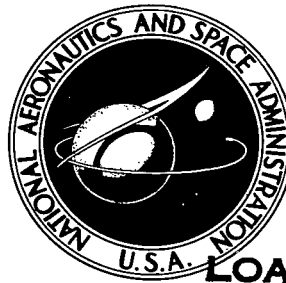


NASA TECHNICAL NOTE



NASA TN D-6691

NASA TN D-6691

LOAN COPY: R
AFWL (D)
KIRTLAND A



TO

THE KINETIC AND MECHANICAL ASPECTS OF HYDROGEN-INDUCED FAILURE IN METALS

by Howard G. Nelson

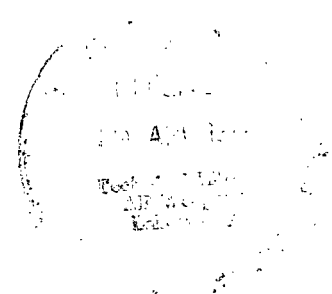
University of California

Los Angeles, Calif. 90024

and

Ames Research Center

Moffett Field, Calif. 94035



NATIONAL AERONAUTICS AND SPACE ADMINISTRATION • WASHINGTON, D. C. • APRIL 1972



0133324

1. Report No. NASA TN D-6691		2. Government Accession No.		3. Recipient's Catalog No.	
4. Title and Subtitle THE KINETIC AND MECHANICAL ASPECTS OF HYDROGEN-INDUCED FAILURE IN METALS				5. Report Date April 1972	
				6. Performing Organization Code	
7. Author(s) Howard G. Nelson				8. Performing Organization Report No. A-4142	
9. Performing Organization Name and Address University of California, Los Angeles, Calif., 90024 and NASA, Ames Research Center Moffett Field, Calif., 94035				10. Work Unit No. 134-03-21-00-21	
				11. Contract or Grant No.	
12. Sponsoring Agency Name and Address National Aeronautics and Space Administration Washington, D. C. 20546				13. Type of Report and Period Covered Technical Note	
				14. Sponsoring Agency Code	
15. Supplementary Notes Submitted to the University of California in partial satisfaction of Ph. D. degree, October 1971, Alan S. Tetelman, Chairman					
16. Abstract An experimental and theoretical study was conducted into the kinetic and mechanical aspects of hydrogen-induced failure of metals. Premature hydrogen-induced failure observed to occur in many metal systems involves three stages of fracture: (1) crack initiation, (2) stable slow crack growth, and (3) unstable rapid crack growth. The presence of hydrogen at some critical location on the metal surface or within the metal lattice has been shown to influence one or both of the first two stages of brittle fracture but has a negligible effect on the unstable rapid crack growth stage. The relative influence of the applied parameters of time, temperature, etc., on the propensity of a metal to exhibit hydrogen-induced premature failure has been investigated and is discussed in terms of (1) the source of the hydrogen species such as a halide-ion-containing aqueous environment, low- and high-pressure hydrogen environments, and hydrogen located initially within the metal lattice and the transport reactions related to each; (2) the specificity of the hydrogen-metal embrittlement couple and the form of the hydrogen-metal embrittlement interaction; (3) the microstructure of the particular alloy system and its effect on both hydrogen transport reactions and intrinsic toughness of the alloy; and (4) the modes of loading. Detailed consideration has been given to the separation of each of these conditions and to their application to the environment-sensitive stages of brittle fracture employing observations of both present and past investigations on several metal systems. Finally, these considerations are discussed in terms of the general mechanism of hydrogen embrittlement and their applicability to premature failure induced by other embrittling species.					
17. Key Words (Suggested by Author(s)) Fracture Hydrogen induced Stress corrosion Corrosion fatigue			18. Distribution Statement Unclassified - Unlimited		
19. Security Classif. (of this report) Unclassified		20. Security Classif. (of this page) Unclassified		21. No. of Pages 143	
				22. Price* \$3.00	

TABLE OF CONTENTS

	<u>Page</u>
LIST OF TABLES	v
LIST OF FIGURES	vi
INTRODUCTION	1
FRACTURE MECHANICS CONCEPTS	2
HOW A CHEMICAL SPECIES CAN INFLUENCE FAILURE	6
KINETIC CONCEPTS	8
HOW TRANSPORT KINETICS CAN INFLUENCE FAILURE	12
HYDROGEN–METAL SYSTEM.	15
STATEMENT OF PROBLEM	20
KINETIC ASPECTS OF HYDROGEN–INDUCED FAILURE	23
SPECIFICITY OF THE HYDROGEN–METAL INTERACTION	23
Materials and procedure	26
Results	28
Discussion	41
Iron-base alloys	41
Nickel-base alloys	42
Titanium-base alloys	43
Molybdenum-base alloys	44
Magnesium-base alloys	44
Copper- and aluminum-base alloys	45
General remarks	45
EMBRITTLEMENT OF AN ENDOTHERMIC OCCLUDER (STEEL)	49
Materials and procedure	50
Experiment and results	50
Fracture toughness tests	50
Crack propagation tests	52
Scanning electron fractography	56
Discussion	56
EMBRITTLEMENT OF AN EXOTHERMIC OCCLUDER (TITANIUM)	64
Materials and procedure	65
Experiments and results	65
Fracture toughness tests	65
Crack propagation tests	68
Discussion	72
MECHANICAL ASPECTS OF HYDROGEN–INDUCED FAILURE	76
HYDROGEN SENSITIVITY OF CRACK INITIATION	76
Materials and procedure	77
Experiments and results	79
Three-point bend tests	79
Hydride formation tests	79
Discussion	82

TABLE OF CONTENTS – Concluded

	Page
DEFORMATION DURING HYDROGEN-INDUCED CRACK GROWTH . . .	85
Material and procedure	86
Results	86
Discussion	88
COMBINED INFLUENCE OF MECHANICALLY AND KINETICALLY INDUCED CRACK GROWTH	92
Materials and procedure	92
Results and discussion	96
Gaseous hydrogen-induced crack growth under static loading	96
Fatigue-induced crack growth in vacuum	98
Corrosion fatigue in hydrogen	100
DISCUSSION	106
KINETIC AND MECHANICAL ASPECTS OF HYDROGEN EMBRITTLEMENT	106
MECHANISM OF HYDROGEN EMBRITTLEMENT	110
Pressure formation	110
Surface interaction	110
Lattice interaction	111
Dislocation interaction	111
Hydride precipitation	112
Hydrogen embrittlement of metals	112
A COMPARISON BETWEEN HYDROGEN EMBRITTLEMENT AND OTHER FORMS OF EMBRITTLEMENT	117
REFERENCES	119

LIST OF TABLES

	Page
1 Hydrogen chemisorption on metal films (ref. 74)	25
2 Alloys, compositions, and heat treatments	27
3 The effect of hydrogen on the fracture behavior of several alloys . . .	30
4 Hydrogen solubility at 1 atm, lattice diffusivity, atom and site dimensions, and heats of adsorption and desorption observed in several endothermic occluding metals	47

LIST OF FIGURES

	Page
1 Parallel and consecutive overall reaction rates contributed by two elementary reactions	13
2 The relationship between the nature of the interaction of hydrogen with metals and the position of the metals in the periodic table (ref. 56)	17
3 Filament placement for the investigation of hydrogen embrittlement of fracture toughness specimens in the presence of atomic-molecular hydrogen .	29
4 SEM fractograph of the molybdenum alloy (TZM); (a) failed in vacuum, (b) failed in molecular hydrogen	31
5 SEM fractograph of the copper alloy (Cu–Be) aged at 400° C; (a) failed in vacuum, (b) failed in molecular hydrogen, (c) failed in atomic-molecular hydrogen	32
6 SEM fractograph of the nickel alloy (201); (a) failed in vacuum, (b) failed in molecular hydrogen	34
7 SEM fractograph of the nickel alloy (Duranickel 301) failed in molecular hydrogen	35
8 SEM fractograph of the aluminum alloy (7075); (a) failed in vacuum, (b) failed in molecular hydrogen	36
9 SEM fractograph of the magnesium alloy (HM21A); (a) failed in vacuum, (b) failed in molecular hydrogen	37
10 SEM fractograph of the titanium alloy (6Al–4V) annealed at 704° C; (a) failed in vacuum, (b) failed in molecular hydrogen	38
11 SEM fractograph of the titanium alloy (6Al–4V) solution treated at 1037° C; (a) stabilized and failed in vacuum, (b) stabilized and failed in molecular hydrogen	39
12 SEM fractograph of the steel alloy (4130); (a) quenched, tempered, and failed in vacuum, (b) quenched, tempered, and failed in molecular hydrogen, (c) quenched, tempered, and failed in atomic-molecular hydrogen	40
13 Filament placement for the investigation of hydrogen-induced slow crack growth in the presence of atomic-molecular hydrogen	51
14 The effect of temperature on K_{scg} in air, molecular hydrogen, and atomic-molecular hydrogen environments	53
15 Molecular hydrogen pressure dependence of embrittlement in an atomic-molecular hydrogen environment	54
16 Temperature dependence of slow crack growth in an atomic-molecular hydrogen environment	55
17 SEM fractograph of a crack propagation specimen failed below 30° C in an atomic-molecular hydrogen environment at a molecular hydrogen pressure of 1.1 N/m ²	57
18 Temperature dependence of slow crack growth in atomic-molecular hydrogen compared with that predicted from equation (28) for a molecular hydrogen environment at the same pressure	59
19 Possible reaction steps involved in the overall transport of hydrogen to the site of the hydrogen embrittlement interaction; (a) transport from a molecular hydrogen environment, (b) transport from an atomic hydrogen environment	62

LIST OF FIGURES – Continued

	Page
20 Representative microstructures of the titanium alloy (6Al–4V); (a) solution treated at 774° C for 40 min, water quenched, and 510° C age for 12 hr, (b) solution treated at 1037° C for 40 min, stabilized at 704° C for 1 hr and 593° C for 1 hr, and air cooled. Kroll's etch	66
21 Environmental hydrogen embrittlement of the titanium alloy (6Al–4V) as a function of hydrogen pressure	67
22 Environmental hydrogen embrittlement of the titanium alloy (6Al–4V) as a function of test displacement rate at a constant hydrogen pressure	69
23 Microscopic hydrogen-induced cracking observed in the titanium alloy (6Al–4V) having an acicular α -phase microstructure; (a) tested at a hydrogen pressure of 9.06×10^4 N/m ² , (b) tested at a hydrogen pressure of 1.3×10^2 N/m ² . Kroll's etch.	70
24 Temperature dependence of slow crack growth in the titanium alloy (6Al–4V) having an acicular α -phase microstructure	71
25 Three-point bend specimen containing a side notch	78
26 The distribution in failure load observed for notched steel alloy (4130) specimens tested at a constant displacement rate of 8.9×10^{-8} m/sec in air and in hydrogen	80
27 The distribution in failure load observed for notched titanium alloy (6Al–4V) specimens tested at a constant displacement rate of 8.9×10^{-8} m/sec in air and in hydrogen	81
28 Cross section of a crater formed on the surface of a titanium specimen by the interaction with the hydrogen environment at the location of the welded thermocouple	83
29 Second-phase stringers formed in titanium from a hydrogen environment showing the existence of cracks following elastic deformation	84
30 Gaseous hydrogen-induced crack growth profile of a large grained Fe–3%Si alloy specimen containing a cleavage precrack on a (100) plane	87
31 SEM fractograph of a large-grained Fe–3%Si alloy specimen failed in hydrogen	89
32 The intersection of a hydrogen-induced cleavage crack with a grain not oriented for continued (100) cleavage	90
33 The transition between hydrogen-induced cleavage and ductile tearing brought about by a change in lattice orientation	91
34 Microstructures of the titanium alloy (5Al–2.5Sn) investigated in this study; (a) fine acicular α -titanium, (b) coarse acicular α -titanium, Kroll's etch . . .	93
35 Double-cantilever-beam specimen	94
36 The effect of applied stress intensity on the rate of hydrogen-induced crack growth under conditions of static loading	97
37 The effect of maximum stress intensity on the rate of fatigue-induced crack growth in a vacuum environment	99
38 The effect of maximum stress intensity on the rate of crack growth in a hydrogen environment under conditions of cyclic loading of specimens having a fine acicular microstructure	101

LIST OF FIGURES – Concluded

	Page
39 The effect of maximum stress intensity on the rate of crack growth in a hydrogen environment under conditions of cyclic loading of specimens having a coarse acicular microstructure	103
40 SEM fractograph of specimens having a coarse acicular microstructure fatigued at 0.005 Hz; (a) fatigued in vacuum, (b) fatigued in hydrogen	105

INTRODUCTION

The capacity of an engineering structure to withstand an applied load is often severely degraded by the presence of hydrogen originating from its equilibrium position within the metal lattice, from a gaseous hydrogen environment in contact with the structure, or from the product of a heterogeneous reaction between a hydrogen-containing molecule and the metal surface. The oldest and most extensively studied form of hydrogen embrittlement is that due to hydrogen within the metal lattice (refs. 1-5). Hydrogen enters the metal during production processes, such as pickling and electrolytic plating operations, where the hydrogen concentrations at the metal surface can be very large (ref. 6). The most recent form of hydrogen embrittlement to be recognized results from the direct exposure of a clean metal surface during deformation to a gaseous hydrogen environment. This form of embrittlement was first studied in detail in 1961 (ref. 7) and has since been regarded with increasing concern. Because of the usefulness of the hydrogen-oxygen reaction as a fuel cell to produce electric current (ref. 8) and as a source of energy for propulsion (ref. 9), this form of embrittlement will become more and more important and may, in the future if not today, control one phase of our technological growth.

The deleterious consequences of hydrogen on an engineering structure come about through an influence on its fracture behavior – either crack initiation or crack growth stage of fracture. The causal interaction between hydrogen and the metal may be the formation of a solid solution of hydrogen in the metal, second phase hydride precipitates, molecular hydrogen within the metal lattice, gaseous products formed as a result of the reaction between hydrogen and impurities, and others. From the numerous studies conducted on hydrogen embrittlement, it can be classified into two distinct types according to its strain rate dependence. The first type of embrittlement is aggravated by increasing strain rates, while embrittlement of the second type decreases with an increase in strain rates until it disappears completely. In this investigation we will concentrate primarily on the second type, yet, understanding that some ideas can be applied to both. The first type, although also important from an engineering standpoint, is due to the presence of a product of a completed reaction within the metal lattice and involves mechanical theory as related to the fracture process. In the second type, a kinetically controlled reaction occurs concurrently with embrittlement and must then involve both kinetics as related to the transport of

hydrogen and its interaction with the metal lattice as well as mechanics related to the fracture process.

Since 1960, considerable advancement has been made in the development and application of linear-elastic fracture mechanics to the fracture process. Because mechanical theory in terms of the fracture mechanics method of analysis and kinetic theory will be used throughout this investigation, concepts underlying these theories as applicable to the hydrogen embrittlement problem are described below.

FRACTURE MECHANICS CONCEPTS

Fracture mechanics concepts originated in the consideration of fracture of brittle materials. A brittle material, by definition, is one that remains elastic up to the point of fracture, glass being the usual example. The work of Griffith (ref. 10) around 1920 represents the birth of fracture mechanics. Griffith treated fracture as a problem of general mechanical stability and established an energy criterion for it, involving the elastic strain energy on the one hand and the free surface energy of the crack on the other, given as

$$\sigma_F = \sqrt{2E\gamma_s / \pi C} \quad (1)$$

where σ_F is the fracture stress of the structure applied normal to an elliptical crack, $2C$ is the crack length, E is the elastic modulus of the material, and γ_s is the true surface energy or the work done in creating new surface area by the breaking of atomic bonds. Unlike a brittle material, a normally ductile material, such as a structural metal, must be expected to yield in some region around the tip of a crack. Griffith's original energy criterion could be applied to fracture in metals, if the work done in plastic straining was taken into account. To apply this modified criterion, it becomes necessary to carry out an elastic-plastic analysis of the cracked material. This is very much more difficult than the purely elastic analysis needed for a brittle material. Because of these difficulties, a simplified approach has been developed that involves a combination of a purely elastic theoretical analysis and appropriate experiments on cracked structures. This is referred to either as "linear elastic fracture mechanics" or "Griffith-Irwin theory." Applying Westergaard's (ref. 11) stress function approach to crack problems, Irwin (ref. 12) found that the stress field in the neighborhood of a crack tip under opening mode stresses of Mode I stresses (tension stresses

perpendicular to the plane of the crack) is given by the equations

$$\left. \begin{aligned} \sigma_{xx} &= \frac{K_I}{(2\pi r)^{1/2}} \cos \frac{\theta}{2} \left(1 - \sin \frac{\theta}{2} \sin \frac{3\theta}{2} \right) \\ \sigma_{yy} &= \frac{K_I}{(2\pi r)^{1/2}} \cos \frac{\theta}{2} \left(1 + \sin \frac{\theta}{2} \sin \frac{3\theta}{2} \right) \\ \tau_{xy} &= \frac{K_I}{(2\pi r)^{1/2}} \sin \frac{\theta}{2} \cos \frac{\theta}{2} \cos \frac{3\theta}{2} \\ \sigma_{zz} &= \nu(\sigma_{xx} + \sigma_{yy}) , \quad \tau_{xz} = \tau_{yz} = 0 \end{aligned} \right\} \quad (2)$$

where r and θ are polar coordinates, ν is Poisson's ratio, and K_I is a parameter termed stress intensity. These equations suggest that the elastic stress field distribution in the neighborhood of crack tips is invariant and that the magnitude of the stress field can be described by a single-term parameter, K_I , designated as the stress intensity factor. For an infinitely sharp elastic crack, in an infinitely wide plate, the stress intensity factor is defined as (ref. 13)

$$K = \sigma \sqrt{\pi C} \quad (3)$$

and thus, is a function of crack size, body configuration, and the applied load. The analytical determination of the stress intensity factors and the crack-tip stress fields is basically a problem in the mathematical theory of elasticity and has been cataloged by Paris and Sih (ref. 14).

The underlying principle of fracture mechanics is that unstable fracture occurs when the stress applied to the cracked structure reaches some value. In terms of the Irwin analysis, this occurs when a parameter defined as the crack extension force, $G = K^2/E$ (in plane stress), is equal to a critical value G_c ; the critical strain-energy release rate for unstable crack extension. When $G = G_c$ then $K = K_c$; K_c (K_{Ic} under Mode I stresses) is considered a

material property, known as the fracture toughness of the material, and represents the material's inherent ability to withstand a given stress field intensity at the tip of a crack. It should be noted, however, that the critical stress intensity parameter is geometry dependent and does not represent a material property when the elastic stress field in the immediate neighborhood of a crack tip is disrupted by plastic deformation. This occurs in engineering materials, particularly under conditions of plane stress, where the plastic zone at the crack tip is much larger than when plane-strain conditions exist.

As mentioned earlier, consideration of plastic deformation at the crack tip complicates fracture mechanics, yet its application to engineering structures is broad. Current theoretical research is particularly focussed on these plasticity aspects (refs. 15-17). For our purposes we need not consider the influence of plastic deformation in terms of fracture mechanics. The following oversimplified thermodynamic approach will serve to emphasize the relevant concepts.

When plastic deformation occurs near the crack tip, a certain amount of plastic work, γ_P , is expended during crack propagation in addition to the elastic work, γ_S , that is required to create the two fracture surfaces. The mechanics of the fracture process, when plastic relaxation occurs at the crack tip, depends on the magnitude of γ_P , and thus, factors affecting γ_P . Brittle fractures may be induced in usually ductile structural metals under conditions where plastic flow is inhibited by low temperatures, an alloy constitution or a mechanical treatment causing an increase in yield stress, or by geometrical constraint causing stress triaxiality, or possibly when chemical alterations reduce the force required to separate the surfaces. This latter point will be discussed in detail later. Considering an energy balance, the stress required to move a crack must involve the total work done in expanding the crack, per unit area of fracture surface. With plastic deformation this work is increased from γ_S to $(\gamma_S + \gamma_P)$. For a moving crack the Griffith equation (eq. (1)) for plane stress is modified to

$$\begin{aligned}\sigma_M &= \sqrt{(2E/\pi C)(\gamma_S + \gamma_P)} \\ &= \sqrt{(2E\gamma_S/\pi C)[1 + (\gamma_P/\gamma_S)]}\end{aligned}\tag{4}$$

when $\gamma_P/\gamma_S > 1$,

$$\sigma_M = \sqrt{(2E\gamma_S/\pi C)(\gamma_P/\gamma_S)}\tag{5}$$

Plastic deformation at the crack tip blunts the crack, and thus relaxes some of the stresses thereby increasing the effective crack tip radius, ρ . The Orowan (ref. 18) modification of the Griffith equation (eq. (1)) to consider the influence of the crack tip radius is given by

$$\sigma_F = \sqrt{(2E\gamma_s/\pi C)(\rho/3a_0)} \quad (6)$$

where a_0 is the interatomic distance within the metal lattice. Equating equations (5) and (6) we obtain

$$\sqrt{(2E\gamma_s/\pi C)(\rho/3a_0)} = \sqrt{(2E\gamma_s/\pi C)(\gamma_p/\gamma_s)}$$

so that

$$\rho/3a_0 = \gamma_p/\gamma_s \quad (7)$$

It is seen from the resulting equation (7) that even though the γ_p term is large compared with γ_s , γ_s is very much a part of the fracture process in that it is a multiplying factor for determining the energy expended on crack growth at a constant crack tip radius.

The above concepts are discussed in much greater detail in reference 19. These concepts are, of course, related to the crack growth stage of fracture. Unfortunately, the crack initiation stage of fracture has not been considered in such detail. This stage of fracture, besides being made complex by variables that are difficult to define, is relatively unimportant in engineering structures. Most structures contain preexisting flaws as a result of processing procedures such as welding. However, this is not the case for many test specimen configurations, where crack initiation is an important part of the fracture process. Because of this, the following qualitative discussion of the crack initiation process is undertaken.

Most models for crack nucleation involve the interaction of dislocations with strong planar defects within the metal lattice, that is, a pile-up of dislocations against an obstacle such as a grain boundary, twin boundary, or precipitated phase. These models have been treated quantitatively by Stroh (refs. 20, 21), Cottrell (ref. 22), and Gilman (ref. 23) and are all common in that the shear stress to initiate a crack is proportional to some function of

surface energy, similar to the equation for crack growth. Specifically, the interaction of a chemical species in a manner to influence crack initiation as well as propagation has been discussed in detail by Robertson and Tetelman (ref. 24). In any case, significant amounts of deformation or very high stress levels, or both, are required before a crack can be initiated in an unflawed metal.

The influence of a notch in a test specimen or structure is significant in that it acts as a stress concentrator. Macroscopic deformation or general yield (crack initiation) can occur at the notch tip at much lower applied loads than if the notch were not present. However, it must be emphasized that the presence of a notch is in no way similar to the presence of a crack in an engineering metal. The stress concentrating effect of a notch is only one parameter that influences crack nucleation. Others include the heterogeneity of deformation, location and orientation of planar defects, and yield and ultimate strengths of the material. Such parameters are generally unpredictable and make crack initiation a random process.

HOW A CHEMICAL SPECIES CAN INFLUENCE FAILURE

From the above brief discussion of concepts related to the crack initiation stage and growth stage of fracture, it is obvious that these are not intrinsic properties of a metal but the results of a collage of specific properties. The influence of a chemical species on the fracture process occurs, then, as the influence of the species on these specific properties such as plastic deformation or dislocation motion, surface energy or lattice bond energy. The degree of influence will depend on the specificity of the system, that is, the specific metal under consideration, the specific material property that has the most significant influence on the fracture process in that metal, and the influence of a specific chemical species on that specific property. In short, the influence of a chemical species on the fracture behavior of a metal is very specific and very complicated. Below we will attempt to consider briefly how any chemical species can influence material properties that in turn influence the crack initiation and growth stages of fracture.

Fracture is a localized process occurring very near the crack tip or at the point of crack initiation; thus it can be affected by a localized concentration of a species very dilute in the metal or in the environment. If this be the case, an activity gradient is required to concentrate the species at these critical locations. Consideration of the species transport will

be discussed in detail in a later section; however, it is important to realize that the effects to be discussed need not be bulk effects.

Plastic deformation has been shown to be essential to some models of crack initiation by creating dislocation pile-ups at obstacles and to hinder crack growth by increasing the crack tip radius. In general the effect of a chemical species is to make it more difficult for deformation to occur. This can come about through 1) the presence of an adsorbed layer or film on a metal surface by influencing the ease of dislocation egress out of that surface through a change in the image force a dislocation sees at the surface (ref. 25) or the formation of a debris layer near the surface (ref. 26); 2) the interaction of the species with the strain fields around a dislocation requiring the dislocation to break free (ref. 27) or to transport the species with it as it moves (ref. 28); 3) a change in heterogeneity of deformation by influencing the stacking fault energy of the dislocation (ref. 29) or its ease of cross-slip (ref. 30); 4) second-phase precipitation at a dislocation (ref. 31) or within the metal lattice (ref. 32). The effect of a chemical species through its effect on deformation will be primarily to increase the rate of stable subcritical crack growth. The magnitude of this effect will depend on the specific metal – if little or no deformation normally occurs at the crack tip during growth, the influence of this effect will be negligible.

The effect of a chemical species on the surface energy or the bond energy of a metal is most often considered to influence fracture (refs. 33-37). As has been discussed, the magnitude of the surface energy term has a direct relation to the ease of both crack initiation and propagation. The lower the surface energy of a metal, the easier it is for crack initiation and propagation. It is most probably because of this obvious dependence that the influence of a chemical species on fracture through surface energy has attracted so much attention. Even with this attention, however, there is little reliable data to establish that a chemical species can influence surface energy to a significant extent, nor is there an established theory by which this could occur. Considerable work has been conducted to explore the effect of a species on surface energy (refs. 38-40); however, the magnitude of the observed effects and even the direction of the effect must be questioned because of recent evidence that establishes the extreme importance of system characterization (refs. 41-42), that is, a total knowledge of surface condition and contamination, purity of the environment, etc. At this point it must remain sufficient to say that a chemical species

may influence surface energy or bond energy to the extent that fracture behavior of a metal *may* be influenced.

Before leaving this discussion, it must be pointed out that a chemical species can influence fracture through other considerations not included above. Second-phase precipitation can occur to such an extent that a crack will initiate and grow in these precipitates, eventually connect together, and result in failure of the structure (ref. 43). The second phase may not be a solid but a gas. In this case a void can be nucleated at some defect in the metal lattice and can grow with or without stress until failure of the structure results (ref. 44). Other considerations can be found throughout the literature; however, these are even more specific and will not be considered here.

KINETIC CONCEPTS

Kinetic theory is defined as a theory that deals with the effects of forces on the motion of bodies. It originated prior to the seventeenth century. Many reactions, be they chemical reactions involving changes in form or transport reactions involving changes in location, are not kinetically simple — they may proceed through a number of reaction steps between the initial and final state of the overall reaction. Each individual reaction step is termed an elementary reaction. Each elementary reaction may or may not be activated. An activated reaction is one in which the reactant must be raised to a higher state of potential energy than the original and final state. Additionally, a reaction can have an order depending on the form of the reaction. In this discussion we will deal simply with first-order reactions that are defined by the reaction equation



Let the initial concentration of A be “a” moles/liter. If after a time t, “x” moles/liter of A have changed state, the remaining concentration of A is (a – x), and “x” moles/liter of B and C have been formed. The rate of formation of B or C is dx/dt, and for a first-order reaction is proportional to the instantaneous concentration of A, so that

$$dx/dt = k_1 (a - x) \quad (9)$$

where k_1 is known as the rate constant.

An overall reaction can be made of elementary reactions of three possible combinations: 1) opposing reactions, 2) consecutive reactions, and 3) parallel reactions. Opposing elementary reactions are given by the equation



where k_1 is the rate constant in the forward direction and k_2 in the reverse. Initially the concentration of A is "a" and B is "b." If after a time t , "x" moles/liter of A have been transformed into B, the concentration of A is $(a - x)$, and that of B is $(b + x)$. The differential rate equation is therefore

$$dx/dt = k_1(a - x) - k_2(b + x) \quad (11)$$

If the reaction occurs for sufficient time that equilibrium exists, the equilibrium constant will be given by $K = k_1/k_2$.

Consecutive reactions occur when the product of one reaction becomes itself the reactant of the following reaction. This is expressed by the equation



As before the differential equations for the rate of change of the concentrations x , y , and z are given as

$$\left. \begin{array}{l} -dx/dt = k_1 x \\ -dy/dt = -k_1 x + k_2 y \\ dz/dt = k_2 y \end{array} \right\} \quad (13)$$

The electrical analog of such a system would be a circuit consisting of impedances connected in series (ref. 45). The overall flux or current passing through the circuit is the same in each element, and is determined by the overall potential divided by the sum of the impedances. If one of the elements in the circuit has an impedance considerably larger than

the others, the smaller impedances can be neglected, as they will have an insignificant effect on the current, its value being essentially determined by the larger one. If, like equation (12), a number of reaction elements are involved consecutively, the overall rate \dot{r} is related to the rates of the component elemental reactions $\dot{r}_1, \dot{r}_2, \dots, \dot{r}_i$ by

$$1/\dot{r} = 1/\dot{r}_1 + 1/\dot{r}_2 + 1/\dot{r}_3 + \dots + 1/\dot{r}_i = \sum_i 1/\dot{r}_i \quad (14)$$

If one of the rates, say \dot{r}_1 , is considerably smaller than the others, it would determine the overall rate

$$\dot{r} \approx \dot{r}_1$$

However, if the rates of two or more steps are of the same order of magnitude, the overall rate will be as given by equation (14).

When a species can react or move to a location in more than one way the elementary reactions are known as parallel reactions and are given by the equation



The rate of an overall reaction composed of a number of parallel elementary reactions is the sum of the rates of each of the elementary reactions. This is analogous to an electrical circuit in which several impedances are connected in parallel (ref. 45). The potential across each impedance is the same, but the current through each varies with its respective impedance. The overall current is the sum of the currents through the parallel legs. By consideration of the conductance analogy, in a complex reaction with parallel steps, the overall rate is related to the rates of the individual steps by

$$\dot{r} = \dot{r}_1 + \dot{r}_2 + \dot{r}_3 + \dots + \dot{r}_i = \sum_i \dot{r}_i \quad (16)$$

Under such conditions, the overall rate is primarily determined by the fastest process, if and only if, one of the rates, say \dot{r}_1 , is considerably greater than the other rates; hence we have

$$\dot{r} \approx \dot{r}_1 \quad (17)$$

Obviously, if the rates of two or more mechanisms are not greatly dissimilar, the overall rate would be expressed by equation (16).

So far we have been concerned with how concentrations affect kinetics and possible combinations of reaction paths available. Next let us consider how the elementary rate constants depend on temperature. The temperature effect has been tremendously useful in providing an insight into the theory of all rate processes.

In 1889, Arrhenius pointed out that the van't Hoff equation for the temperature coefficient of the equilibrium constant was

$$d \ln k / dT = \Delta E / RT^2$$

so a reasonable equation for the variation of elementary rate constants with temperature might be

$$d \ln k / dT = E / RT^2 \quad (18)$$

where T is absolute temperature, R is the gas constant, and E is called the activation energy of the reaction. The activation energy is the potential-energy hill that must be climbed to reach the activated state between the initial and final state of the elementary reaction. If E is not itself temperature dependent (usually the case), equation (18) upon integration yields

$$k = A \exp(-E/RT) \quad (19)$$

where A is the constant of integration and is called the frequency factor or preexponential factor. Equation (19) is the famous Arrhenius equation for the rate constant.

In an overall reaction composed of numerous elementary reactions under steady-state conditions, the concentrations of all reactants will be constant at a given temperature and will vary as a function of temperature through the temperature dependence of the rate constants. Over a wide range of temperatures, the activation energy spectrum for an overall

reaction may exhibit several discrete values, each associated with a specific rate-controlling elementary reaction. Figure 1 is a schematic illustration of this effect for two overall reactions (ref. 45) – one in which the elementary reactions are consecutive and the other in which the reactions are parallel. This figure is a semilogarithmic rate plot of two individual elementary reactions crossing each other at a temperature T_t . At the intersection temperature T_t , the individual rates are equal; elsewhere, one step will have a rate significantly greater than the other. The important point in figure 1 is the difference in form of the two overall reactions depending on whether they are made up of consecutive or parallel elements. Such a plot can thus separate the form of the reaction paths in an overall reaction made up of numerous elementary reactions.

The above concepts are an agglomeration of concepts discussed in detail in several texts on chemical kinetic theory. One of the major sources of information has been reference 46.

HOW TRANSPORT KINETICS CAN INFLUENCE FAILURE

If a chemical species is observed to influence fracture behavior of a metal, the species must have been at some critical location before the metal was stressed or have been transported to this location during deformation. An example of the former is the embrittlement of a metal by the presence of massive precipitates in the metal lattice; examples of the latter are forms of embrittlement identified by an inverse strain rate dependence. This inverse strain rate dependence is a result of an overall kinetic reaction involved in the transport of the species from its equilibrium or quasiequilibrium position in the system to some critical location that can influence fracture. The rate in which a metal becomes embrittled, then, will depend on the reaction kinetics of the overall reaction. We will next consider the elementary reactions potentially involved in various forms of embrittlement.

The overall transport reaction will be very different depending on whether the embrittling species originates in the environment surrounding the metal or is present in equilibrium within the metal lattice. When the species originates in the metal lattice, lattice diffusion will be the primary transport reaction; however, other reactions such as phase formation, dissolution onto an internal surface (of a void perhaps), and desorption into the

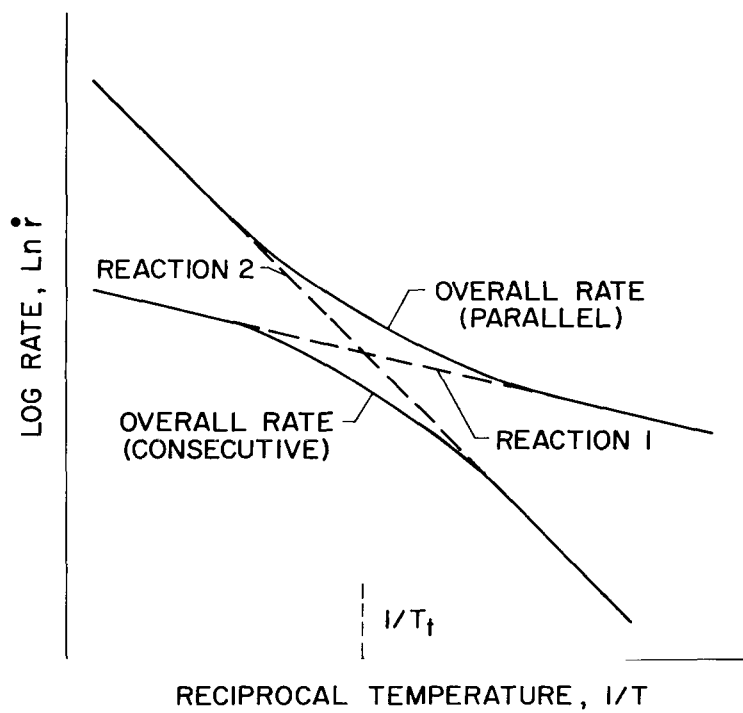


Figure 1.— Parallel and consecutive overall reaction rates contributed by two elementary reactions.

void cavity may also be involved, depending on where and how the species influences fracture.

When the species originates in the environment, the overall transport reaction will be very complex reflecting the form of the species in the environment, the purity of the environment, and the nature of the metal surface. For the simple case of embrittlement caused by a very high purity gaseous hydrogen environment where the interaction influencing fracture occurs well within the metal and does not involve a phase precipitation, the elementary reactions may be:

1. Gas-phase diffusion of molecular hydrogen to the crack surface

$$r_1 = k_1 P \quad (20)$$

where k_1 is the rate constant and P is molecular hydrogen pressure.

2. Molecular hydrogen strikes the metal surface, dissociates, and is adsorbed as atoms

$$r_2 = k_2 P(1 - \theta)^2 \quad (21)$$

where θ is the hydrogen surface coverage.

3. A pair of adsorbed hydrogen atoms combines and evaporates as a molecule

$$r_3 = k_3 \theta^2 \quad (22)$$

4. An adsorbed atom passes into the metal

$$r_4 = k_4 \theta [1 - (u/u_s)] \quad (23)$$

where u is the hydrogen concentration just inside the metal surface and u_s is the saturation concentration of hydrogen in the metal.

5. A hydrogen atom in the metal leaves the lattice and enters the metal surface

$$r_5 = k_5 u(1 - \theta) \quad (24)$$

6. A molecule strikes the surface and dissociates, one atom staying on the surface and the other entering the metal

$$r_6 = k_6 P(1 - \theta)[1 - (u/u_s)] \quad (25)$$

7. A hydrogen atom near the metal surface diffuses to the critical location to cause embrittlement

$$r_7 = D[(u - u_\ell)/\ell] \quad (26)$$

where D is the diffusion coefficient and u_ℓ is the hydrogen concentration at the critical location ℓ distance from the metal surface.

Obviously the form of the overall reaction rate equation will be very complex and will involve elementary reactions occurring in opposite directions, consecutively, and in parallel. Additionally, the form of the temperature dependence and pressure dependence of transport will be complex unless, over the temperature and pressure ranges investigated, one or two of the elementary reactions controls the overall reaction. Barrer (ref. 47) and others (refs. 48-49) considered the contributions of elementary reactions to the overall reaction controlling gas-phase permeation through a metal membrane and found that almost any form of pressure and temperature dependence for the overall reaction can be justified.

The point of this somewhat detailed discussion is that the species transport is a very complex, yet very important, process that determines the rate in which embrittlement occurs in a metal. Further, embrittlement may or may not be observed in a particular metal or a particular environment simply as a result of what are normally considered secondary effects, such as the influence on an elementary reaction of minute concentrations of contaminant in the environment or on the metal surface. Transport reactions are truly specific, so an evaluation of embrittlement of a system must include the complete characterization of that system.

HYDROGEN-METAL SYSTEM

The hydrogen-metal system is one of the most extensively studied bielement systems so numerous reviews are available. One of the more recent and probably the most extensive particularly concerning ferrous alloys is that by Oriani (ref. 50).


Sieverts (ref. 51) in 1929 demonstrated that the solubility of hydrogen in iron and, in fact, most metals is proportional to the square root of external pressure;

$$u = sP^{1/2} \quad (27)$$


where u is the concentration of dissolved hydrogen in equilibrium with gaseous hydrogen at pressure P , and s is a constant of proportionality. This relation (Sieverts' law) establishes through the equilibrium rate equations that hydrogen is present in a metal lattice in dissociated (atomic) form. Oriani (ref. 50) concludes from a review of available information that dissolved hydrogen, at least in the transition metals, is a proton that has given up its electrons to the electron gas of the metal. This screened proton is capable of rather substantial perturbation of the metal lattice – for hydrogen in α -iron, the partial molal volume has been observed to be around $2 \times 10^{-6} \text{ m}^3/\text{g-atom}$ (refs. 52, 53), about one-third the value of that caused by dissolved carbon (ref. 54). The combination of small diameter of the hydrogen atom ($1.06 \times 10^{-10} \text{ m}$) and relatively large observed partial molal volumes suggests that hydrogen is located in the interstitial position rather than the substitutional position within the metal lattice (ref. 50). In α -iron evidence indicates that hydrogen occupies the octahedral interstitial site (ref. 55); however, for metals in general the exact interstitial site (octahedral or tetrahedral) has not been firmly established.

The products of the interaction of hydrogen with metals can be hydrides, solid solutions, or a binary phase mixture of solid solutions and hydrides. The nature of the products of the interaction of metals with hydrogen depends on the specific metal. Hurd (ref. 56) divides metals into four groups depending on the form of the hydride; ionic hydrides, hydrides of transition metals, intermediate hydrides, and covalent hydrides. Each group corresponds to a position of the elements in the periodic table (fig. 2). As discussed in detail by Kolachev (ref. 57), a separation must be made between solid solutions of hydrogen in metals and hydrides. The transition metals of Groups IIIB-VB form solid solutions and hydrides as the result of direct reaction with hydrogen, while metals of Groups VIB-VIIIB normally form only solid solutions that cannot really be considered hydrides. Under specific sets of conditions real hydrides of several metals of Groups VIB-VIIIB can also be obtained (refs. 58, 59).

PERIOD	GROUP																	
	IA	IIA	IIIB	IVB	VB	VIB	VIIB	VIIIB			IB	IIB	IIIA	IVA	VA	VIA	VIIA	O
I	¹ H																	² He
II	³ Li	⁴ Be											⁵ B	⁶ C	⁷ N	⁸ O	⁹ F	¹⁰ Ne
III	¹¹ Na	¹² Mg											¹³ Al	¹⁴ Si	¹⁵ P	¹⁶ S	¹⁷ Cl	¹⁸ Ar
IV	¹⁹ K	²⁰ Ca	²¹ Sc	²² Ti	²³ V	²⁴ Cr	²⁵ Mn	²⁶ Fe	²⁷ Co	²⁸ Ni	²⁹ Cu	³⁰ Zn	³¹ Ga	³² Ge	³³ As	³⁴ Se	³⁵ Br	³⁶ Kr
V	³⁷ Rb	³⁸ Sr	³⁹ Y	⁴⁰ Zr	⁴¹ Nb	⁴² Mo	⁴³ Tc	⁴⁴ Ru	⁴⁵ Rh	⁴⁶ Pd	⁴⁷ Ag	⁴⁸ Cd	⁴⁹ In	⁵⁰ Sn	⁵¹ Sb	⁵² Te	⁵³ I	⁵⁴ Xe
VI	⁵⁵ Cs	⁵⁶ Ba	⁵⁷⁻⁷¹ La-Lu	⁷² Hf	⁷³ Ta	⁷⁴ W	⁷⁵ Re	⁷⁶ Os	⁷⁷ Ir	⁷⁸ Pt	⁷⁹ Au	⁸⁰ Hg	⁸¹ Tl	⁸² Pb	⁸³ Bi	⁸⁴ Po	⁸⁵ At	⁸⁶ Rn
IONIC			TRANSITION									INTER-MEDIATE		COVALENT				



EXOTHERMIC HYDROGEN OCCLUDERS



ENDOTHERMIC HYDROGEN OCCLUDERS

Figure 2.— The relationship between the nature of the interaction of hydrogen with metals and the position of the metals in the periodic table (ref. 56).

The hydrides of the transition metals have metallic properties that can be explained by the theory of metallic bonds. Hydrides are less dense than the metal; they have a volume increase of 10 to 20 percent. In the formation of hydrides by the absorption of hydrogen by dense metals, appreciable tensile stresses exist around the hydrides. They are generally porous brittle materials of low strength. Under ordinary conditions hydrides exist at concentrations of metal atoms in excess of stoichiometric compositions; that is, $\text{TiH}_{1.70}$ - $\text{TiH}_{1.75}$, $\text{ZrH}_{1.92}$, and $\text{VH}_{0.7}$ - $\text{VH}_{0.9}$, but the formation of compounds with a higher content of hydrogen is difficult. Elements of Groups VIB-VIIB do not form hydrides during hydrogen exposure, because these metals have no free states in the band of the bonding electrons.

From Sieverts' law (eq. (27)) the constant of proportionality, s , is either the chemical equilibrium constant or the rate constant between molecular hydrogen in the gas phase to atomic hydrogen within the metal lattice just below the surface, and is temperature dependent. An isobaric plot of logarithm s versus the reciprocal of absolute temperature (an Arrhenius type plot, eq. (19)) will yield a value of energy for the process. In actuality, the exact meaning of this energy term is difficult to assess depending on whether true equilibrium exists between hydrogen in the gas phase and that absorbed in the metal lattice. Confusion concerning this point exists throughout the literature (refs. 49, 60). Be that as it may, as we pass from metals of Group VB to those of Groups VIB-VIIIB in figure 2, the temperature dependence of the absorption term, s , changes. The transition elements of Groups IIIB-VB absorb hydrogen exothermally, and elements of Groups VIB-VIIIB (except palladium) absorb hydrogen endothermally. The former are characterized by a negative value of energy with uptake decreasing with increasing temperature at a constant pressure; the latter by positive energy with uptake increasing with increasing temperature. In endothermic occluding metals, the maximum amount of hydrogen possible within the metal at a constant pressure is several orders of magnitude less than metals that are exothermic occluders. For example, in α -iron at a hydrogen pressure of 1 atm, equilibrium lattice solubility is only 5×10^{-4} ppm by weight at room temperature, which corresponds to about 3×10^8 atoms of hydrogen per atom of iron (ref. 61). In titanium, the entire metal can be converted to a hydride yielding nearly 2 atoms of hydrogen per 1 atom of titanium (ref. 62).

Hydrogen transport within a metal lattice occurs by an interstitial diffusion mechanism in general agreement with the Zener model (ref. 63). In metals having a body-centered-cubic crystal structure such as α -iron (ref. 64) and β -titanium (ref. 65), the rate of hydrogen transport is much less temperature sensitive than most solid-state diffusion processes exhibiting activation energies of the order of 12,500 J/mole (3,000 calories/mole) and transport rates of the order of 10^{-8} m²/sec near room temperature. In face-centered-cubic metals such as γ -iron (ref. 64) and hexagonal-close-packed metals such as α -titanium (ref. 66), hydrogen transport rate is substantially slower and the temperature dependence considerably greater.

In summary, hydrogen can enter a metal from the liquid state or the gas state by any process producing atomic hydrogen at the metal surface. The amount of atomic hydrogen present on the metal surface is directly dependent on the overall transport process and is influenced by a number of physical characteristics of the particular surface and environment. The amount of hydrogen present in the metal lattice at interstitial positions is dependent on the specific nature of the metal. Metals that are exothermic occluders to hydrogen, such as titanium, can hold enormous quantities of hydrogen while metals that are endothermic occluders, such as iron, can only hold extremely low quantities. Hydrogen transport within the metal lattice occurs by an interstitial mechanism and is also very dependent on the crystal structure of the metal. Transport in metals having a more open crystal structure (bcc) is less temperature dependent and more rapid than those having a more closed structure (fcc and hcp).

STATEMENT OF PROBLEM

Hydrogen embrittlement as a result of hydrogen within the metal lattice has been a problem for several decades; however, only in the past decade has the real breadth of this problem been indicated. Hydrogen need not be originally present within the metal lattice to cause a degradation of the load-carrying ability of a metal structure, but can originate from the environment – by the direct exposure of a clean metal surface during deformation to a gaseous hydrogen environment or by heterogeneous reactions, occurring even at room temperature, between the metal and hydrogen-containing molecules and compounds, such as water and numerous organic species. As the growth of technology increases and new materials, applications, and processing procedures are developed, it becomes increasingly apparent that solutions to specific hydrogen problems are no longer adequate and many times, in fact, can lead to erroneous interpretation of the general phenomena. A vast majority of the more than 1000 investigations conducted on the deleterious effects of hydrogen on metals has been specific because of the nature of the phenomena. Hydrogen attack occurs most often in components of a system that are most highly stressed, and thus critical to the system. A failure of such a component demands immediate action and a specific solution. This approach contributes little to an understanding of the phenomena, an understanding that must be attained in the near future.

The embrittlement of metals by a gaseous hydrogen environment affords a potentially powerful tool for the quantitative understanding of the overall hydrogen embrittlement phenomena. When combined with the fracture mechanics approach to fracture and the kinetic theory approach to hydrogen transport, complete characterization of the embrittling system becomes possible. When the hydrogen is originally present only in the environment: concentration effects, purity effects, etc., can be established through the instantaneous change of the environment; interaction with the metal must occur at the metal surface or, at the least, hydrogen must enter the metal through this surface; the origin of the species is absolutely defined such that rate effects can be compared through kinetic theory; influence of the species on the stages of fracture can be defined through fracture mechanics; and the specificity of embrittlement can be better established through the characterization of the embrittling system.

The first reported evidence of the embrittlement of a metal by a gaseous hydrogen environment was in 1955 (ref. 67). In 1961 Hofmann and Rauls (ref. 7) observed a significant reduction in the time to failure of steel tested in an environment of 1.01×10^4 kN/m² (100 atm) hydrogen as compared with an air environment. In 1963 Cavett and Van Ness (ref. 68), in an extension of a study in which hydrogen was charged into the metal under 6.9×10^4 kN/m² (10,000 psig) hydrogen pressure at high temperatures, observed a degrading effect of this environment on a steel and a nickel base alloy even at room temperature. Between 1963 and 1965 there were numerous scattered reports of the effect of an environment on the ductility of metals (refs. 69-72). This phenomena became of engineering importance in June 1965 when the National Aeronautics and Space Administration observed the premature failure of a gaseous hydrogen storage vessel designed for service at 3.45×10^4 kN/m² (5000 psi). This welded vessel, which was fabricated from A 517-F (T-1) steel in the quenched and tempered condition, failed at 2.69×10^4 kN/m² (3900 psi) (ref. 73). Since this failure there have been several investigations on the effect of a high pressure, high purity gaseous hydrogen environment on metals. One of the most extensive, involving several engineering materials, is reference 74. During this initial phase (and even today) many people considered the gaseous hydrogen problem to be related to the presence of a high pressure hydrogen environment. Hancock and Johnson (ref. 75) demonstrated that this is not the case because significant effects can be observed in hydrogen at least as low as 1 atm pressure.

The purpose of this investigation is to contribute significantly to the understanding of the embrittlement of metals by hydrogen such that this knowledge may be used to predict, if not prevent, failure in engineering structures. Kinetic theory will be used in conjunction with a gaseous hydrogen environment to clarify:

1. The specificity of the hydrogen-metal embrittlement interaction
2. The form and the location of the embrittlement interaction in an endothermic occluding metal (steel)
3. The form and the location of the embrittlement interaction in an exothermic occluding metal (titanium)

Mechanical considerations will be used in conjunction with a gaseous hydrogen environment to clarify:

1. The sensitivity of the crack initiation stage of fracture to a hydrogen environment
2. The influence of a hydrogen environment on deformation associated with embrittlement
3. The combined influence of mechanical and chemical effects on embrittlement

By providing at least partial clarification of the above areas, it is hoped that important factors affecting the embrittlement of a metal by a chemical species will be elucidated so that meaningful engineering evaluations of specific systems can be conducted in the future.

KINETIC ASPECTS OF HYDROGEN-INDUCED FAILURE

SPECIFICITY OF THE HYDROGEN-METAL INTERACTION

To understand whether a particular hydrogen-metal system is susceptible to embrittlement, the specificity of the system in terms of the kinetic transport reactions must be considered with respect to the specific influence of hydrogen on the three consecutive stages of environmentally induced fracture (ref. 76) — crack initiation, subcritical crack growth, and rapid failure. The easiest of these to consider is rapid failure. There is to date no positive demonstration of an influence of hydrogen on the final, rapid fracture stage or on the critical stress intensity at which the onset of rapid fracture is observed. The most plausible explanation for this hydrogen insensitive characteristic is that hydrogen effects are governed by time dependent rate processes requiring hydrogen transport to a specific location on or within the metal, or interaction with the metal itself. This final stage of fracture occurs with such a high velocity that, under all known conditions, the controlling hydrogen rate kinetics are not competitive with these rapid crack growth rates. This is not the case, however, for the first two stages of fracture. Depending on the form of loading and the expected life of an engineering structure, hydrogen rate kinetics can become competitive and sufficient time may be available for hydrogen to influence these stages of fracture. Of these two potentially environment-sensitive stages of fracture, because of the somewhat haphazard nature of crack initiation, the subcritical crack growth stage is by far the least complex and the most easy to handle. It is for this reason that subcritical crack growth is the embrittlement parameter used in this section to investigate the specificity of the hydrogen-metal interaction.

As we have seen, the overall transport process in the transport of hydrogen from the gas phase to a location where it may interact with the metal to cause embrittlement can be extremely complex and will involve a number of elementary reaction steps. One portion of this overall transport reaction is termed chemisorption and is the process that results in the transport of a species from the gas phase to some location on the surface of the metal. In general, chemisorption is not one elementary reaction but several and can be very involved. Be that as it may, the chemisorption reaction is essential for environmental embrittlement, no matter the location or form of the embrittlement interaction. Let us consider in a cursory manner what is known of the process of hydrogen chemisorption on metal films.

The process of hydrogen chemisorption has been reviewed in some detail by Hayward and Trapnell (ref. 77). Table 1, a portion of the data reviewed, is a list of metals separated as to the speed of the chemisorption process.

1. Very fast chemisorption occurs in a few seconds and, if an activation energy is involved, it must be exceedingly small.
2. Slow chemisorption is definitely an activated process.
3. No chemisorption is where no hydrogen is adsorbed up to 0° C.

Table 1 shows that all metals that exhibit fast chemisorption are transition metals except for barium (Group IIA). The transition metals copper, silver, and gold (Group IIB) and manganese (Group VIIB) and the remaining nontransition metals that have been studied do not chemisorb hydrogen or do so very slowly. Thus, three very important engineering metals, aluminum, copper, and magnesium, do not chemisorb hydrogen, at least up to 0° C. Because chemisorption is essential to the embrittlement of a metal from the environment, it is predicted from table 1 that copper, aluminum, and magnesium should not be affected by the presence of hydrogen. It is important to realize with respect to the data of table 1, especially in those metals where chemisorption has not been observed up to 0° C, that the speed of chemisorption cannot be projected to greater temperatures. It is possible in some cases that the activation energies for chemisorption are such that it will proceed at higher temperatures, but it is equally likely in others that chemisorption is endothermic, in which case it will not occur however high the temperature. Additionally, table 1 is the chemisorption process from a molecular hydrogen gas. If atomic hydrogen is the adsorbing species, the chemisorption process may change drastically. On copper, for example, atomic hydrogen adsorbs readily at low temperatures but desorbs as molecules if the film is warmed to room temperature (ref. 78). Others have seen significant chemisorption of hydrogen atoms on copper at room temperature (ref. 79).

The purpose of this study was to consider the specificity of hydrogen embrittlement in terms of the ability of hydrogen to affect the fracture mode and fracture behavior of precracked specimens of several engineering alloys. Both a molecular hydrogen environment and a partially dissociate hydrogen environment were used as the source of the hydrogen species. The results of this study were used with those of previous studies to better establish the specificity of the hydrogen-metal embrittlement interaction.

TABLE 1.— HYDROGEN CHEMISORPTION ON METAL FILMS (REF. 74)

Very fast chemisorption	Slow chemisorption	No chemisorption up to 0° C
Ti	Mn	K
Zr	Ge	Cu
Nb		Ag
Ta		Au
Cr		Zn
Mo		Cd
W		Al
Fe		In
Co		Pb
Ni		Sn
Rh		
Pd		Mg (ref. 56)
Pt		
Ba		

Materials and procedure— The materials used in this study are given in table 2 with their nominal compositions and heat treatments. All heat treatments were performed in a vacuum furnace. For those requiring a rapid quench rate, the furnace was backfilled with argon immediately before quenching (while the specimen was kept at temperature) and then the specimen was removed and quenched in less than 2 sec.

Fracture toughness tests were conducted on precracked bend specimens loaded in three-point bending. These specimens were 1.90×10^{-2} m (0.750 in.) wide, 3.17×10^{-3} m (0.125 in.) thick. They contained a side notch plus precrack of between 7.9×10^{-4} and 1.59×10^{-3} m (0.312 and 0.0625 in.) total length. These specimens, which had a support span of 7.6×10^{-2} m (3.0 in.), obviously did not conform to the ASTM thickness guideline for plane-strain fracture toughness specimens but, since the data to be obtained were intended to be only comparative in nature, this was considered relatively unimportant. Stress-intensity values were calculated from the maximum load measured on the load-displacement record by using a fourth-degree polynomial expression for pure bending (ref. 80). The nonstandard stress-intensity values calculated in this manner are designated as K_{scg} , the stress intensity for the initiation of measurable subcritical crack growth. (When negligible subcritical crack growth occurs, as in air, K_{scg} equals the nonstandard critical stress intensity for failure, K_Q).

All tests were conducted at room temperature at a constant displacement rate, \dot{d} of 1.48×10^{-9} m/sec (3.5×10^{-6} in./sec) in a stainless-steel chamber. The chamber was evacuated by the use of zeolite-trapped mechanical pump, a titanium sublimation pump, and a sputter-ion pump to a pressure of better than 7×10^{-5} N/m² (5×10^{-7} torr) prior to backfilling with hydrogen to the desired test pressure. The hydrogen, as received, contained an active impurity level less than 100 ppm (N₂, O₂, H₂O) and was additionally purified by passing it slowly through a liquid nitrogen-chilled trap.

The hydrogen test environments were molecular hydrogen at a pressure of 90.6 kN/m² (680 torr) and an atomic-molecular hydrogen mixture at a molecular hydrogen pressure of 1.1 N/m² (8×10^{-3} torr). The selection of the latter pressure was based on results observed on AISI 4130 steel (described in the following section). The hydrogen test environment at pressures of 1.1 N/m² (8×10^{-3} torr) contained significant quantities of contaminants (of the order of 10 percent carbon monoxide and 1 percent water as determined by a residual-gas analysis sampling system made up of a small stainless-steel chamber, a controlled

TABLE 2.— ALLOYS, COMPOSITIONS, AND HEAT TREATMENTS

Alloy	Composition	Heat treatment	Yield strength, n/m ²
Molybdenum alloy (TZM)	Mo—0.5Ti—0.08Zr	As received— annealed	13.9×10 ⁸
Copper alloy (Cu—Be)	Cu—1.8Be	Solution annealed at 900° C and aged at 343° C for 4 hr	10.9×10 ⁸
		Solution annealed at 900° C and aged at 399° C for 3 hr	8.48×10 ⁸
Nickel alloy (201)	99.5 Ni	As received— annealed	1.03×10 ⁸
Nickel alloy (301)	Ni—4.37Al	As received— solution treated, quenched, and aged	11.7×10 ⁸
Aluminum alloy (7075)	Al—5.6Zn—2.5Mg— 1.6Cu	As received— solution treated, and aged	5.03×10 ⁸
Magnesium alloy (HM21A)	Mg—2Th—1Mn	As received— solution treated, cold worked, and aged	1.72×10 ⁸
Titanium alloy (6-4)	Ti—6Al—4V	Annealed at 704° C	8.96×10 ⁸
		Solution treated at 1037° C and stabilized	12.4×10 ⁸
Steel alloy (4130)	Fe—1Cr—0.2Mo— 0.30C	Oil quenched from 843° C and tempered at 250° C for 2 hr	13.9×10 ⁸
Stainless-steel alloy (310)	Fe—25Cr—21Ni	As received— annealed	3.10×10 ⁸
Stainless-steel alloy (A286)	Fe—25Ni—15Cr	As received— solution treated, quenched, and aged	8.20×10 ⁸

leak, and a quadrupole residual gas analyzer). This contamination could not be eliminated by baking the chamber, and appeared to result from displacement reactions occurring between hydrogen and contaminants on the chamber walls. Such contamination was negligible at high pressures (i.e., 90.6 kN/m^2) of hydrogen.

An atomic-molecular hydrogen mixture was created at the crack opening by the dissociation of molecular hydrogen on $5 \times 10^{-5} \text{ m}$ (0.002 in.) diameter tungsten filaments heated to approximately 2000° C . Although the presence of a hot tungsten filament on which molecular hydrogen can dissociate adds additional elementary reactions to the formation of atomic hydrogen on the crack surface, Brennan and Fletcher (ref. 81) have shown that molecular hydrogen adsorption, dissociation, and atomic hydrogen desorption occur very rapidly on a hot tungsten surface. The filament location for the test specimen is shown in figure 3. Specimen temperature was controlled with a liquid nitrogen-cooled shroud surrounding the specimen and grips and by quartz-lamp heaters placed near the specimen. Specimen temperature was monitored by the use of thermocouples welded to the specimen adjacent to the fatigue crack tip.

Results— Fracture toughness tests were conducted at a constant displacement rate at room temperature in environments of vacuum at $6.7 \times 10^{-3} \text{ N/m}^2$ (5×10^{-7} torr), of molecular hydrogen at 90.6 kN/m^2 (680 torr), and of atomic-molecular hydrogen mixtures at a molecular hydrogen pressure of 1.1 N/m^2 (8×10^{-3} torr). Table 3 is a summary of the results of this study indicating the value of K_{scg} (an average of at least two tests) observed in the three test environments for a number of alloys. Additionally, fractographic analysis was conducted on all specimens that fractured. Scanning electron micrographs of typical fracture surfaces are given in figures 4 through 12. This table and these figures show that the molybdenum alloy (TZM) exhibited a significant reduction in K_{scg} in molecular hydrogen as compared to that in vacuum (table 3); however, there was no discernible difference in the fracture surface of these specimens (fig. 4). Failure of this alloy both in vacuum and in hydrogen occurs by the brittle, cleavage mode.

The copper alloy (Cu-Be) was tested in both the underaged and fully aged conditions. Neither molecular hydrogen nor atomic hydrogen was observed to influence the fracture behavior of this alloy (table 3). The mode of failure in the three environments was identical and appeared to be a form of ductile tearing typified by lacelike-appearing dimples (fig. 5).

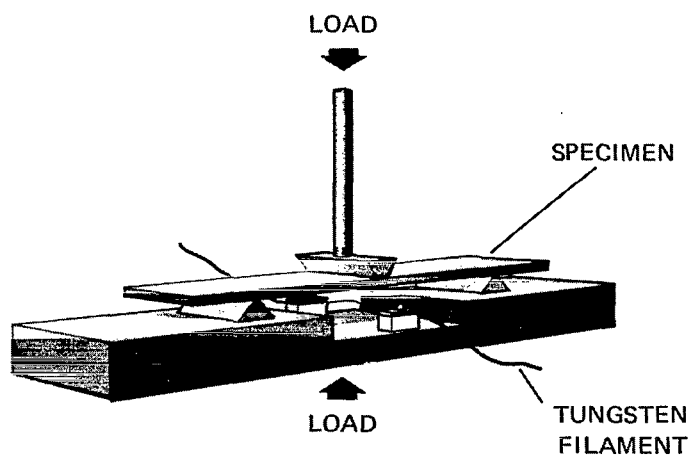


Figure 3.— Filament placement for the investigation of hydrogen embrittlement of fracture toughness specimens in the presence of atomic-molecular hydrogen.

TABLE 3.— THE EFFECT OF HYDROGEN ON THE FRACTURE BEHAVIOR
OF SEVERAL ALLOYS

Alloy	K_{scg} , MN/m ² -m ^{1/2}		
	Vacuum ($K_{scg} = K_Q$)	$P_{H_2} = 90.6$ kN/m ²	$P_{H_2} = 1.07$ N/m ²
Molybdenum alloy (TZM)	123.4	74.6	---
Copper alloy ¹ (Cu-Be)	39.3	37.6	37.5
Copper alloy ² (Cu-Be)	82.4	87.9	92.3
Nickel alloy (201)	No failure	No failure	---
Nickel alloy (301)	162.6	54.9	---
Aluminum alloy (7075)	23.5	24.6	24.6
Magnesium alloy (HM21A)	6.12	6.40	5.85
Titanium alloy ³ (6-4)	115.6	105.3	---
Titanium alloy ⁴ (6-4)	149.7	52.1	---
Steel alloy (4130)	64.0	27.3	48.8
Stainless-steel alloy (310)	No failure	No failure	No failure
Stainless-steel alloy (A286)	No failure	No failure	No failure

¹ Aged at 343° C for 4 hr

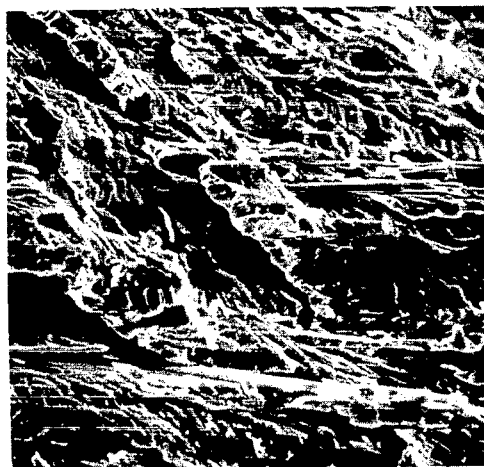
² Aged at 399° C for 3 hr

³ Annealed at 704° C

⁴ Solution treated at 1037° C and stabilized



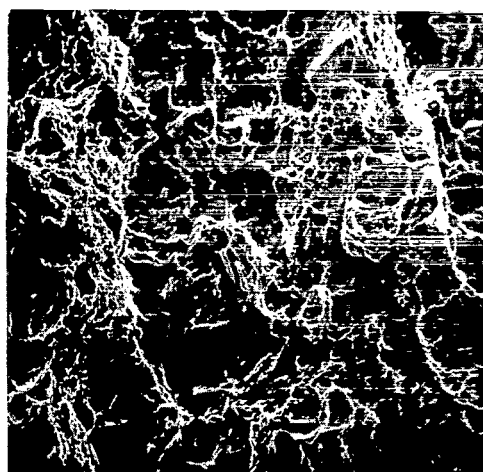
(a)



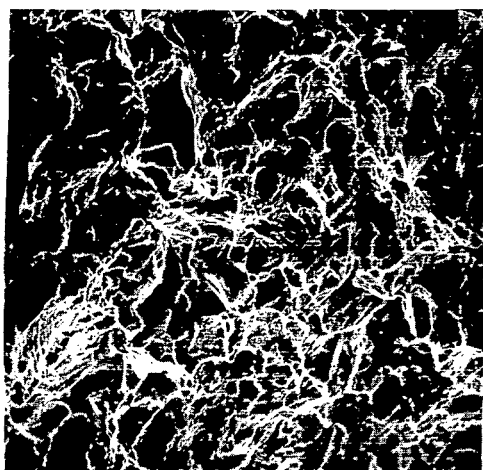
(b)

20 μm
|—————|

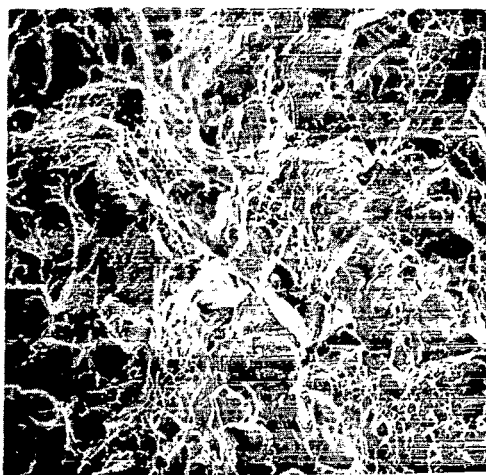
Figure 4.— SEM fractograph of the molybdenum alloy (TZM): (a) failed in vacuum,
(b) failed in molecular hydrogen.



(a)



(b)



(c)

20 μm
└───┘

Figure 5.— SEM fractograph of the copper alloy (Cu—Be) aged at 400° C; (a) failed in vacuum, (b) failed in molecular hydrogen, (c) failed in atomic-molecular hydrogen.

The pure nickel alloy (201) was found to be so ductile that the fatigue crack would not propagate to failure under the three-point bend mode of loading at the strain-rate employed (table 3); however, a small amount of crack propagation did occur ahead of the fatigue crack in both vacuum and molecular hydrogen environments. The appearance of these areas of crack growth is shown in figure 6. In vacuum the fracture surface appears ductile with substructure indicative of gross plastic deformation of the fracture surface following fracture. Similar substructure is present on the surface failed in molecular hydrogen; however, the overall appearance of the surface indicates a more brittle mode of failure with some intergranular separation and transgranular cleavage facets. The nickel alloy (Duranickel 301) is a precipitation hardening alloy and was tested in the fully hardened condition. A molecular hydrogen environment has a significant effect on this alloy with a large reduction in K_{scg} and a complete change in fracture mode. In vacuum the fracture surface of this alloy is identical to that observed in the nickel (201) alloy (fig. 6(a)); in hydrogen, however, failure occurs entirely by intergranular separation, completely void of any evidence of ductile tearing (fig. 7).

The aluminum alloy (7075), like the copper alloy, is completely unaffected by either a molecular or an atomic hydrogen environment (table 3) with failure in every case occurring by ductile tearing (fig. 8). Additionally, identical results are observed for the magnesium alloy (HM21A) (table 3 and fig. 9).

The titanium alloy (6Al-4V) is an alpha-beta alloy with the microstructure very dependent on heat treatment (ref. 82). This alloy was tested in the annealed condition, which has a microstructure of equiaxed, primary α -phase with a noncontinuous dispersion of β -phase in the α -phase boundaries. The solution-treated and stabilized structure consists of acicular α -phase platelets in prior β -phase grains with a more or less continuous β -phase separating each α -phase platelet. Table 3 shows that the annealed structure is only slightly affected by a molecular hydrogen environment whereas the solution-treated and stabilized structure is greatly affected. The fracture mode in vacuum is ductile tearing in both structures. In hydrogen the annealed structure yields a fracture that is very feathery in appearance (fig. 10) and seems to contain small cleavage facets and significant amounts of subsurface cracking — both intergranular and transgranular. In the solution-treated and stabilized structure, fracture in hydrogen appears primarily by intergranular separation (fig. 11). Additionally, this surface contains a substructure of rather evenly spaced



(a)



(b)

40 μm
|-----|

Figure 6.— SEM fractograph of the nickel alloy (201); (a) failed in vacuum, (b) failed in molecular hydrogen.



40 μm


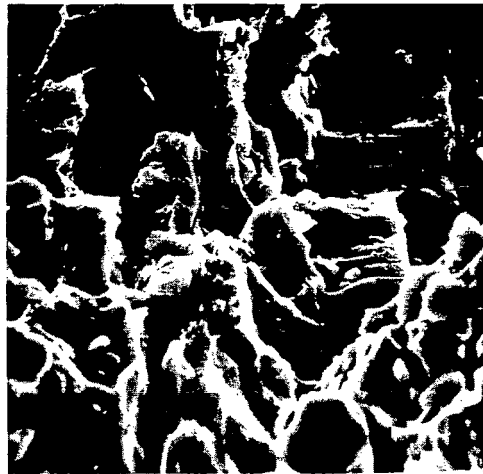
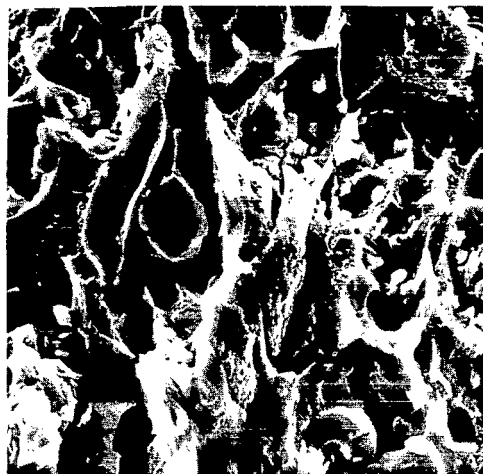
A horizontal scale bar with vertical end caps, indicating a length of 40 micrometers.

Figure 7.— SEM fractograph of the nickel alloy (Duranickel 301) failed in molecular hydrogen.



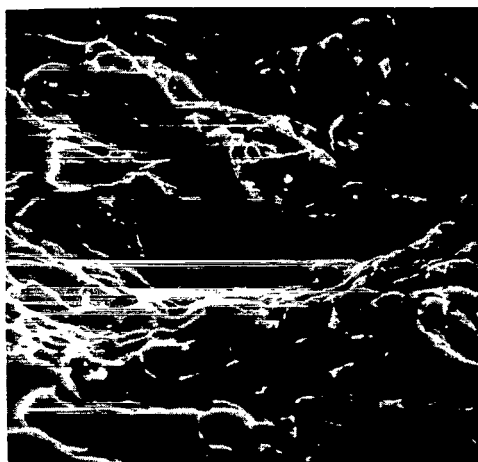
(a)



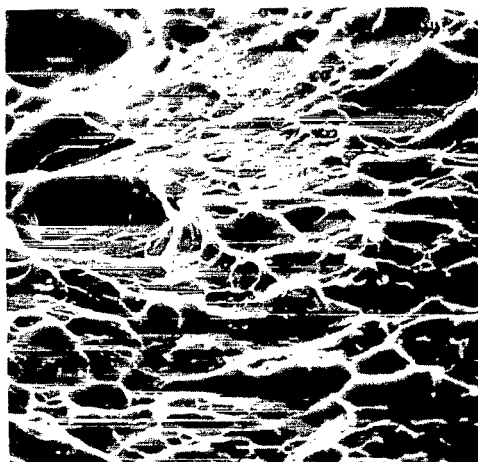
(b)

20 μm
|-----|

Figure 8.-- SEM fractograph of the aluminum alloy (7075); (a) failed in vacuum,
(b) failed in molecular hydrogen.



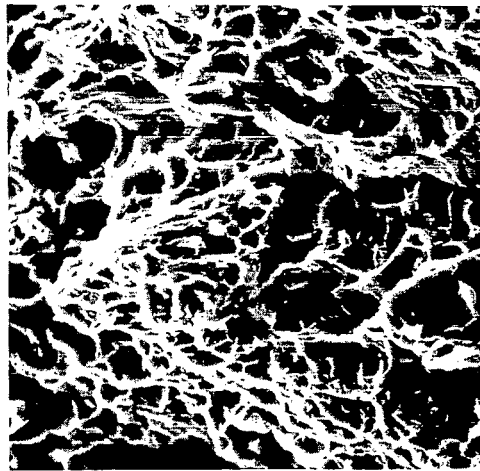
(a)



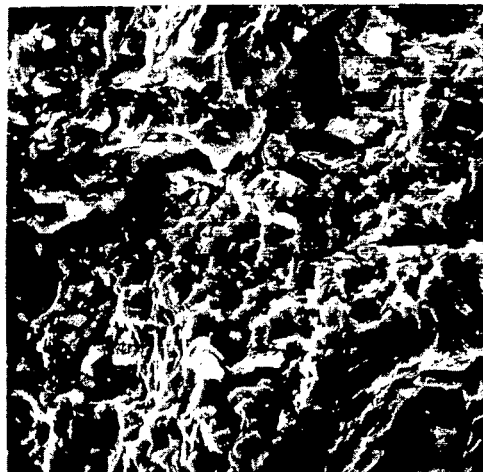
(b)

40 μm
|-----|

Figure 9.— SEM fractograph of the magnesium alloy (HM21A); (a) failed in vacuum,
(b) failed in molecular hydrogen.



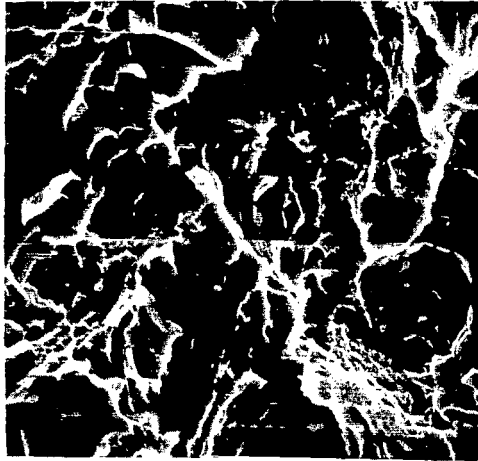
(a)



(b)

20 μm
|-----|

Figure 10.— SEM fractograph of the titanium alloy (6Al-4V) annealed at 704° C;
(a) failed in vacuum, (b) failed in molecular hydrogen.



(a)



(b)

20 μm
|-----|

Figure 11.— SEM fractograph of the titanium alloy (6Al–4V) solution treated at 1037° C;
(a) stabilized and failed in vacuum, (b) stabilized and failed in molecular hydrogen.

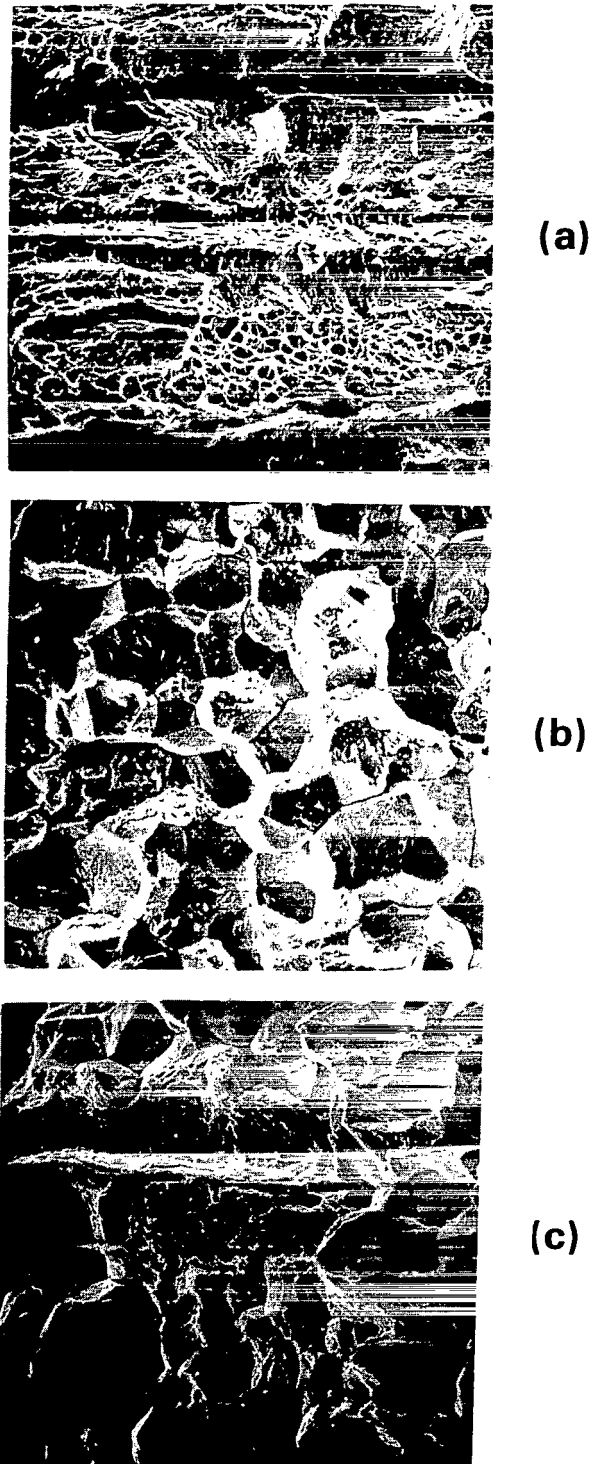


Figure 12.— SEM fractograph of the steel alloy (4130); (a) quenched, tempered, and failed in vacuum, (b) quenched, tempered, and failed in molecular hydrogen, (c) quenched, tempered, and failed in atomic-molecular hydrogen.

terrace-like steps. (The possible significance of this substructure is discussed in detail in a following section.)

The steel alloy (4130) exhibited the most striking results of all of the alloys tested. The microstructure of this alloy was tempered martensite and was significantly affected by both a molecular hydrogen and an atomic hydrogen environment (table 3). The degree of reduction in K_{scg} was most severe in molecular hydrogen. Figure 12 shows that the fracture mode in vacuum was ductile tearing, in molecular hydrogen it was entirely intergranular separation, and in atomic hydrogen it was a combination of both ductile tearing and intergranular separation. This is the first observation to indicate that a low pressure molecular hydrogen environment containing a large ratio of atomic hydrogen can significantly affect the fracture behavior of an alloy.

The stainless steel alloys (310 and A286) are very stable austenitic alloys unlike some stainless steels such as type 304, which will transform to martensite on deformation. Although these alloys are of medium strength, the fatigue crack would not propagate under the bending mode of loading in any of the environments; in fact, in all cases gross deformation occurred at the crack tip and the tip was blunted.

Discussion— In this section we will attempt to establish some order to the specificity of the hydrogen-metal embrittlement interaction in terms of the observations of this study and observations by other investigators. We will review pertinent observations made concerning the hydrogen-metal interaction in specific base-metal systems. Next, in an effort to understand the specificity of embrittlement, we will consider the susceptibility of these systems to various forms of hydrogen embrittlement in terms of what is known of the hydrogen-metal interaction.

Iron-base alloys: Iron-base alloys have microstructures made up of α -phase (bcc) and γ -phase (fcc) iron in various forms. At room temperature the α -phase is stable; however, with the correct alloy additions, primarily nickel and chromium, the γ -phase can be stabilized. Both of these phases of iron are endothermic occluders of hydrogen and form solid solutions with hydrogen with an energy of absorption of 27,200 J/mole (6,500 cal/mole) in α -iron and slightly greater in γ -iron (ref. 83). The solubility of hydrogen at 1 atm in α -iron is around 10^{-7} m³/100g at 200° C and somewhat greater in γ -iron (ref. 83). Likewise, lattice diffusion of hydrogen occurs more easily in the γ structure than in the α with the latter having a value near 10^{-8} m²/sec at 200° C (ref. 83).

Although there appears to be little significant difference between the interaction of hydrogen with the α - and γ -phases of iron, the susceptibility of these structures to hydrogen embrittlement varies greatly. Alloys having the α -type microstructures of martensite and ferrite have been found to be very susceptible to hydrogen attack (gaseous hydrogen, refs. 68-71); hydrogen-containing molecules, refs. 84-86; hydrogen in solution within the metal lattice, refs. 87-89). Failure occurs exclusively by intergranular separation (fig. 12). This behavior is contrasted with that of alloys that retain a stable austenitic (γ -phase) microstructure. These alloys appear quite immune to hydrogen attack, as demonstrated by the stainless steels of this study (table 3) and others (refs. 90, 91). If, however, the austenitic structure is not stable but transforms to martensite as the result of deformation, etc., the austenitic alloy is then susceptible to hydrogen embrittlement (refs. 92-95). There is as yet no proven explanation for this phase sensitivity of the iron-base alloys to hydrogen attack. Two possible explanations involve the difference in the form of the hydrogen interaction with the two phases or changes in the hydrogen transport reactions. Neither possibility, however, is as yet supported by differences observed in hydrogen interaction or transport.

Nickel-base alloys: Nickel has a face-centered-cubic structure and reacts very strongly with hydrogen, as do palladium and platinum (ref. 57), all three are of Group VIIB (fig. 2). Hydrogen adsorption occurs rapidly on the surface of nickel (table 1); at temperatures above 100° C, however, no physical adsorption of hydrogen appears to take place (ref. 57). Under normal conditions, hydrogen exists in the nickel lattice as a solid solution, but it has also been observed to form a hydride phase at the grain boundaries and near the surface of the metal during electrolytic charging or at high pressures (ref. 58). The solubility of hydrogen in solid solution is somewhat greater than that in α -iron and has a value of around 10^{-6} m³/100g at atmospheric pressure at 200° C with the energy of absorption being approximately 12,300 J/mole (3,000 cal/mole) (ref. 96). Lattice diffusion in nickel is on the order of 10^{-11} m²/sec at 200° C (ref. 97) or about three orders of magnitude slower than that observed in α -iron.

Nickel-base alloys, like martensitic and ferritic steels, are observed to be extremely sensitive to hydrogen attack from gaseous hydrogen (refs. 74, 98), hydrogen containing molecules in the environment (ref. 99), and hydrogen charged into the lattice (refs. 100-102). In this study it is seen that the nickel alloy (Duranickel 301) is severely

degraded by a hydrogen environment (table 3), with failure occurring by complete intergranular separation (fig. 7). Even high purity nickel (201) is affected by a hydrogen environment to some degree (fig. 6). Additionally, an interesting form of hydrogen embrittlement has been observed in nickel (ref. 58) where hydrides formed in the grain boundaries become unstable and decompose, which leads to the formation of cracks because of the high pressure that develops.

Titanium-base alloys: The reaction between hydrogen and titanium is similar to the other metals of Group IVB and VB (fig. 2), zirconium, hafnium, vanadium, columbium, and tantalum (ref. 57). These metals are exothermic occluders of hydrogen and form hydrides readily (ref. 57). Titanium has two basic lattice structures: the α -phase that is closed-packed-hexagonal and stable at room temperature and the β -phase that is face-centered-cubic and easily stabilized to room temperature. Most engineering titanium alloys have microstructures that are a mixture of the α - β phases. The two phases differ in that hydrogen forms a solid solution in α -titanium only to extremely low hydrogen concentrations before hydride is formed (ref. 103), whereas hydrogen is readily soluble in β -titanium, which it stabilizes (ref. 104). Lattice diffusion of hydrogen in α -phase titanium occurs at approximately 10^{-11} m²/sec at 200° C (ref. 105) and, by extrapolation from high temperatures, in β -phase titanium at 10^{-10} m²/sec at 200° C (ref. 105).

Embrittlement as a result of hydrogen charging has been observed in titanium (ref. 106), zirconium (ref. 43), columbium (ref. 107), tantalum (ref. 108), vanadium (ref. 109), and uranium (ref. 110). A gaseous hydrogen environment has been observed to influence the fracture behavior of titanium (ref. 74), tantalum (ref. 111), and columbium (ref. 111). Additionally, titanium is influenced by environments of hydrogen-containing molecules (ref. 112). In all forms of hydrogen embrittlement of titanium, susceptibility of embrittlement appears to be dependent on alloy microstructure. In charged hydrogen, pure β -titanium appears relatively insensitive to hydrogen (ref. 113) as does pure α -titanium (ref. 114); when the microstructure is a combination of these two phases, however, hydrogen attack is severe (ref. 106). Similar results were observed in a gaseous hydrogen environment discussed in this section and a following section in which this effect is studied extensively. In this section it was seen that the Ti-6Al-4V alloy was much more susceptible to gaseous hydrogen when the structure consisted of acicular α in a β -matrix

(fig. 11) as compared with an α -matrix with discontinuous β in the boundaries (fig. 10), table 3.

Titanium, like the other exothermic occluding metals mentioned above, forms the brittle second-phase hydride precipitate in the α -phase matrix. When present in massive quantities, this precipitate can affect the fracture behavior of the alloys. This form of embrittlement, unlike that discussed above, is most severe at high strain rates (ref. 115).

Molybdenum base alloy: The Group VB (fig. 2) metals of molybdenum, tungsten, and chromium are similar in that they are very rapid adsorbers of hydrogen (table 1) and are endothermic occluders absorbing relatively small amounts of hydrogen compared with other transition metals. The solubility of hydrogen in molybdenum is approximately 10^{-9} m³/100g at 1 atm at 200° C with an energy of absorption of around 29,300 J/mole (7,000 cal/mole) (refs. 60, 116). Diffusion of hydrogen in molybdenum occurs at a rate of 10^{-12} m²/sec (refs. 60, 116) at 200° C and is comparable to that in nickel and titanium.

The embrittlement of these alloys by hydrogen has received little attention; molybdenum, however, has been observed to be influenced by cathodically charged hydrogen (ref. 117). Additionally, hydrogen has been shown to influence plastic deformation in molybdenum by the formation of impurity atmospheres on dislocations (ref. 118). The present study appears to be the first environmental hydrogen study on these alloys. The results indicate that the molybdenum alloy (TZM) is susceptible to environmental embrittlement (table 3). The failure mode of this alloy was not influenced, as might be expected, because failure in vacuum also occurred by brittle cleavage (fig. 4). No firm conclusions should be based on this one study; nevertheless, it appears that environmental hydrogen can influence crack growth in this molybdenum alloy.

Magnesium-base alloys: The interaction of hydrogen with magnesium is similar to that with beryllium, the other Group IIA (fig. 2) metals of engineering importance. Magnesium does not interact with molecular hydrogen at room temperature. Even vaporized magnesium, which has an active surface, does not adsorb molecular hydrogen (ref. 57). Atomic hydrogen is, however, readily adsorbed on magnesium. The solubility of hydrogen in magnesium is quite large, about 2×10^{-5} m³/100g, with a slight increase with increasing temperature (ref. 119). Hydrides can be formed in magnesium only under very high pressures or by cathodically charging (ref. 57).

A number of Soviet investigators studied the influence of hydrogen on magnesium and magnesium alloys (ref. 57) and found a degrading effect only when hydrides were present because of supersaturation. Extensive embrittlement was observed in a water vapor environment as the result of crystallographic hydride precipitation (ref. 120). In the present study the crack growth characteristics of the magnesium alloy (HM21A) were not influenced by the presence of either a molecular or a partially dissociated hydrogen environment (table 3 and fig. 9). This would be expected based solely on hydrogen transport kinetics (table 1), at least in the molecular hydrogen environment.

Copper- and aluminum-base alloys: Neither copper nor aluminum adsorb molecular hydrogen at room temperature (table 1). The solubility of hydrogen in copper is fairly low with a value of the order of 10^{-9} m³/100g at 1 atm at 200° C with a heat of absorption of near 37,600 J/mole (9,000 cal/mole) (ref. 51). The solubility of hydrogen in aluminum is considerably less than in copper and is of the order of 10^{-13} m³/100g with an energy of absorption of near 83,400 J/mole (20,000 cal/mole) (ref. 121). Diffusion of hydrogen in copper (122) and aluminum (ref. 123) is nearly identical having a value of the order of 10^{-10} m²/sec at 200° C.

Hydrogen can significantly influence the mechanical properties of copper and aluminum if it exists in solution above the saturation level in the metal lattice. In both alloys supersaturated hydrogen precipitates at defects, generally grain boundaries, and forms voids. In aluminum these voids grow and cause failure by a ductile separation at the boundaries (ref. 124). In copper, however, the porosity along the grain boundaries appears to weaken the material and leads to a brittle intergranular failure (ref. 125). Copper and aluminum alloys have never been observed to be affected by a molecular hydrogen environment (refs. 74, 94, 98) with the possible exception of a study that indicates that the fatigue crack growth rate of an aluminum alloy is significantly affected by a hydrogen environment (ref. 126); however, attempts to duplicate this result have been unsuccessful (refs. 127, 128). In the present study neither a molecular hydrogen nor a dissociated hydrogen environment was observed to influence the crack growth behavior of copper (table 3 and fig. 5) or aluminum alloys (table 3 and fig. 8). Again, as with magnesium, this would be expected based on the difficulty of hydrogen chemisorption (table 1).

General remarks: Hydrogen affects the fracture behavior of all engineering metals, although for some metals this influence occurs only under very specific conditions. All

metals that are endothermic occluders of hydrogen are influenced in one way or another by the precipitation of hydrogen from the supersaturated lattice obtained by cooling a saturated lattice from elevated temperatures. In the alloys of magnesium, aluminum, and austenitic iron, this influence is not observed to be accompanied by a change in fracture mode but appears to result from porosity or void formation at defects, such as grain boundaries, with failure being by ductile separation. In metals such as α -iron, nickel, and copper, failure appears to be associated with a change in fracture mode with failure occurring by brittle intergranular separation, implying an interaction between hydrogen and the metal lattice. Table 4 is a compilation from the literature of experimental observations involving the interaction of hydrogen with several endothermic occluding metals. Each of these phenomena will be considered in an attempt to point out potential qualitative correlations to the observed hydrogen embrittlement phenomenon.

The first column of table 4 gives the observed values of equilibrium solid solubility of hydrogen in a metal under 1 atm hydrogen pressure normalized to a common temperature of 200° C. With the exception of austenitic iron, those metals that have the highest equilibrium solubility appear to be the most embrittled. Comparing molybdenum and copper may be difficult. In the present study molybdenum appeared to be embrittled by gaseous hydrogen while copper did not, although both have similar values of solubility. The insensitive nature of aluminum to hydrogen is consistent with its low solubility. The second column is a list of heats of solution of hydrogen in these metals. The heat of solution is the energy state of the hydrogen atom within the metal lattice relative to its equilibrium state as gas phase molecular hydrogen. These values could be loosely interpreted as a measure of lattice disturbance produced by the introduction of a hydrogen atom into a metal. Table 4 shows that the maximum heat of solution is observed for aluminum and the minimum for nickel, just the reverse of what is observed in terms of severity of embrittlement. Possibly a better correlation could be developed based on a parameter that is some function of both solubility and heat of solution (say solubility times heat) and interpreted as the total lattice disturbance, that is, the lattice disturbances per hydrogen atom times the number of hydrogen atoms present. Even with this, however, the insensitive character of austenitic steel to hydrogen would not be consistent with the apparent correlation.

TABLE 4.— HYDROGEN SOLUBILITY AT 1 ATM, LATTICE DIFFUSIVITY, ATOM AND SITE DIMENSIONS,
AND HEATS OF ADSORPTION AND DESORPTION OBSERVED IN SEVERAL
ENDOTHERMIC OCCLUDING METALS

Metal	Solubility			Diffusivity			Dimensional			Adsorption		Desorption	
	S _{200° C} , ppm	ΔH _{sol} , kJ/mole	Ref.	D _{200° C} , m ² /sec	Q _{Dif} , kJ/mole	Ref.	r _{ave} , pm	$\epsilon, \frac{r_i - r_{ave}}{r_i}$	Ref.	-ΔH _{chem} , kJ/mole	Ref.	Q _{des} , kJ/mole	Ref.
Iron-α	10 ⁻¹	27.2	83	10 ⁻⁸	12.1	129	82.3	0.0025	57	133.9	132	---	
Iron-γ	10 ⁻¹	22.6	83	10 ⁻¹¹	44.8	130	81.9	-.093	57	---		---	
Nickel	1	12.3	96	10 ⁻¹¹	36.0	131	91.8	.0935	57	125.5	132	83.7	134
Molybdenum	10 ⁻³	29.3	60	10 ⁻¹²	61.5	60	72.0	-.322	57	167.4	133	150.6	134
Copper	10 ⁻³	38.3	51	10 ⁻¹⁰	23.3	122	111.8	.36	57	50.2	133	64.9	135
Aluminum	10 ⁻⁷	106.3	121	10 ⁻¹⁰	41.8	123	94.2	-.202	57	---	78	---	

The third and fourth columns in table 4 list the rate of hydrogen diffusion transport and the activation energy for hydrogen diffusion, respectively. There appears to be little or no correlation between these parameters and the propensity of a metal to exhibit hydrogen embrittlement.

The next columns list the effective radius of the electron shell of hydrogen in the various metals as well as the relative differences between the effective radius of hydrogen ions and the radius of the interstices in which they are apparently located. These values were calculated by Kolachev (ref. 57) based on calculations made by Gubanov (ref. 136) using the Thomas-Fermi method of atomic radius determinations. Here too, there appears to be little correlation between these values and the observed influence of hydrogen on metals.

The two remaining data columns of table 4 list the heat of chemisorption and the activation energy for desorption relative to hydrogen and a metal surface. The meanings of these parameters as discussed by Hayward and Trapnell (ref. 77) are somewhat nebulous; however, they are related in a complex way to the character of the hydrogen-metal surface bond. Although the published data are somewhat sparse, there appears to be little correlation between the sensitivity of a metal to hydrogen embrittlement and the magnitude of these parameters.

In summary, there appears to be little correlation between the occurrence of hydrogen embrittlement in several endothermic hydrogen occluding metals and other properties of the metal related to the hydrogen-metal interaction. The best correlation appears when one considers the parameters of solubility; however, even here the correlation is not consistent for all the metals considered. In general, the parameters listed in table 4 are difficult to determine and sensitive to secondary considerations such as surface contamination and surface condition and in some cases may be questionable. Additionally, as discussed previously, embrittlement in some metals may be controlled by different kinetic reactions than other metals and thus a correlation with a common parameter may never be possible. For example, gaseous hydrogen embrittlement of copper, aluminum, and magnesium may never be observed. This must not be interpreted to mean that hydrogen cannot influence these metals, but that the transport kinetics limit the accessibility of hydrogen to these metals.

In exothermic metals such as titanium, zirconium, vanadium, and tantalum, the influence of hydrogen appears severe with failure generally associated with the formation of

a hydride. In these alloys, particularly titanium lattice transport of hydrogen seems to significantly influence embrittlement. This point will be discussed extensively later.

EMBRITTLEMENT OF AN ENDOTHERMIC OCCLUDER (STEEL)¹

The embrittling effect of hydrogen on the fracture behavior of martensitic steels is significant and has been studied extensively for several decades. In reference 138 the observed features of gaseous hydrogen embrittlement (refs. 74, 139) are compared with solution-induced hydrogen embrittlement (refs. 2, 76). It was deduced that both forms of hydrogen embrittlement may result from the same hydrogen-metal interaction; however, the overall form of the embrittlement process differs because of the transport of hydrogen to the point of hydrogen-metal interaction. In both forms of embrittlement, any one of the elementary transport reactions can control the rate of hydrogen-induced, slow crack growth under a particular set of conditions.

In reference 138 it was suggested that hydrogen-induced, slow crack growth in a quenched and tempered steel exposed to a low-pressure ($\approx 101 \text{ kN/m}^2$) molecular hydrogen environment is controlled by a heterogeneous reaction involved in the transport of hydrogen from its molecular form in the gas phase to its atomic form on the crack surface. This reaction was tentatively identified as a thermally activated chemisorption process involving a physisorbed precursor. It was further determined, by comparisons of hydrogen-induced crack growth rates and hydrogen diffusion rates, that hydrogen transport within the lattice cannot be involved in the gaseous hydrogen embrittlement process and that, therefore, the location of the hydrogen-metal interaction is at or just below the crack tip surface. If these deductions are true, additional knowledge of the kinetics of hydrogen-induced, slow crack growth in a molecular hydrogen environment does little to help understand the hydrogen-metal interaction responsible for embrittlement. Only if this rate-controlling reaction step, occurring on the crack surface, can be eliminated or accelerated can there exist a possibility of studying the kinetics of the hydrogen-metal interaction.

The objective of this portion of the investigation was to eliminate the controlling surface-reaction step involving molecular hydrogen by exposing the propagating crack to a partially dissociated hydrogen environment. It was seen in the previous section that an atomic-molecular hydrogen environment can influence the fracture behavior of a steel alloy

¹ This study has also been reported as reference 137.

(4130) (table 3 and fig. 12). Under these experimental conditions, then, a study of the effects of temperature, hydrogen concentration, etc., as well as the determination of the kinetics of slow crack growth, may yield a more definite insight as to the location and mechanism involved in the hydrogen-metal interaction of an endothermic occluder of hydrogen, steel. Additionally, such a study may serve to emphasize that hydrogen embrittlement can many times be complicated by secondary considerations, such as hydrogen transport reactions, and that specific features, such as maximum embrittlement occurring at a particular temperature, may be simply a manifestation of the transport process and not an inherent quality of embrittlement itself.

Materials and procedure – The material employed in this study was AISI–SAE 4130 steel, quenched in oil from 843° C, and tempered for 2 hours at 250° C. This treatment resulted in a steel having a hardness of Rc 47; tensile yield and ultimate strengths of approximately 1378 kN/m² (200 ksi) and 1520 kN/m² (220 ksi), respectively, and an elongation to failure of approximately 6 percent.

Two types of tests were conducted: fracture toughness tests and crack growth-rate tests. Fracture toughness tests were three-point bend tests, as discussed in the previous section. Beam displacement rate was controlled at 2.1×10^{-8} m/sec (5×10^{-5} in./min). Crack growth-rate measurements were conducted on precracked, double-cantilever beam specimens having a 1.33×10^{-3} m thickness in the plane of the propagating crack and were monitored by the use of a compliance technique previously described (ref. 138).

All tests were conducted in a stainless-steel chamber evacuated to a pressure of less than 6.6×10^{-5} N/m² (5×10^{-7} torr) prior to backfilling with hydrogen. As in the previous section, an atomic-molecular hydrogen mixture was created at the crack opening by the dissociation of molecular hydrogen on a hot tungsten filament. The filament location is shown in figure 3 for the fracture toughness tests and in figure 13 for the crack growth-rate tests. Specimen temperature was controlled by the use of a liquid nitrogen-cooled shroud and quartz-lamp heaters. Specimen temperature was monitored by thermocouples welded to the specimen adjacent to the path of the propagating crack.

Experiment and results– The experiment consisted of fracture toughness tests, crack propagation tests, and scanning electron fractography.

Fracture toughness tests: Fracture toughness tests were conducted at various temperatures in environments of air at 101 kN/m² (1 atm), molecular hydrogen near

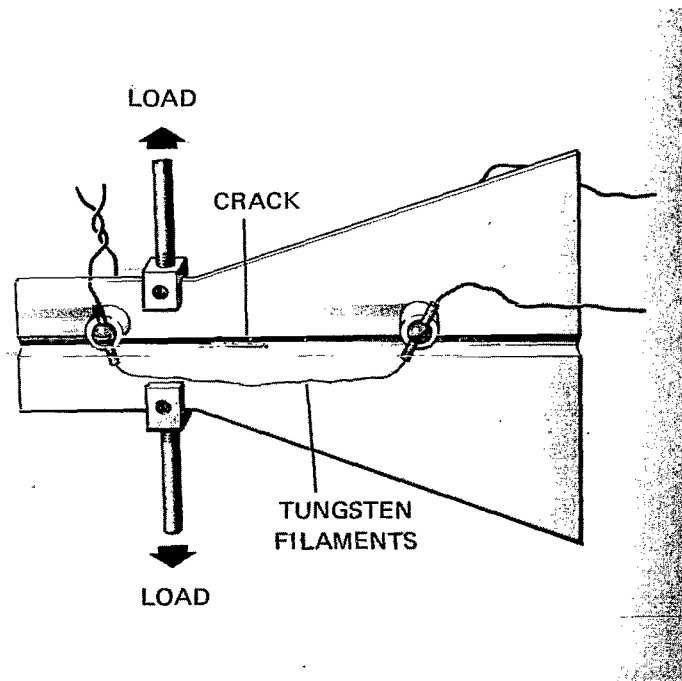


Figure 13.— Filament placement for the investigation of hydrogen-induced slow crack growth in the presence of atomic-molecular hydrogen.

101 kN/m² (1 atm), and atomic-molecular hydrogen mixtures at very low molecular hydrogen pressures to compare the magnitude of K_{scg} and its temperature dependence. Figure 14 is a plot of K_{scg} as a function of temperature observed in the various test environments and shows that K_{scg} , in an air environment, is nearly independent of temperature within the range of this study. In a molecular hydrogen environment, a severe reduction in K_{scg} occurs below 120° C, with maximum embrittlement (≈ 50 percent reduction in K_{scg}) for these test conditions occurring near room temperature. These results are nearly identical to those observed in reference 138. An atomic-molecular hydrogen environment also causes embrittlement (fig. 14) and the temperature dependence and magnitude of K_{scg} vary significantly from those observed in molecular hydrogen alone. Of great significance is the fact that embrittlement is noted at temperatures up to at least 164° C (the highest temperature of this study) in the atomic-molecular hydrogen environment.

In addition, figure 14 shows that, in an atomic-molecular hydrogen environment, K_{scg} is pressure dependent in the vicinity of room temperature. This is seen more easily in figure 15, a plot of K_{scg} as a function of molecular hydrogen pressure at 23° C observed in an atomic-molecular hydrogen environment. It is significant to note that, except for the lowest pressure, embrittlement increases as pressure decreases, with maximum embrittlement occurring near 1.1 N/m² (8×10^{-3} torr) for these test conditions.

Crack propagation tests: Crack propagation studies led to the results shown in figure 16, a plot of crack growth rate versus the reciprocal of absolute temperature for a specimen under a constant stress intensity of 45 MN/m² m^{1/2} (41 ksi-in^{1/2}) in an atomic-molecular hydrogen environment at a molecular hydrogen pressure of 1.1 N/m² (8×10^{-3} torr). All data in this figure were taken from one specimen to minimize material variations. The data in figure 16 obey, within experimental scatter, a linear relationship on this Arrhenius-type plot, indicating an exponential temperature dependence typical of a thermally activated process. A least-mean-square analysis results in an apparent activation energy of 28,500 J/mole (6,800 cal/mole) for dissociated hydrogen-induced, slow crack growth. At temperatures above approximately 30° C (other experimental conditions the same), the rate of crack growth was observed to decrease rapidly with time of exposure. After the occurrence of this so far unexplained behavior, additional crack growth at temperatures below 30° C would not occur without first reinitiating crack growth by

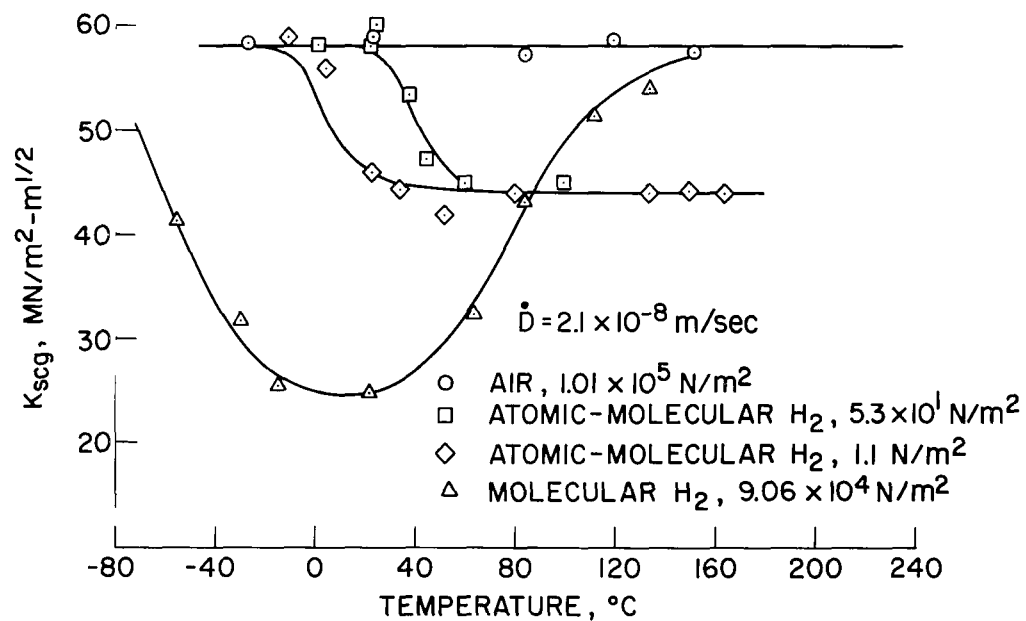


Figure 14.— The effect of temperature on K_{scg} in air, molecular hydrogen, and atomic-molecular hydrogen environments.

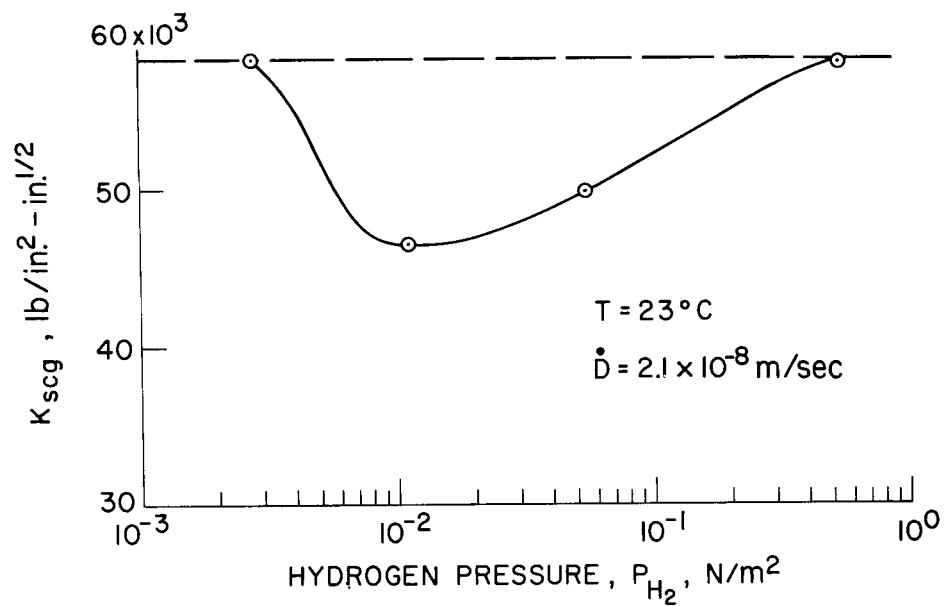


Figure 15.— Molecular hydrogen pressure dependence of embrittlement in an atomic-molecular hydrogen environment.

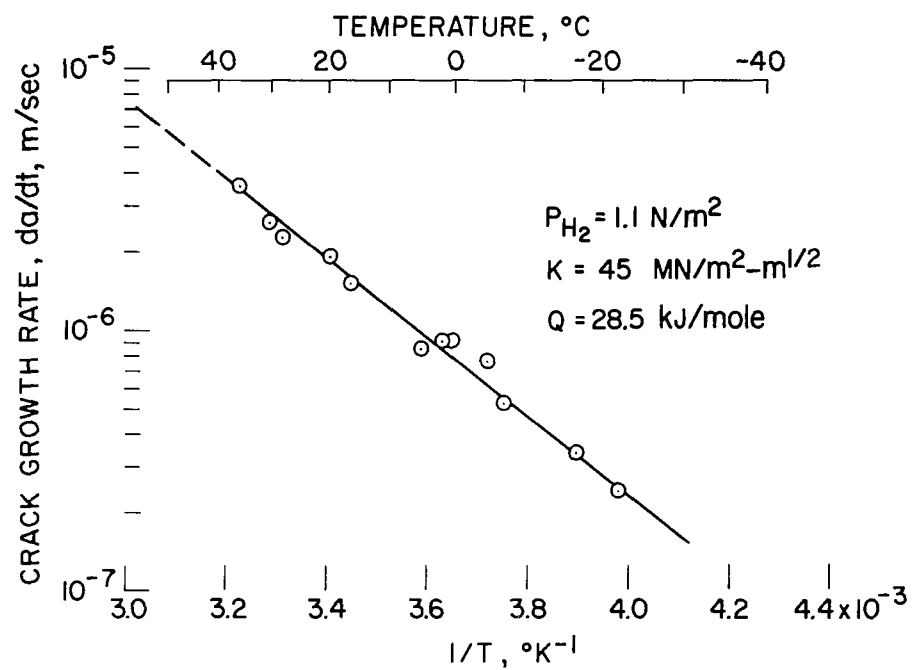


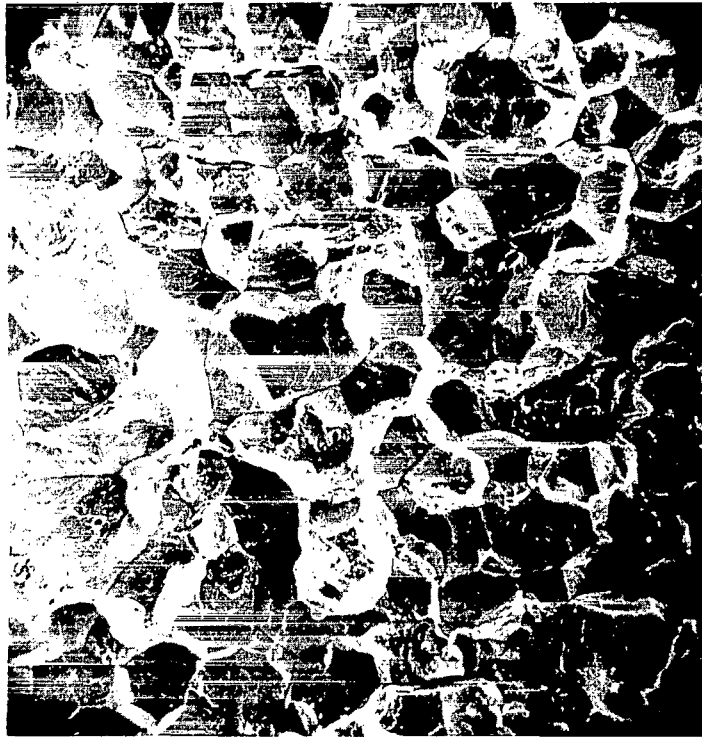
Figure 16.— Temperature dependence of slow crack growth in an atomic-molecular hydrogen environment.

cycling the applied load several times or by loading in the presence of a molecular hydrogen environment near 101 kN/m^2 (1 atm). For this reason, we have not as yet made meaningful crack propagation-rate measurements at higher temperatures, even though this is a most interesting region as indicated from the fracture toughness tests.

Scanning electron fractography: The fracture surfaces of fracture toughness specimens tested in air, molecular hydrogen, and atomic-molecular hydrogen environments were studied by scanning electron fractographic techniques. The fracture surfaces for these specimens appeared identical to those observed in a previous section for similar conditions (fig. 12), that is, a ductile tear failure in air, a complete intergranular failure in molecular hydrogen, and a mixed mode of ductile tearing and intergranular separation in atomic-molecular hydrogen. Additionally, as might be predicted from the comparable values of K_{scg} obtained, fracture toughness specimens tested in molecular hydrogen above 120°C and in dissociated hydrogen below 0°C produced ductile-tear fractographs of nearly identical appearance and similar to figure 12(a).

Unlike the fracture toughness specimens embrittled by atomic-molecular hydrogen, the fracture surface of the crack propagation test specimen failed in an atomic-molecular hydrogen environment below 30°C exhibited complete intergranular failure (fig. 17). This fracture appearance, of course, is identical to that observed in the fracture toughness specimens tested in a molecular hydrogen environment (fig. 12(b)).

Discussion— Embrittlement of a metal in a gaseous hydrogen environment must involve the transport of hydrogen to some critical location on or near the metal surface or well within the metal lattice. The equation that describes the overall transport rate can take any number of forms depending on whether the elementary reactions are opposing, equation (11); consecutive, equation (14); or parallel, equation (16). In reference 138 it was speculated that the controlling reaction step for hydrogen-induced, slow crack growth in molecular hydrogen is an elementary reaction occurring consecutively, equation (14). If this is the case, then the elimination in this study of the heterogeneous reaction involving molecular hydrogen as the slow reaction step in the overall transport process should result in: (1) a change in the molecular hydrogen pressure dependence of embrittlement; (2) a substantial increase in the rate of slow crack growth over what would be expected if the environment did not contain atomic hydrogen; and (3) an alteration in the form of the



40 μm
|————|

Figure 17.— SEM fractograph of a crack propagation specimen failed below 30° C in an atomic-molecular hydrogen environment at a molecular hydrogen pressure of 1.1 N/m².

temperature dependence of embrittlement (a change in the observed kinetics for hydrogen-induced, slow crack growth).

The results of the present study indicate that the heterogeneous molecular hydrogen reaction no longer controls slow crack growth in the presence of an atomic-molecular hydrogen environment. Hydrogen-induced, slow crack growth in the presence of a molecular hydrogen environment was observed to obey the relation (ref. 138):

$$\dot{R} = C_3 \left[\frac{C_4 P T^{-1/2} \exp(-\Delta H/RT)}{\sigma_0 + C_4 P T^{-1/2} \exp(-\Delta H/RT)} \right] P^{1/2} \exp \left(\frac{E_m}{RT} \right) \quad (28)$$

where $-\Delta H$ is the heat of molecular hydrogen adsorption, E_m is the energy of hydrogen adatom migration, P is molecular hydrogen pressure, T is absolute temperature, R is the gas constant, σ_0 is the total number of initial adsorption sites, and C_3 and C_4 are constants defined by the experiment. Figure 15 shows that embrittlement in atomic-molecular hydrogen first increases and then decreases with decreasing molecular hydrogen pressure, exhibiting a maximum near 1.1 N/m^2 (8×10^{-3} torr). This would not be expected if the heterogeneous molecular hydrogen reaction were controlling slow crack growth, as defined in equation (28). In an atomic-molecular hydrogen environment, on the other hand, the flux of atomic hydrogen at the crack tip would be expected to exhibit a maximum at some pressure near 1.1 N/m^2 (8×10^{-3} torr) (ref. 140) – the pressure at which the mean free path for molecular hydrogen equals approximately 1 cm (the specimen-filament distance). At lower pressures, the flux of atomic hydrogen at the crack is decreased because fewer hydrogen molecules strike the hot tungsten filament than at higher pressures; at higher pressures, the flux at the crack is decreased because of prior collisions of the atomic hydrogen with hydrogen atoms and molecules because of a shortened mean free path.

As would be expected if a reaction involving molecular hydrogen no longer controlled the embrittlement process, significant embrittlement was observed in atomic-molecular hydrogen at very much lower pressures than would occur in molecular hydrogen alone. For comparison, figure 18 shows hydrogen-induced, slow crack growth rates observed in the presence of atomic-molecular hydrogen at 1.1 N/m^2 (8×10^{-3} torr) molecular hydrogen (fig. 16) with those expected from equation (28), assuming only molecular hydrogen to be

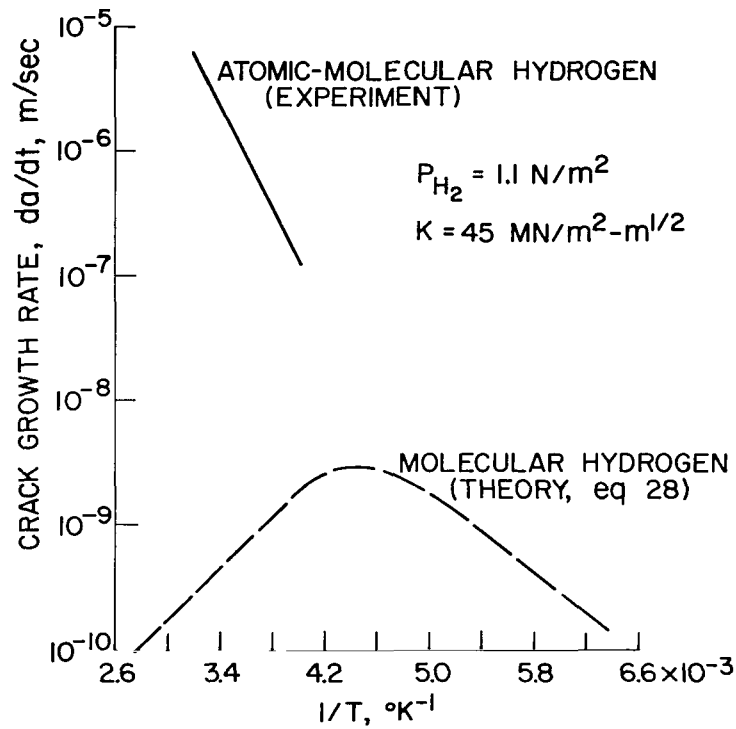


Figure 18.— Temperature dependence of slow crack growth in atomic-molecular hydrogen compared with that predicted from equation (28) for a molecular hydrogen environment at the same pressure.

present at this pressure. At the temperatures of the experiments (fig. 18), crack growth rates in atomic-molecular hydrogen were orders of magnitude faster than would be expected if atomic hydrogen was not present. Also, it is enlightening to consider the quantity of atomic hydrogen available to cause such hydrogen-induced, slow crack growth. As a maximum, the atomic hydrogen pressure at the crack opening can only be of the order of the molecular hydrogen gas pressure. In reality, however, considering the kinetics of dissociation on hot tungsten (ref. 81), the mean free path at these molecular hydrogen pressures (ref. 140), the location and configuration of the filament and crack, the instability of dissociated hydrogen, etc., the effective atomic hydrogen pressure will most probably be several orders of magnitude less than the molecular hydrogen pressure so it is estimated very roughly, based on geometrical considerations alone, to be of the order of $1.3 \times 10^{-3} \text{ N/m}^2$ ($1 \times 10^{-5} \text{ torr}$) or less at the molecular hydrogen pressure of 1.1 N/m^2 ($8 \times 10^{-3} \text{ torr}$).

Considering the temperature dependence of embrittlement, the fracture toughness studies (fig. 14) show that a drastic change in form from that found in molecular hydrogen occurs when atomic hydrogen is present in the molecular hydrogen environment. In 90.6 kN/m^2 (680 torr) molecular hydrogen, embrittlement is maximal near room temperature and decreases as the temperature is raised or lowered. A change in fracture mode also occurs with temperature, consistent with observed K_{scg} , from nearly total intergranular failure at room temperature (fig. 12(b)), mixed mode in the transition regions, and ductile tear at low and high temperatures (fig. 12(a)). These observations agree with the results of reference 138. In atomic-molecular hydrogen at 5.3×10^1 and 1.1 N/m^2 (4×10^{-1} and $8 \times 10^{-3} \text{ torr}$) (fig. 14), an embrittlement maximum is not observed within the temperature range of this study; instead, a brittle-to-ductile transition occurs with its temperature of transition dependent on hydrogen pressure – it is displaced to lower temperatures with increased atomic hydrogen concentration in the atomic-molecular environment. Unlike what was observed in molecular hydrogen at 90.6 kN/m^2 (680 torr), atomic-molecular hydrogen resulted in only a partial change in fracture mode of the fracture toughness specimens. At low temperatures and high values of K_{scg} , the fracture surface exhibited a ductile-tear appearance similar to figure 12(a); at high temperatures, however, the fracture surface never gained the total intergranular appearance observed in molecular hydrogen but remained as mixed mode failure (fig. 12(c)), showing only small areas of intergranular failure. It is believed that the lesser degree of embrittlement observed in the

fracture toughness studies in atomic-molecular hydrogen, compared to that observed in 90.6 kN/m² (680 torr) molecular hydrogen (fig. 12(b)), is the result of the experimental conditions of this study. This conclusion is supported by the inconsistencies observed between the fracture toughness and crack growth-rate portions of the study. Unlike the fracture toughness specimens, the fracture appearance of hydrogen-induced, slow crack growth in atomic-molecular hydrogen was totally intergranular below 30° C (fig. 17) and was nearly identical in appearance to the surface of the fracture toughness specimen exhibiting maximum embrittlement in molecular hydrogen (fig. 12(b)). Above 30° C, crack growth rate was observed to decrease with time and the fracture mode changed from intergranular to mixed mode failure. Possible explanations for these anomalous behaviours might lie in the inherent instability of atomic hydrogen, which recombines to its molecular form by means of three-body collisions (ref. 77) or the effect of contaminants present at these low molecular hydrogen pressures (ref. 75). Both explanations might be affected by numerous experimental parameters such as crack configuration and testing mode.

The forms of the temperature dependence of embrittlement (fig. 14) and slow crack growth rate (fig. 16) in the presence of atomic-molecular hydrogen suggest that the controlling reaction within this temperature range is a simple thermally activated elementary reaction involving atomic hydrogen. In molecular hydrogen the temperature dependence is more complex (eq. (28) and fig. 14) and involves control by more than one elementary reaction. From figure 16, assuming an equation of the Arrhenius form (eq. (19)), the activation energy for hydrogen-induced, slow crack growth was determined to be 28,500 J/mole (6,800 cal/mole). In an effort to establish a plausible elementary reaction controlling crack growth in atomic-molecular hydrogen, the overall transport reaction will be considered and this energy will be compared to known, possible, elementary hydrogen-transport reactions.

For comparison, a very much simplified schematic illustration of possible elementary reactions involved in hydrogen transport is shown in figure 19(a) for a molecular hydrogen environment (the conditions of reference 138 and in figure 19(b)) for an atomic-molecular hydrogen environment (the conditions of this study). It can be speculated that the difference between these two overall reactions is that in molecular hydrogen, molecular hydrogen adsorption and dissociation is involved, whereas in atomic hydrogen, the hydrogen atom can directly chemisorb on the metal surface. Comparing the kinetics of the elementary

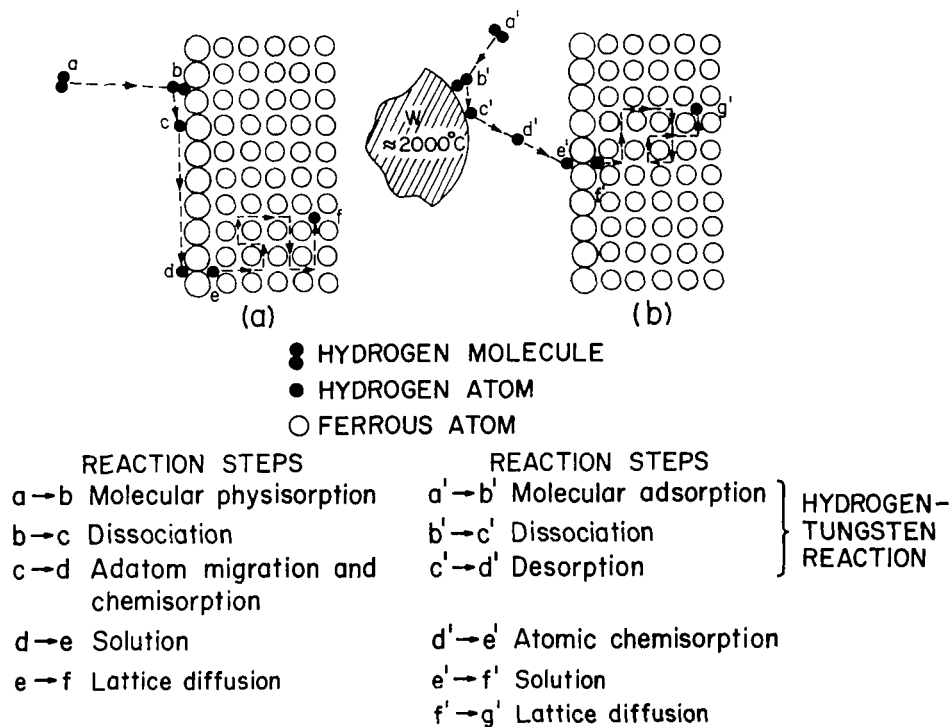


Figure 19.— Possible reaction steps involved in the overall transport of hydrogen to the site of the hydrogen embrittlement interaction; (a) transport from a molecular hydrogen environment, (b) transport from an atomic hydrogen environment.

transport reactions in atomic hydrogen (fig. 19(b)) with those observed for hydrogen-induced, slow crack growth (fig. 16), the reactions occurring on the tungsten filament and gas phase migration of atomic hydrogen can be eliminated because in the former the filament temperature was kept constant while in the latter the pressure was kept constant throughout the experiments. Additionally, the chemisorption of atomic hydrogen can be eliminated since this reaction is very rapid (ref. 141) on metals and would involve an exothermic heat of reaction as do other atomic hydrogen chemisorption reactions (ref. 79). The two remaining reactions are the hydrogen solution reaction (the reaction by which hydrogen is dissolved into an interstitial site in the ferrous lattice) and lattice diffusion of hydrogen. A study² of hydrogen transport kinetics in quenched and tempered AISI-SAE 4130 steel with the same heat treatment as the material of the present study found that the activation energies for gas-phase permeation and lattice diffusion were 35,000 and 7,900 J/mole (8,400 and 1,900 cal/mole), respectively, with a resulting activation energy for absorption (solution) of 27,200 J/mole (6,500 cal/mole). From these results, if concentration gradient diffusion were involved (eq. (26)) the activation energy for crack growth should be 35,000 J/mole (8,400 cal/mole), which is not the case. We conclude then that the solution reaction is the elementary reaction controlling slow crack growth. If this is the case, the hydrogen-lattice interaction resulting in embrittlement must be located just below the crack tip and not well within the metal lattice, since diffusion transport in the lattice (shown to be a slower reaction than the other reaction steps in these hydrogen and stress gradients, ref. 138) cannot be involved.

The exact elementary reaction cannot be concluded unequivocally even though, using the rationale of the above discussion, the hydrogen-metal embrittlement interaction is isolated to a location near the tip of the crack and the correlation between the activation energies for crack growth in atomic-molecular hydrogen and the hydrogen solution reaction is excellent. Oriani³ has put forth a valid criticism of this interpretation of the exact meaning of the energy for solution as determined in a permeation experiment and claims that this is not an activation energy for a reaction but rather a heat of solution resulting

²Unpublished work "Hydrogen Permeation and Diffusion in 4130 Steel and α -Iron," by Howard G. Nelson.

³Letter to H. G. Nelson from R. A. Oriani, United States Steel Corp., Bain Laboratory for Fundamental Research, Monroeville, Pa., Sept. 18, 1970.

from thermodynamic equilibrium between hydrogen in the gas phase and hydrogen within the metal lattice. This may be the case, but there are numerous examples where the heats of solution cannot be explained by thermodynamic equilibrium (refs. 60,142). The hydrogen transport process is too complex to unequivocally identify an energy with a particular elementary reaction so we can only conclude that the energies for the two particular processes are similar (crack growth and solution) and thus can be controlled by the same elementary reaction. In both cases this reaction is a surface or near surface associated process.

EMBRITTLEMENT OF AN EXOTHERMIC OCCLUDER (TITANIUM)⁴

Titanium, like zirconium and other metals previously discussed, differs from steel in that titanium is an exothermic occluder of hydrogen, which can react with titanium to form a hydride phase. In α -titanium this phase is stable at very low hydrogen concentrations, even at room temperature. The dispersed, stable, hydride phase is accepted by most investigators to be the cause of at least one form of hydrogen embrittlement observed in α - β titanium alloys, that is, high strain-rate, or, impact hydrogen embrittlement (ref. 144). A second form of hydrogen embrittlement, known as slow-strain-rate embrittlement, has also been attributed by some to the presence of a hydride phase (ref. 144); however, this form of embrittlement in many respects resembles the hydrogen-induced cracking observed in endothermic occluders (steel), and has thus been attributed by others (ref. 145) to the presence of nascent hydrogen in the titanium lattice.

A gaseous hydrogen environment can influence the fracture behavior of titanium alloys (ref. 74); the degree of susceptibility being dependent on the form of the α - β microstructure (table 3 and figs. 10 and 11). The objective of this portion of the present study was to consider more fully the effects of variations in the α - β microstructure on the susceptibility to and severity of environmental hydrogen embrittlement of an α - β titanium alloy. These observations were correlated with potential elementary hydrogen transport reactions in an effort to qualitatively identify the reactions controlling embrittlement, as well as the location of the embrittlement interaction. Additionally, such a study should serve to elucidate the form of slow-strain-rate embrittlement, that is, whether the formation of a hydride phase is involved.

⁴Portions of this study have been reported in reference 143.

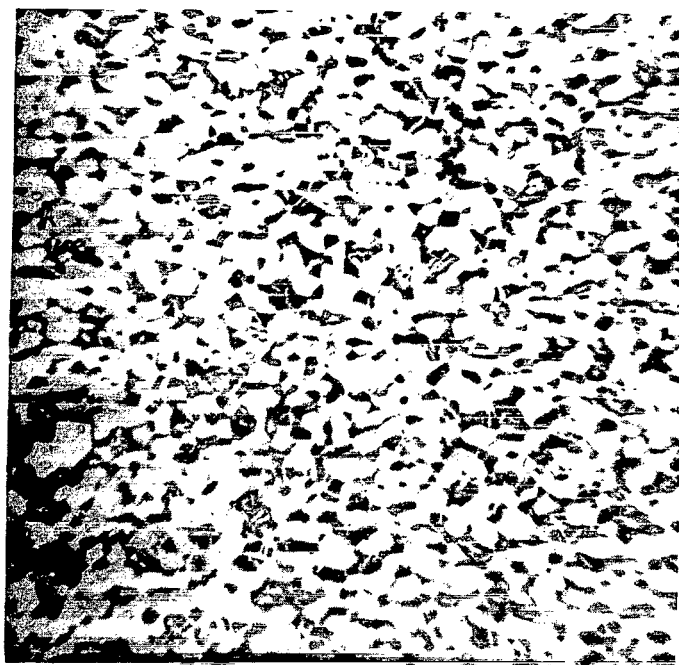
Materials and procedure— The material used in this study was commercially obtained Ti–6Al–4V alloy received in the mill-annealed condition. Prior to testing, all specimens were either solution treated at 774° C for 40 min, water quenched, and aged at 510° C for 12 hr; or solution treated at 1037° C for 40 min, stabilized at 704° C for 1 hr and 593° C for 1 hr, and air cooled.

Test specimens and procedure are as have been described. Fracture toughness tests were conducted on precracked bend specimens that were loaded in three-point bending (fig. 3). The nonstandard stress-intensity values were calculated and designated K_{scg} . Crack growth-rate measurements were conducted on precracked, tapered, double-cantilever beam (TDCB) specimens (fig. 13) and the rate of crack propagation was monitored by the use of a compliance technique.

All tests were conducted in a stainless-steel chamber that could be evacuated to a pressure of better than 6.6×10^{-5} N/m² (5×10^{-7} torr) prior to backfilling with hydrogen to the desired test pressure. The fracture toughness tests were conducted at a constant displacement rate of 8.9×10^{-8} m/sec (3.5×10^{-6} in./sec).

Experiments and results— The microstructures resulting from the two heat treatments employed in this study are shown in figure 20. The low-temperature solution treatment and age (fig. 20(a)) resulted in primary α -phase, equiaxed grains forming a continuous matrix with the retained β -phase finely dispersed in the α boundaries. The solution treatment that was well into the β -field followed by a stabilization (fig. 20(b)) resulted in a structure of coarse acicular α -phase, that is, transformed α -platelets in a β -matrix.

Fracture toughness tests: Fracture toughness tests were conducted on specimens at various hydrogen pressures ranging from 90.6 kN/m² (680 torr) to 1.3 N/m² (1×10^{-2} torr). Figure 21 shows the results of these tests where embrittlement, as defined by the ratio of K_{scg} in hydrogen to K_Q in air, is plotted as a function of the pressure of the hydrogen environment. At the constant displacement rate of these tests (8.9×10^{-8} m/sec (3.5×10^{-6} in./sec)), hydrogen at a pressure near 1 atm embrittles both structures, but has a greater effect on the Ti–6Al–4V alloy with an acicular α microstructure than on that with an equiaxed, primary α microstructure. Additionally, as the hydrogen pressure is decreased, the degree of embrittlement observed in the specimens having an acicular microstructure is decreased until, at a hydrogen pressure of approximately 1.3 N/m² (1×10^{-2} torr) no embrittlement is observed. In contrast with these observations, the degree



(a)



(b)

10 μ m
H

Figure 20.— Representative microstructures of the titanium alloy (6Al-4V): (a) solution treated at 774° C for 40 min, water quenched, and 510° C age for 12 hr, (b) solution treated at 1037° C for 40 min, stabilized at 704° C for 1 hr and 593° C for 1 hr, and air cooled. Kroll's etch.

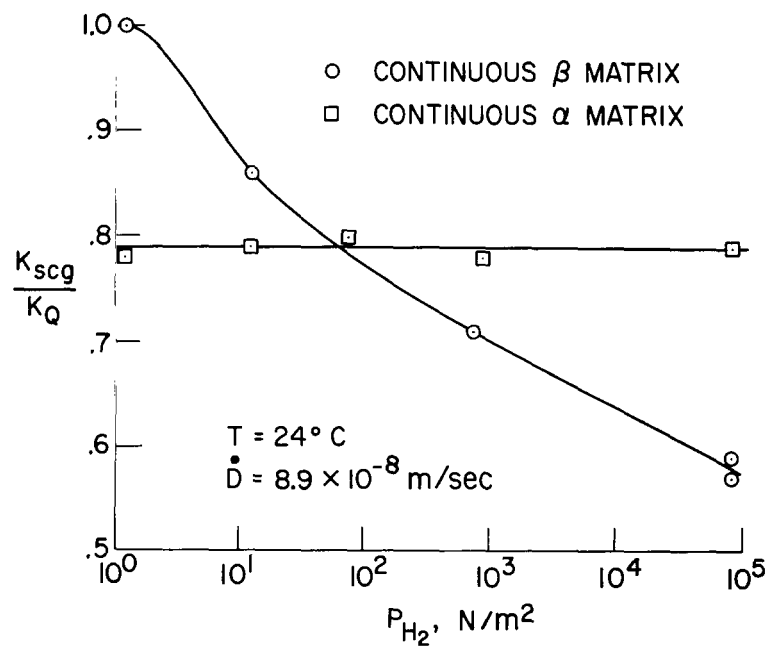


Figure 21.— Environmental hydrogen embrittlement of the titanium alloy (6Al-4V) as a function of hydrogen pressure.

of embrittlement in specimens with a primary α microstructure appears to be unaffected by a decrease in the environmental hydrogen pressure down to at least 1.3 N/m^2 (1×10^{-2} torr), the lowest pressure of this study.

The influence of test displacement rate on the severity of embrittlement (K_{scg}/K_Q) observed in specimens having the two different structures was studied at a constant hydrogen pressure of 90.6 kN/m^2 (680 torr). Figure 22 shows the results of this study. As is seen for a given microstructure, there exists a large influence of displacement rate on the severity of embrittlement with severity increasing with decreasing displacement rate. Further, the microstructure characterized as having a continuous β matrix (i.e., the acicular α structure) is more severely embrittled for a given displacement rate; if the displacement rate were reduced sufficiently, however, it appears that the microstructure of fine equiaxed α without the continuous β network would also exhibit severe embrittlement.

The microscopic fracture path of hydrogen-induced slow crack growth was also investigated in specimens having both types of microstructures tested at a constant displacement rate of $8.9 \times 10^{-8} \text{ m/sec}$ ($3.5 \times 10^{-6} \text{ in./sec}$). In specimens having an equiaxed primary α microstructure, growth appeared to be primarily transgranular through the α -phase grains with some intergranular growth present at all pressures investigated. In specimens having an acicular α microstructure, hydrogen pressure was observed to have an effect on microscopic fracture path. Figure 23 shows typical subsurface cracks observed in acicular specimens failed in hydrogen at 90.6 kN/m^2 (680 torr) (fig. 23(a)) and at $1.3 \times 10^2 \text{ N/m}^2$ (1 torr) (fig. 23(b)). At the higher hydrogen pressure, cracking occurs in an intergranular manner along prior β and transformed α platelet boundaries. At the lower hydrogen pressure, cracking is primarily transgranular through the prior β grains and across the transformed α platelets.

Crack propagation tests: Hydrogen-induced, slow crack growth was studied from -45° C to 80° C to establish the controlling reaction kinetics of this rate process. Figure 24 is a plot of crack growth rate versus the reciprocal of absolute temperature obtained from the TDCB-type specimen having an acicular microstructure. Crack growth rate increases with increasing temperature from -45° C to 23° C and then appears to remain constant. Scanning electron fractography was conducted along the fracture surface. At the lower temperatures the fracture was macroscopically flat with failure occurring by intergranular

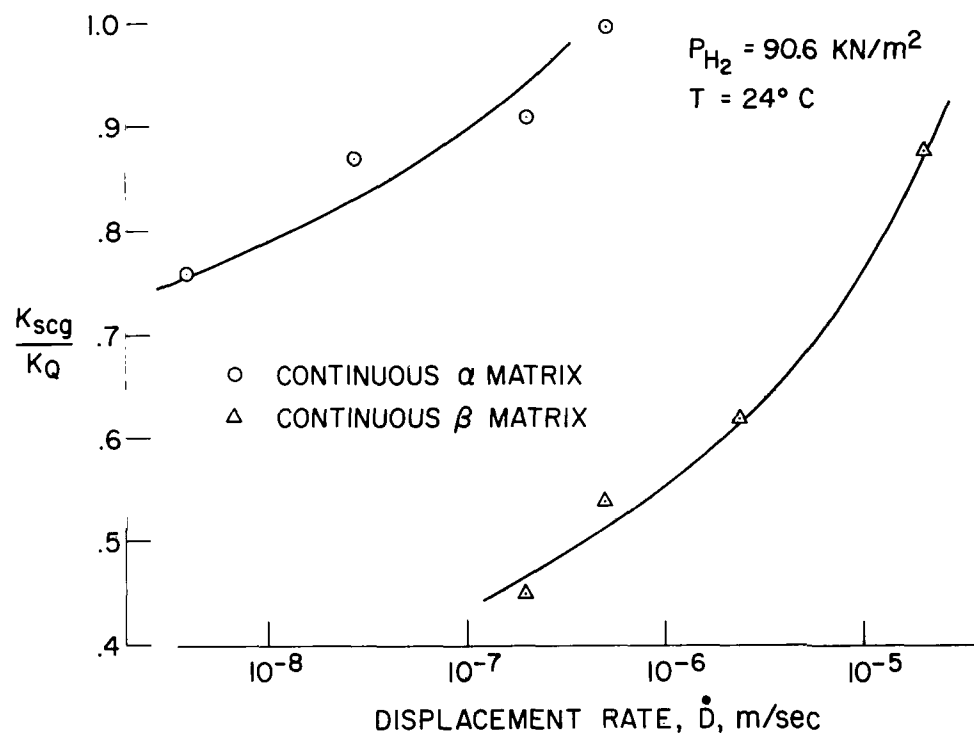
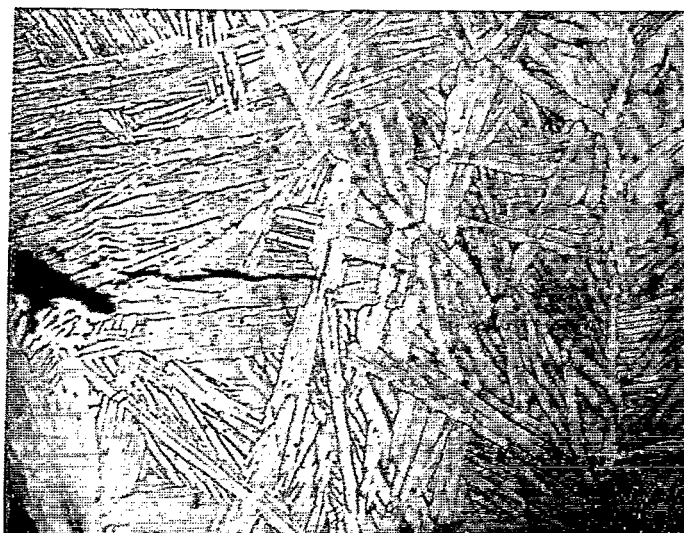


Figure 22.— Environmental hydrogen embrittlement of the titanium alloy (6Al-4V) as a function of test displacement rate at a constant hydrogen pressure.



(a)



(b)

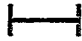
20 μm


Figure 23.— Microscopic hydrogen-induced cracking observed in the titanium alloy (6Al-4V) having an acicular α -phase microstructure; (a) tested at a hydrogen pressure of $9.06 \times 10^4 \text{ N/m}^2$, (b) tested at a hydrogen pressure of $1.3 \times 10^2 \text{ N/m}^2$. Kroll's etch.

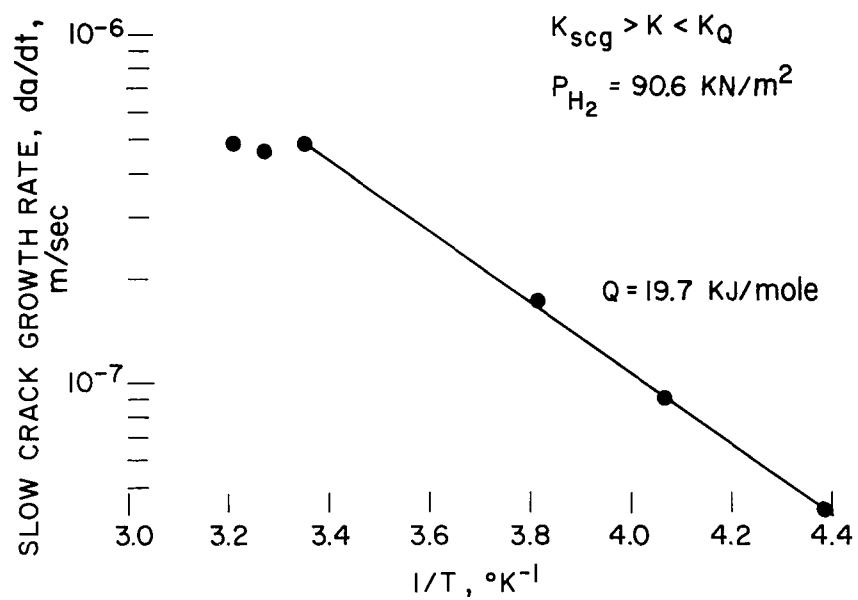


Figure 24.— Temperature dependence of slow crack growth in the titanium alloy (6Al–4V) having an acicular α -phase microstructure.

separation, similar to figure 11(b). At temperatures near room temperature failure continued intergranular; however, severe macroscopic crack branching occurred. Such crack branching invalidates growth rate measurements so observed rates above 23° C will not be considered. Employing the Arrhenius type analysis (eq. (19)) from -45° C to 23° C, assuming a thermally activated rate process, yields an activation energy of 19,700 J/mole (4,700 cal/mole).

Similar slow-crack-growth-rate measurements were attempted in TDCB specimens having a primary equiaxed α -phase microstructure. Such attempts were totally unsuccessful because of the severe crack branching that occurs in this microstructure at all temperatures investigated.

Discussion— The interdependence between the experimental parameters of time (displacement rate), temperature, pressure, and microstructure, and the severity of embrittlement comes about through the involvement of these parameters in the overall transport reactions or interaction process. Considering the titanium system, the hydrogen transport processes are basically the same as those involved in the embrittlement of steel and will include molecular hydrogen adsorption on the metal surface, hydrogen dissociation, and others, depending on the location of the embrittlement interaction. These processes are, in general, thermally activated involving a linear dependence on time, an exponential dependence on temperature, a power dependence on hydrogen pressure, and possibly some direct dependence on the metal's microstructure. The latter dependence is particularly true if the embrittlement reaction occurs well within the metal lattice where hydrogen diffusion must be an elementary reaction step. Unlike steel, however, hydrogen can interact with α -titanium exothermally and form a stable titanium-hydride phase. This phase is extremely brittle and its presence in the titanium matrix is the basis of many theories of hydrogen embrittlement of titanium (ref. 144).

From the above considerations we are able to qualitatively consider the overall process of environmental hydrogen embrittlement of the Ti-6Al-4V alloy. This alloy was found to be susceptible to embrittlement in both heat-treated conditions with severity of embrittlement strongly dependent on alloy microstructure, displacement rate, and hydrogen pressure. Specifically, at a constant displacement rate the equiaxed α microstructure was found to be less susceptible to embrittlement in hydrogen at a pressure near 1 atm than the acicular α microstructure (fig. 22). Additionally, in the equiaxed microstructure, severity

of embrittlement was found to be independent of pressure; whereas in the acicular microstructure it was dependent on pressure (fig. 21). It is emphasized that the primary difference between these microstructures is that in the equiaxed structure, the α -phase is continuous and in the acicular the β -phase is continuous.

The extreme dependence of environmental-hydrogen embrittlement on the form of the α - β microstructure suggests that hydrogen transport within the metal lattice is involved in the embrittlement process, at least for these structures containing a β -matrix. From information available in the literature, it has been established that at room temperature hydrogen transport in β -phase titanium is several orders of magnitude more rapid than in α -phase titanium (ref. 146). These relative transport rates can explain the data of figure 22 where it is shown that the displacement-rate (time) required to observe a given degree of embrittlement at a constant pressure is several orders of magnitude slower for the microstructure having a continuous α -matrix than for the microstructure having a continuous β -matrix. The continuous β -matrix appears to act as a "short-circuit" transport path that allows more hydrogen to get to a given point within the metal lattice in a given time. As the environmental hydrogen pressure is decreased, the hydrogen concentration near the surface in the β -phase is lowered, concentration-gradient-induced diffusion in the β -phase is decreased, and embrittlement becomes pressure dependent (fig. 21).

Because hydrogen transport within the titanium lattice appears to be involved for microstructures having a β -matrix, the location of the embrittlement interaction must be within the metal ahead of the crack tip. This deduction, together with the intergranular failure mode observed in this microstructure, agrees with the embrittlement theory of Craighead *et al.* (ref. 106) for hydrogen-charged α - β titanium alloys. These authors put forth the idea that hydrogen within the β -phase segregates at the α / β boundaries and results in embrittlement characterized by intergranular separation. The exact form of the embrittlement interaction occurring at the α / β interface is unclear; however, embrittlement as a result of hydride formation has been demonstrated (ref. 147) as one possible mode. The fractographic observations on the specimens having an α acicular microstructure lend support to the idea of intergranular failure by the brittle failure of a hydride film (fig. 20(b)). In this microstructure the fracture surface always contains a terrace-like substructure that can easily be interpreted as stepwise crack growth by the formation and rupture of a brittle hydride film (ref. 148).

For the microstructure having a continuous α -matrix (equiaxed α), cracking undoubtedly occurs along α/β boundaries in a manner similar to that described for β -matrix material; however, because of the relatively small volume fraction of β -phase and the discontinuous nature of the α/β boundaries, this mode of cracking does not contribute significantly to either the mechanical behavior or fracture appearance of α -matrix materials. In these microstructures, the type of hydrogen-induced cracking that results in the observed embrittlement is transgranular in nature and may result from an interaction between α -titanium and hydrogen either at the surface or within the α -grains. In any case the hydrogen must interact directly with the α -phase titanium. The form of this interaction may be speculated by consideration of the hydrogen- α titanium- γ hydride equilibrium. Employing the equation of either McQuillan (ref. 104) or Giorgi-Ricca (ref. 149) for the equilibrium hydrogen concentration at the $\alpha/(\alpha+\gamma)$ solvus, the equilibrium hydrogen pressure can be calculated to be approximately 6.7×10^{-12} N/m² (5×10^{-14} torr) near room temperature, at pressures above which hydride formation will occur. That is, at the lowest pressure of the present study (1.3 N/m² (1×10^{-2} torr)) hydride formation on α -titanium should be controlled by nonsteady-state reaction kinetics and should be independent of the environmental hydrogen pressure, consistent with the observations of the present study (fig. 21). Additionally, transgranular cracking observed in this microstructure is consistent with the idea of hydride formation (refs. 150, 151) within the α -phase titanium grains.

Based on the above ideas, hydrogen-induced cracking in titanium involves the competition between intergranular failure at the α/β boundaries and transgranular failure through the α -grains. The rate of cracking of the latter process for all extensive purposes is independent of pressure, whereas the former process is dependent on pressure. Consistent with this is the pressure dependence of the failure mode observed in the acicular α microstructure, the continuous β -matrix material (fig. 23). At high pressures, cracking along the α/β boundaries is rapid and failure is intergranular (fig. 23(a)); however, at some pressure the two processes become competitive and mixed mode failure is observed (fig. 23(b)). At low pressures, intergranular cracking does not occur, the α -phase titanium is shielded from the environment by the β -phase titanium and failure occurs by ductile-tearing with little or no influence of hydrogen on fracture (fig. 21).

The form of the temperature dependence of hydrogen-induced, slow crack growth in the acicular α -microstructure (fig. 24) suggests control within this temperature range by a

simple, thermally activated elementary reaction exhibiting an activation energy of 19,700 J/mole (4,700 cal/mole). As discussed for steel in the previous section, it is difficult to unequivocally identify the rate controlling elementary reaction because of the complex nature of the overall hydrogen transport process; however, two elementary reactions are suggested based on the speculated location of the hydrogen-embrittlement interaction in this β -matrix material. At first perusal, the most obvious is nonsteady-state diffusion transport within β -phase titanium. Several investigators (refs. 105, 146, 152) have observed the activation energy for diffusion transport of hydrogen in β -phase to be approximately 20,900 N/mole (5,000 cal/mole). This, of course, is similar to that observed in the present study for slow crack growth. (Steady-state transport must involve the heat of solution (ref. 104) as well as the activation energy for diffusion through equation (eq. (26)) and thus, does not apply.) The observed pressure dependence of embrittlement of this structure (fig. 21), however, is not consistent with nonsteady-state transport. Nonsteady-state transport is independent of pressure (ref. 47), which negates this as a possible controlling elementary reaction. The second elementary reaction in titanium exhibiting first-order reaction kinetics and a similar activation energy, 20,900 N/mole, is the initial stage of hydride precipitation in α -titanium (refs. 153, 154). The inclusion of this reaction in the embrittlement process is consistent with the idea that failure occurs at the α/β boundaries in continuous β -matrix material as a result of hydride precipitation. To date this appears to be the most plausible rate controlling elementary reaction for the embrittlement of this material.

MECHANICAL ASPECTS OF HYDROGEN-INDUCED FAILURE

HYDROGEN SENSITIVITY OF CRACK INITIATION

The crack initiation stage of fracture is relatively unimportant in most engineering structures because the great majority contain preexisting flaws due to processing, etc. However, this is not the case in all structures or, more importantly, in many test specimen configurations often used for the evaluation of hydrogen embrittlement. For this reason it is important to understand the potential influence of hydrogen on the crack initiation stage of fracture.

Most models for crack initiation involve the interaction of dislocations with strong planar defects within the metal lattice (refs. 20-23) and are common in that the stress to initiate a crack is proportional to some function of surface energy. In general, crack initiation is an internal process that occurs within the metal structure and not on or very near the metal surface. It can be more easily understood how hydrogen *within* a metal lattice can influence this stage of fracture than hydrogen originally present only in the environment. In endothermic occluding metals, Tetelman *et al.* (ref. 44) have demonstrated that crack initiation can occur in a supersaturated metal lattice by the precipitation of molecular hydrogen at an internal defect. Such internal defects are numerous in metals and their interaction with hydrogen is further demonstrated by the anomalous hydrogen diffusion behavior that is sometimes observed (refs. 129, 155). In exothermic occluders hydrogen-induced, crack initiation has been demonstrated to occur *within* a metal as a result of crack initiation in a brittle hydride precipitate (ref. 156) or by the interaction of dislocations with this precipitate (ref. 157).

Crack initiation as the result of the interaction of environmental hydrogen with a metal is difficult to access. Because diffusion in metals is slow at ordinary hydrogen pressures at room temperature, it must be assumed to be a surface or near surface process. In endothermic metals it is difficult to understand how an environment can affect surface behavior sufficiently to influence the crack initiation stage of fracture unless the stress at that surface approaches the strength of the metal lattice. This need not be the case in exothermic metals. The formation of the brittle second-phase precipitate on the metal surface by the reaction with the environment may act similar to the presence of a brittle hydride within the metal lattice. Crack initiation in both types of metals, like the process

of crack propagation discussed previously, must involve hydrogen adsorption, which is essentially nonexistent on metal oxides (ref. 77). Therefore, if the influence of environmental hydrogen is to be observed, it must be preceded by the formation of a clean metal surface, that is, the removal or fracturing of the normally present surface oxide layer by plastic deformation, abrasion, or such. The influence of an oxide layer is relatively unimportant in crack growth rate behavior because the presence of a crack offers a sufficient stress concentrator to fracture an oxide at low applied loads. This is not the case, in general, for crack initiation stage of fracture. If because of the properties of the oxide or if the metal does not deform significantly during loading and the oxide is never fractured, the most susceptible alloy will not demonstrate the degrading effects of the environment. It is essential, then, that a stress concentrator exist so local plastic deformation will occur early in the loading process.

The purpose of this portion of the present investigation was to establish the influence of hydrogen on the delayed failure of notched specimens of an endothermic occluding metal (steel) and an exothermic occluding metal (titanium) in an effort to elucidate the role of environmental hydrogen in the crack initiation process.

Materials and procedure— The material used in this study was commercially obtained AISI–SAE 4130 steel, Ti–6Al–4V titanium alloy, and Ti–70A commercially pure titanium alloy. The 4130 steel was heat-treated to give a martensitic structure by quenching in oil from 843° C and tempering for 2 hr at 250° C. The Ti–6Al–4V alloy was heat-treated to an acicular α -microstructure by solution treating for 40 min and then stabilized.

Tests were conducted on notched (not precracked) bend specimens loaded in three-point bending. These specimens were 1.90×10^{-2} m (0.75 in.) wide, 3.17×10^{-3} m (0.125 in.) thick with a side notch to a depth of 8.0×10^{-4} m (0.031 in.) (fig. 25).

All tests were conducted in a stainless-steel chamber that could be evacuated to a pressure of better than 6.6×10^{-5} N/m² (5×10^{-7} torr) prior to backfilling with hydrogen to the desired test pressure. The bend tests were conducted at a constant displacement rate of 8.9×10^{-8} m/sec (3.5×10^{-6} in./sec).

Surface hydride formation studies were conducted in three-point bending employing the test facility (fig. 3). In these tests the tungsten filament was used as an electron source to heat the test specimen. The chamber was pumped to better than 6.6×10^{-5} N/m² (5×10^{-7} torr). The normally present oxide layer was removed from the specimen surface by

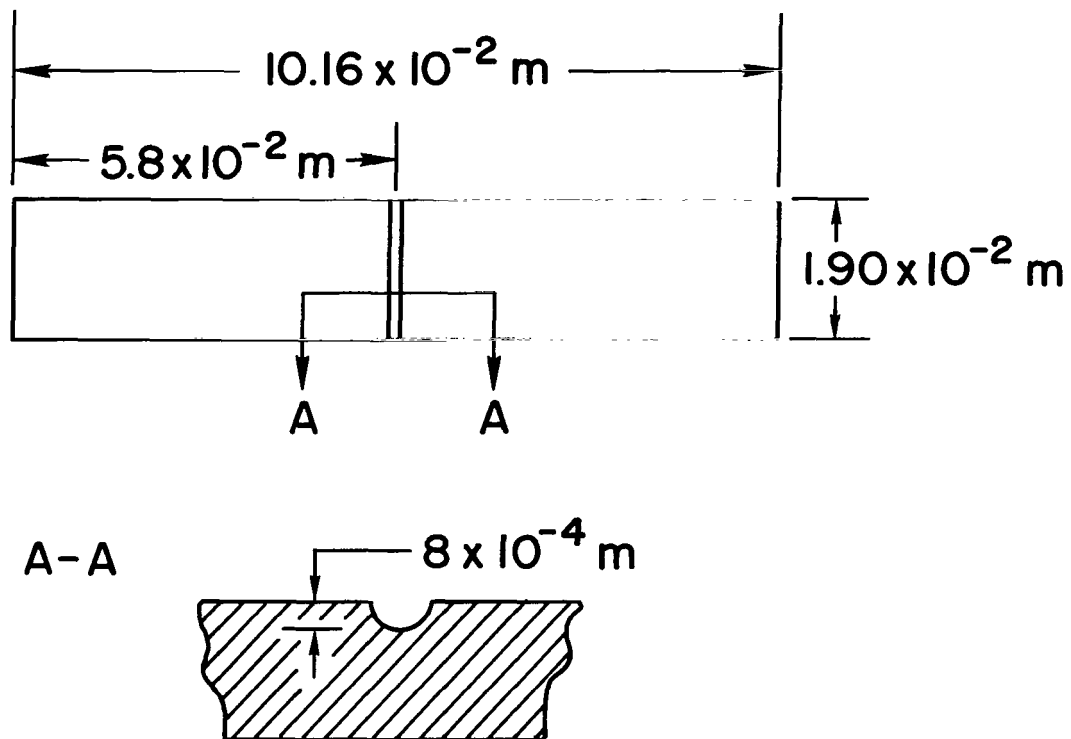


Figure 25.— Three-point bend specimen containing a side notch.

heating the specimen to approximately 750° C for about 1 hr (ref. 154). This was accomplished by the use of a potential of near 5000 volts placed between the hot filament (approximately 2500° C) and the specimen. Specimen temperature was determined by the use of an iron-constantan thermocouple spot-welded near the notch on the tension side of the bend specimen. Following the soak period, the specimen was cooled in vacuum to room temperature and hydrogen was introduced into the chamber to a pressure of 90.6 kN/m² (680 torr).

Experiments and results— The experiments consisted of three-point bend tests and hydride formation tests.

Three-point bend tests: Bend tests were conducted on the 4130 steel and Ti–6Al–4V alloy to establish the hydrogen sensitivity of these materials when a notch to concentrate deformation, but not a precrack, is present in the specimens. The distributions in failure load observed for the 4130 steel specimens tested in air and hydrogen are shown on figure 26. All specimens tested in air failed between 4 and 4.2 kN (900 and 950 lb); however, in hydrogen one specimen failed at a load of as low as 2.2 kN (500 lb) with the number of failures increasing as the failure load in air is approached. Additionally, a significant number of specimens failed in hydrogen at the same range of loads as those tested in air. The distributions in failure loads observed for the Ti–6Al–4V alloy tested in air and hydrogen are shown in figure 27. All specimens tested in air failed between 2.2 and 2.4 kN (500 and 550 lb). In hydrogen, unlike the distribution observed in steel (fig. 26), all titanium specimens failed at loads near, but less than, those observed in air. No titanium specimen failed in hydrogen at the same load range as in air. In both the steel and titanium specimens tested in hydrogen, once the crack initiated at the notch, propagation to failure was very rapid.

Hydride formation tests: Tests were conducted in a hydrogen environment at room temperature on commercially pure titanium free of surface oxide to establish the propensity of this all- α titanium alloy to form a surface hydride layer and the ability of this layer to fragment under load and initiate a crack. A number of test runs were conducted in which “clean” titanium specimens were cyclically strained both in the elastic and into the plastic regime. Under these conditions no surface hydride layer was observed with a light microscope. In one test run, however, a violent reaction occurred between the titanium alloy and the hydrogen environment immediately following the introduction of hydrogen

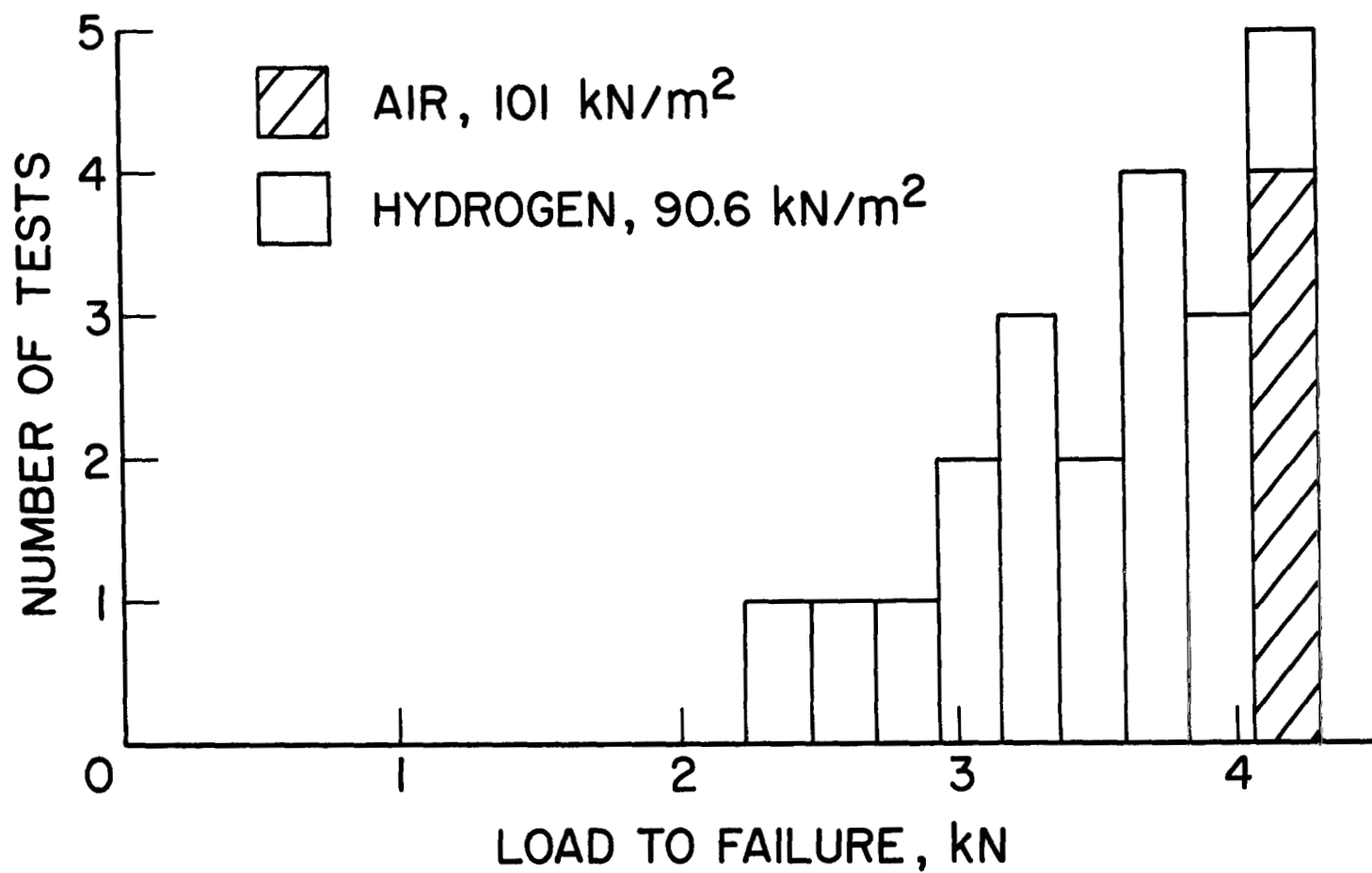


Figure 26.— The distribution in failure load observed for notched steel alloy (4130) specimens tested at a constant displacement rate of 8.9×10^{-8} m/sec in air and in hydrogen.

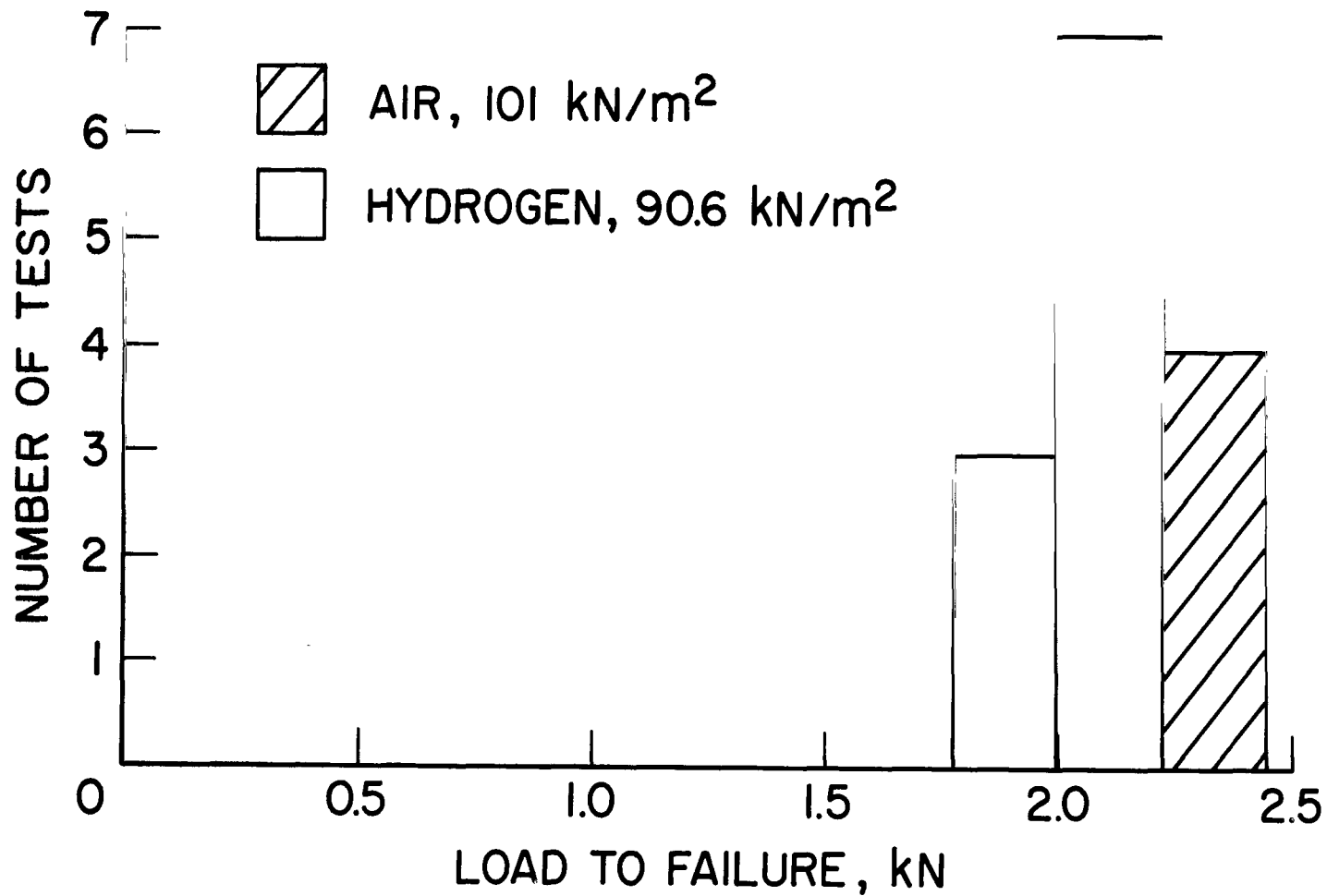
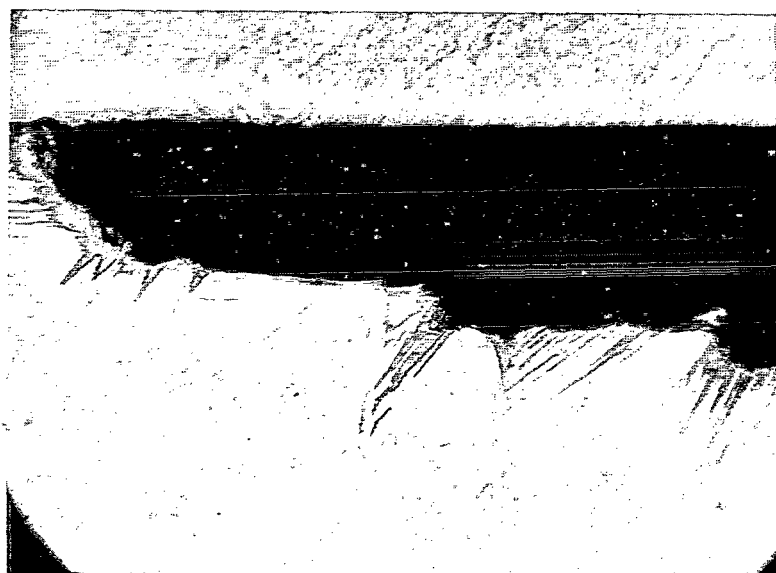


Figure 27.— The distribution in failure load observed for notched titanium alloy (6Al-4V) specimens tested at a constant displacement rate of 8.9×10^{-8} m/sec in air and in hydrogen.

into the test chamber. This reaction continued for approximately 3 min, ejecting material continuously, with a resulting crater 3.17×10^{-3} m (0.125 in.) deep and 9.52×10^{-3} m (0.375 in.) in diameter formed on the specimen surface near the original location of the welded iron-constantan thermocouple. A cross section of part of this crater is shown in figure 28. Long stringers of apparent second-phase material extend from the edge and base of the crater into the alloy. The specimen was next strained by three-point bending in the elastic region. Figure 29, a photomicrograph of these second-phase stringers following straining, shows that each stringer contains a crack extending the full length of the stringers from the surface of the crater.

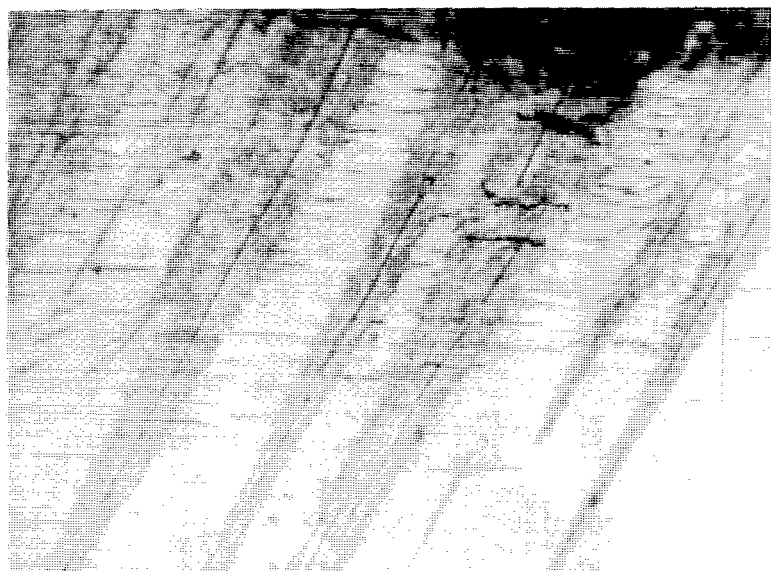
Discussion— The results of this study (figs. 26 and 27) demonstrate the less sensitive and less predictable nature of fracture behavior of notched specimens as compared with specimens containing a precrack (table 3) tested in a hydrogen environment. These observations can be interpreted in terms of the relatively insensitive and haphazard character of the crack initiation stage of fracture, as previously discussed. Specifically, in the endothermic occluding alloy (steel) the influence of hydrogen on the failure load of notched specimens ranged from severe in a few specimens with most specimens exhibiting little or no observable effect (fig. 26). The range of sensitivity observed in this alloy is probably related to the strong influence of physical variables such as notch smoothness and surface defects. In the exothermic occluding alloy (titanium), failure load in hydrogen was observed to be more predictable, although never as severe as that observed for steel (fig. 26) and always less than that in air (fig. 27). These observations suggest that crack initiation in titanium, compared with steel, originates from a fairly predictable process. Such a process may be the formation of a thin surface hydride layer in which the crack can initiate at loads slightly less than necessary for failure in air.

Hydride formation is thermodynamically feasible (refs. 104, 149) and probably occurs on the clean surface of all- α titanium alloys (ref. 158). A continuous thin layer of hydride can, in fact, protect the titanium from further hydride formation (ref. 158). There is little doubt that under the right conditions severe hydride formation and spallation can occur. Similar observations have been made at room temperature in columbium and in tantalum where severe fragmentation has been observed as the result of hydride formation originating at a thermocouple attachment (refs. 159, 160). If fragmentation occurs in titanium alloys,



100 μm
|-----|

Figure 28.— Cross section of a crater formed on the surface of a titanium specimen by the interaction with the hydrogen environment at the location of the welded thermocouple.



20 μm
┌──┐

Figure 29.— Second-phase stringers formed in titanium from a hydrogen environment showing the existence of cracks following elastic deformation.

crack initiation in the stringers is essentially spontaneous because of the brittle nature of the hydride phase (fig. 29).

From the above discussion, one of the most important considerations in the evaluation of a test result, particularly related to environmental hydrogen embrittlement, is a knowledge of the relationship of the parameter being measured in the test to the fracture process. For example, test configurations such as the smooth tensile bar, the notched tensile bar, and the burst disc (extensively used in France to measure environmental hydrogen embrittlement, ref. 161) can lead to erroneous conclusions concerning the susceptibility of the alloy tested. In these test configurations crack initiation must occur prior to the propagation stage of fracture, whereas in actual service conditions preflaws almost always exist. Crack initiation is haphazard, and most of the variables on which it depends are not sensitive to the environment so it is less dependent on the environment than the propagation stage of fracture. When such tests are employed, an alloy that is extremely sensitive to embrittlement in the propagation stage and insensitive in the initiation stage will exhibit little or no deleterious influence of hydrogen. In such tests those alloys that indicate susceptibility to hydrogen should be considered affected by hydrogen; however, those that are indicated to be unaffected must be considered potentially susceptible until proven otherwise. This problem can be circumvented by the use of a precracked specimen where crack initiation is no longer a required process.

DEFORMATION DURING HYDROGEN-INDUCED CRACK GROWTH

One of the classic experiments related to the embrittlement of hydrogen-charged endothermic occluding metals is that by Tetelman (ref. 162). He observed the formation of microcracks on $\{100\}$ planes in Fe-3%Si single crystals in the absence of applied load by the precipitation of molecular hydrogen during electrolytic charging at 23° C or when crystals were quenched from elevated temperatures in a hydrogen atmosphere. This work has since been extended (refs. 163, 164) to include a rather extensive analysis of plastic deformation accompanying crack propagation. From these studies, Tetelman (ref. 76) has been successful in describing hydrogen-induced, discontinuous crack growth as a modification of the theory first proposed by Zapffe (ref. 165) in which growth was controlled by the diffusion of hydrogen to these internal cracks to maintain the necessary pressure. Recently, Bernstein (ref. 166) extended the study of failure in Fe-3%Si

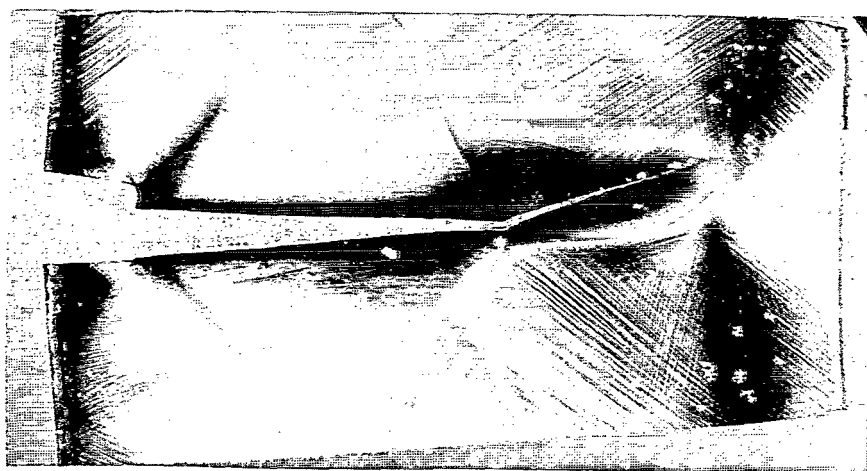
polycrystal material to a gaseous hydrogen environment and found a significant decrease in ductility with a cleavage mode of fracture.

The purpose of this portion of the investigation was to establish in an endothermic occluding alloy (Fe-3%Si) whether crack growth in a hydrogen environment occurs in a continuous or discontinuous manner, the extent of plastic deformation associated with crack growth, and the influence of grain boundaries on the propensity of the material to fail by intergranular or transgranular separation. The technique employed was similar to that used by Tetelman (ref. 162) in which plastic deformation was revealed by a dislocation decoration procedure (ref. 167).

Material and procedure— The material used was the iron alloy having the composition Fe-3.50Si-0.005C that could be etch-pitted. The 3.17×10^{-3} m thick polycrystalline material (as received) was given a critical strain of approximately 5 percent and annealed at approximately 1200° C for 1 hr. This procedure resulted in a grain size of 1×10^{-2} to 2×10^{-2} m in diameter. X-ray diffraction orientation analysis was conducted and specimens 2×10^{-2} m wide and 4×10^{-2} m long were sectioned from the sheet such that a major grain, having its (100) plane perpendicular to the long axis of the specimen, intersected the edge of the specimen.

As previously described, the test chamber was evacuated to better than 6.6×10^{-5} N/m² (5×10^{-7} torr) prior to backfilling with hydrogen. The specimens were notched into the major grain by use of a jeweler's saw. Cleavage cracks along the (100) plane were extended from the notches by cooling the specimens to liquid-nitrogen temperature and spreading the notches with a wedge. Specimens were pulled to failure in vacuum and in 90.6 kN/m² (680 torr) hydrogen and were etch-pitted using the normal technique (ref. 167).

Results— Tests were conducted on specimens containing a (100) cleavage precrack, loaded perpendicular to this plane in either a vacuum or a hydrogen environment. All specimens pulled in vacuum failed by a chisel-point type failure associated with gross deformation and the inability of the existing cleavage precrack to continue propagation. In a hydrogen environment the cleavage precrack continued to propagate by cleavage on the (100) plane at low applied loads. Figure 30 is a profile of a specimen tested in a hydrogen environment. The saw cut can be seen at the left edge of the specimen. The precrack originally extended midway across the large grain from the saw cut. In this figure the light



3000 μm


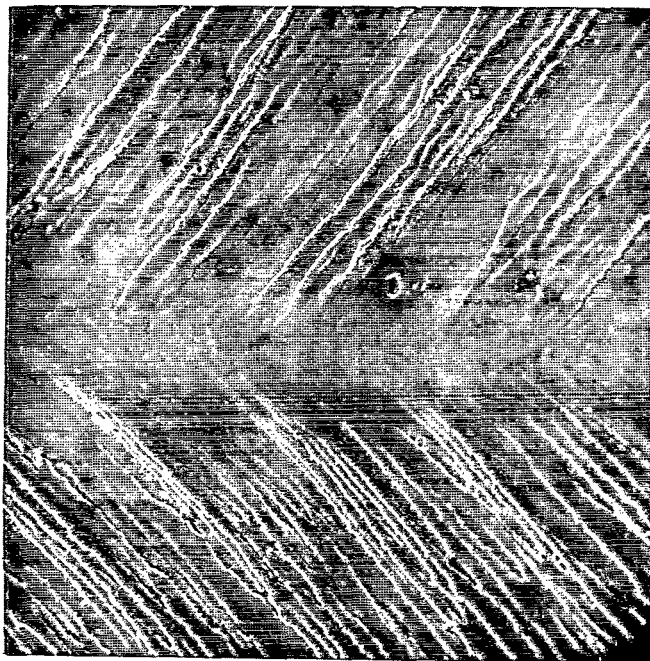
A horizontal scale bar with vertical end caps, indicating a length of 3000 micrometers.

Figure 30.— Gaseous hydrogen-induced crack growth profile of a large grained Fe—3%Si alloy specimen containing a cleavage precrack on a (100) plane.

areas indicate dislocation decorated material and the dark areas indicate dislocation free material. Figure 31 is a fractograph of a portion of the hydrogen-induced fracture of the specimen shown in figure 30. Hydrogen-induced crack growth occurs by the continuation of (100) cleavage, is negligibly affected by a grain boundary if a properly oriented cleavage plane exists in the second grain for continued propagation, and results in little or no deformation associated with it, even at the point of crack initiation. Figure 32, a photomicrograph of the crack tip of this specimen at a higher magnification, shows that crack growth stops at a grain boundary, with extensive deformation, when the new grain (the third grain) does not contain a cleavage plane of the correct orientation. Figure 32 is a further example of this behavior in another specimen where the crack continues by what appears to be a tearing mode with extensive deformation.

Discussion— The results of the present study indicate that hydrogen-induced crack growth in this endothermic occluding Fe-3%Si alloy occurs by transgranular cleavage (figs. 30 and 31) with no evidence of intergranular separation even when cleavage is not possible (figs. 32 and 33). Bernstein (ref. 166) has reviewed the observed modes of hydrogen-induced failure in iron and found them to be dependent on such variables as interstitial level and carbon-oxygen level. Such variables were not controlled in the present study; however, there is little doubt as to the mode of failure in at least this Fe-3%Si material.

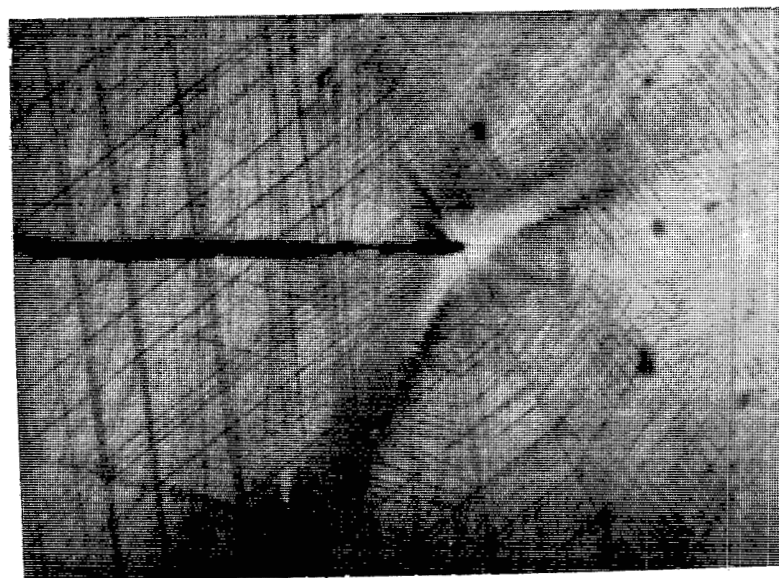
Unlike the discontinuous nature of hydrogen-induced crack growth observed in hydrogen-charged specimens (refs. 162, 163) crack growth observed in the presence of a gaseous hydrogen environment appears continuous to the extent that crack growth does not result in areas of plastic deformation where the crack stops and starts. Further, no observable deformation occurred on the continuation of a preexisting, stopped, cleavage crack in a hydrogen environment. The apparent lack of deformation associated with hydrogen-induced crack propagation in this material suggests that crack growth occurs at the crack tip or not significantly ahead of the crack tip and that the surface energy or the bond energy of the iron lattice is reduced by the presence of the hydrogen environment. The alternative possibility that plastic deformation is influenced by the hydrogen environment appears negated by the lack of decorated dislocations near the crack and the difficulty of hydrogen to penetrate the iron lattice at these pressures and temperatures, as discussed previously.



40 μm

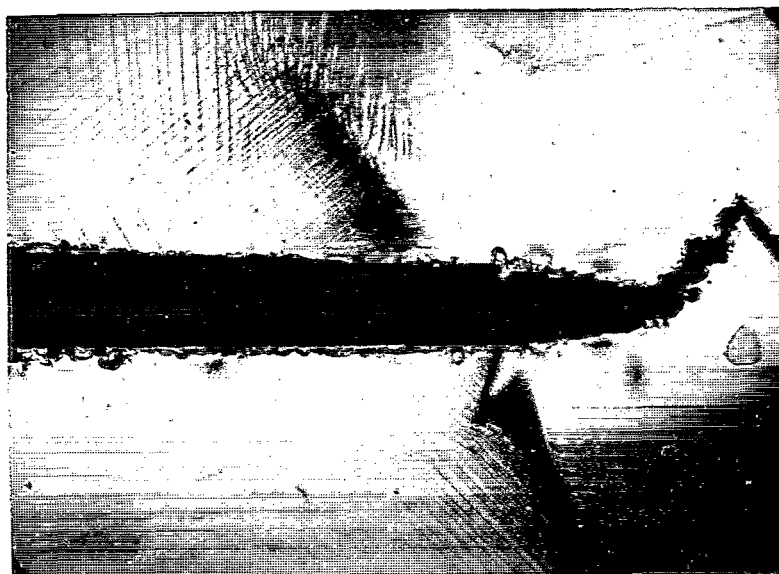
A horizontal scale bar with vertical end caps, indicating a length of 40 micrometers.

Figure 31.— SEM fractograph of a large-grained Fe—3%Si alloy specimen failed in hydrogen.



50 μm
└───┘

Figure 32.— The intersection of a hydrogen-induced cleavage crack with a grain not oriented for continued (100) cleavage.



300 μm
└────────┘

Figure 33.— The transition between hydrogen-induced cleavage and ductile tearing brought about by a change in lattice orientation.

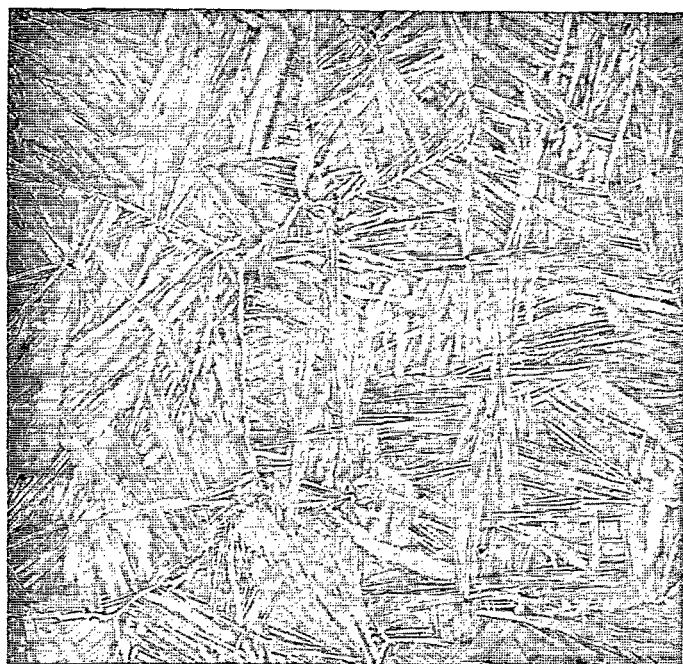
COMBINED INFLUENCE OF MECHANICALLY AND KINETICALLY INDUCED CRACK GROWTH

Stable crack growth at subcritical stress-intensity levels can occur in materials as a consequence of kinetic reactions involving the material and a chemical species, such as hydrogen. An additional form of subcritical crack growth occurs when a metal is cyclically loaded. This form of crack growth, termed fatigue crack growth, does not involve a chemical species but is solely the result of mechanical considerations occurring at the crack tip (ref. 168). The combined phenomenon of kinetically and mechanically induced crack growth is termed corrosion fatigue and is due to the combined action of chemical and fatigue attack on metals.

In this portion of the investigation we will consider the stable, subcritical crack growth stage of fracture under conditions of corrosion fatigue. Specifically, a comparison will be made under conditions of static and cyclic loading between the behavior of an exothermic occluding titanium alloy in a gaseous hydrogen environment with its behavior in a vacuum environment. Titanium can exhibit a broad range of susceptibility to environmental-hydrogen embrittlement depending on alloy microstructure, so a variation of this parameter under conditions of fatigue attack will dramatize the importance of the kinetic and mechanical aspects of hydrogen-induced crack growth. Additionally, the corrosion fatigue characteristics of this hydrogen-metal system will have been established.

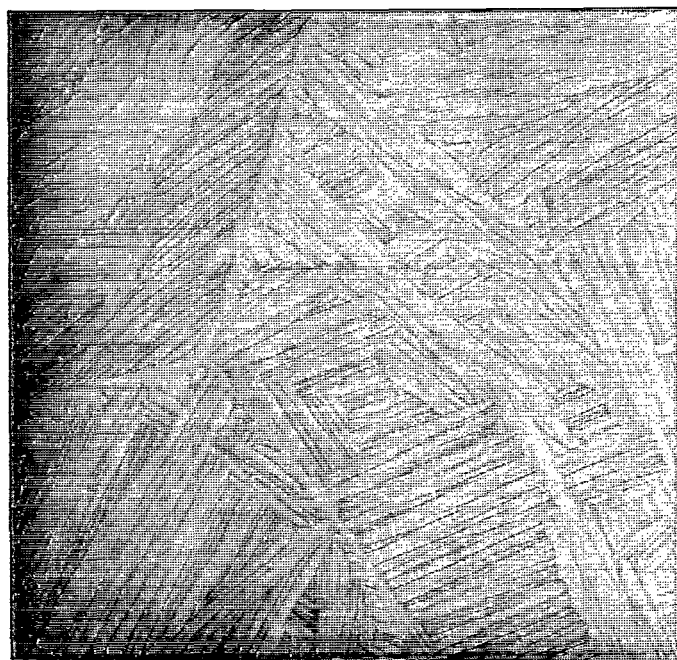
Materials and procedure— The materials were two heats of commercially obtained Ti-5Al-2.5Sn alloy plate both of which had an original thickness of 1.27×10^{-2} m (0.50 in.). Test specimens were machined such that the propagating crack would be transverse to the rolling direction of the plates. Specimens were heat treated at 1010° C and 1065° C in a vacuum furnace for 15 minutes and furnace cooled with the resulting microstructures shown in figure 34. Both microstructures contained acicular α -phase platelets with some β -phase in the boundaries; for those heated to the higher temperature, however, the acicular structure was coarse while to the lower temperature it was fine, the former having much less phase boundary area than the latter.

The test specimen configuration, compliance calibration, and analysis used were identical to those employed in reference 169 and thus will be reviewed only briefly. Specimen configuration was of the double-cantilever-beam type (fig. 35). Load was applied to the specimen by the use of a closed-loop, servo-controlled, hydraulic actuator, and



200 μm
|-----|

(a)



400 μm
|-----|

(b)

Figure 34.— Microstructures of the titanium alloy (5Al–2.5Sn) investigated in this study;
(a) fine acicular α -titanium, (b) coarse acicular α -titanium. Kroll's etch.

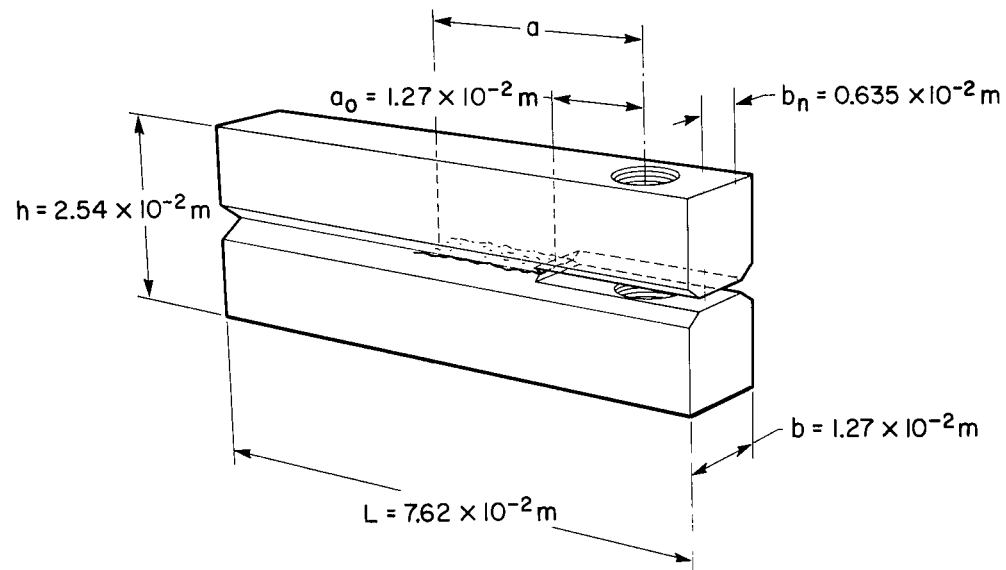


Figure 35.— Double-cantilever-beam specimen.

crack-opening displacement was measured by a linear variable differential transformer mounted across the crack at the loading points. The compliance calibration was determined for this specimen and, by an analytical technique described below, these compliance values were used to calculate stress-intensity values and crack-growth rates.

Specifically, the compliance curve was found to be represented by

$$C = Aa^n \quad (29)$$

where a is the crack length and constants A and n have values of 1.43×10^{-5} in.-deflection/(in.-length) ^{n} -lb and 2.22, respectively, for the Ti-5Al-2.5Sn alloy specimens. Through the use of elastic mechanics, the following equation was developed by Williams and Nelson (ref. 169) to describe the stress intensity as a function of applied load and crack-opening displacement.

$$K_I = 5.96 \times 10^2 P^{0.725} \delta^{0.275} \text{ (ksi-in.}^{1/2}\text{)} \quad (30)$$

where P is load in pounds and δ is crack-opening displacement in inches. For any fixed load or displacement, therefore, the instantaneous stress intensity can be determined from the instantaneous crack-opening displacement or load, respectively. From the same equations used for the development of equation (30) crack length can be shown to be given by

$$a = \delta^{1/n} P^{-1/n} A^{-1/n} \quad (31)$$

Differentiating a with respect to δ , dividing by dt , and substituting the compliance constants A and n , we obtain

$$da/dt = 6.84 \times 10^1 \delta^{-0.549} P^{-0.450} (d\delta/dt) \quad (32)$$

for a and δ in inches and P in pounds. For any fixed load and known crack-opening displacement, the crack growth rate can be determined from the instantaneous time change in crack-opening displacement. Likewise, differentiating equation (31) with respect to P , dividing by dt , and substituting the compliance constants, we obtain

$$da/dt = -6.84 \times 10^{-1} \delta^{0.450} P^{-1.450} (dP/dt) \quad (33)$$

For any fixed displacement and known load the crack growth rate can now be determined from the instantaneous time change in load.

As in the previous portions of this investigation, tests were conducted in a test chamber that could be evacuated prior to backfilling with hydrogen to a pressure of 90.6 kN/m² (680 torr). Prior to testing, each specimen was precracked by fatiguing in vacuum to extend the notch approximately 1.27×10^{-2} m beyond the machined notch. Fatigue tests were conducted either in a vacuum or a hydrogen environment by the use of a square-wave generator under conditions of $R = 0$ where load was cycled between near zero and some preselected maximum value. Cyclic tests were conducted at frequencies of 5×10^{-1} and 5×10^{-3} Hz, which correspond to 1 sec and 100 sec at maximum load and equal times at zero load. Crack-opening displacement was monitored as a function of time. Static tests were conducted in hydrogen by rapidly loading the specimen to a preselected crack-opening displacement and holding it at that value while the load was monitored as a function of time.

Results and discussion—

Gaseous hydrogen-induced crack growth under static loading: In a previous section we saw that the embrittlement of precracked Ti–6Al–4V alloy in a gaseous hydrogen environment was strongly dependent on both test displacement rate (fig 22) and microstructure (fig. 21). These observations were explained in terms of the operative crack growth processes controlled by hydrogen transport and hydride-formation reaction kinetics. It was suggested that the β -phase titanium acts as a “short-circuit” transport path that allows more hydrogen to get to a given point in given time and interact at the phase boundaries to cause rapid intergranular crack growth and fracture. When the environment sees little or no β -phase titanium, hydrogen must interact with the α -phase directly on or very near the crack tip resulting in slow transgranular crack growth and failure. The rate of macroscopic crack growth observed in a specimen will depend on both the amount of β -phase present in the boundaries and the amount of boundary area present in the microstructure.

The observed influence of two types of microstructure on subcritical crack growth rate in hydrogen environment for the Ti–5Al–2.5Sn alloy of the present study is shown in figure 36, which is a plot of the log of the hydrogen-induced crack growth rate as a function

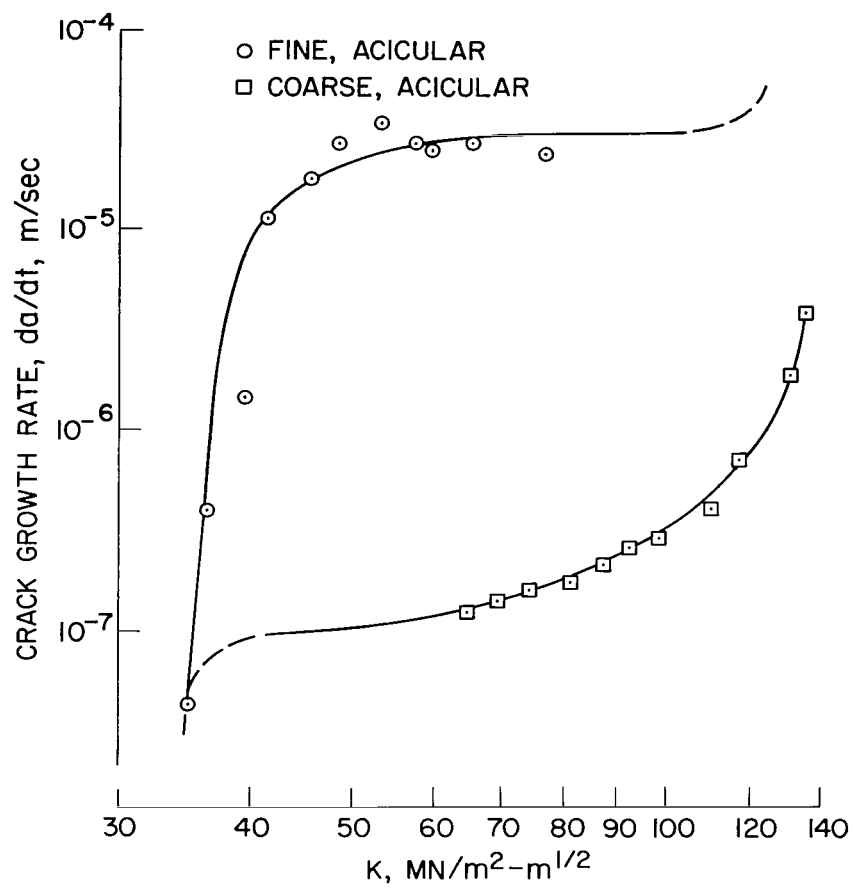


Figure 36.— The effect of applied stress intensity on the rate of hydrogen-induced crack growth under conditions of static loading.

of the log of the applied stress intensity under conditions of static load for coarse acicular and fine acicular α -phase microstructures. Only a portion of the entire curve was obtained for each microstructure because of the experimental limitations of the test apparatus. Crack growth rates could not be measured with reasonable accuracy at very high rates because of the poor response of the measuring system at these rates, or at very low rates because of the significant influence, at these rates, of minor amounts of contaminants present in the hydrogen environment, possibly from the chamber walls, etc. Figure 36 shows that the form of the stress-intensity dependence of the growth rate appears similar to that observed by others for titanium alloys tested in an aqueous chloride environment (ref. 170); that is, for a given microstructure there exists a large range of stress-intensity values over which the subcritical crack growth rate is increasing very slowly. Above and below this range, crack growth rate changes very rapidly for a small change in stress intensity. Additionally, the influence of microstructure on the hydrogen-induced subcritical crack growth rates observed in this section is consistent with that observed for Ti-6Al-4V alloy in the previous section. In figure 36 it is seen that crack growth rates at intermediate values of stress intensity are two to three orders of magnitude faster for specimens having a fine acicular microstructure than for those having a coarse acicular microstructure (a large amount of phase boundary area as compared with a small amount of boundary area, respectively, fig. 34).

Fatigue-induced crack growth in vacuum: Tests were conducted in a vacuum environment ($<6.6 \times 10^{-1}$ N/m² (5×10^{-3} torr)) to establish the rate of subcritical crack growth that occurs in Ti-5Al-2.5Sn alloy under cyclic loading in an inert atmosphere. Figure 37 shows the results of this portion of the study and is a plot of log maximum stress intensity versus log crack growth rate for the fine acicular structure at a frequency of 5×10^{-1} Hz and for the coarse acicular structure at 5×10^{-1} and 5×10^{-3} Hz. In this figure, as well as all of the following figures in which cyclic crack growth rates are reported, the measured rates under cyclic loading, where the specimen is under load half of the time, have been doubled so that these rates can be compared with crack growth rates under static loading, where the specimen is under load all of the time. At the higher frequency the differences in microstructures have little or no effect on the rate of fatigue-induced crack growth. For the coarse acicular structure, by converting crack growth per unit time to growth per cycle, frequency can be shown to have little or no effect on crack growth at the two frequencies investigated (i.e., $da/dN = \text{constant}$, where N is the number of cycles).

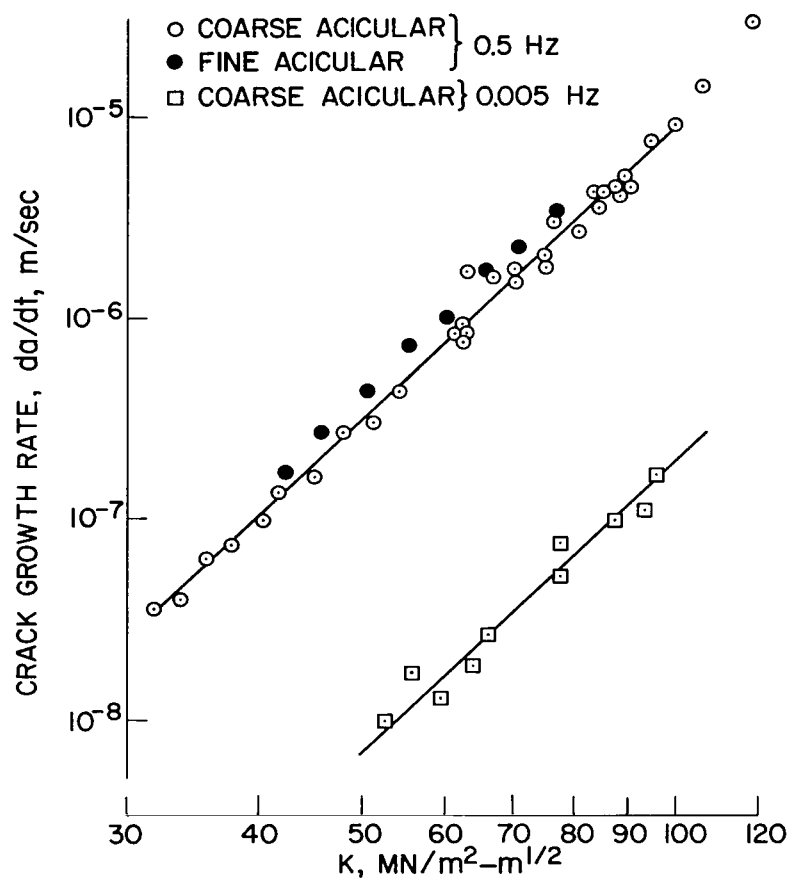


Figure 37.— The effect of maximum stress intensity on the rate of fatigue-induced crack growth in a vacuum environment.

Additionally, the applicability of the exponential relation between fatigue-induced crack growth and stress intensity is demonstrated. The log-log curves obey a linear relationship, independent of microstructure and frequency, given by

$$da/dN \propto da/dt = C(K_{\max})^5 \quad (34)$$

This relationship with the stress-intensity exponent of 5 is the same as that observed by Crooker et al. (ref. 171) for the titanium alloy Ti-7Al-2Cb-1Ta and the exponent is well within the range of 2 to 10 observed by other investigators for several alloy systems.

Corrosion fatigue in hydrogen: Corrosion fatigue, or in the particular case of this study, hydrogen-induced crack growth under cyclic loading, can be thought of as the combined influence of environment (chemical) and cyclic loading (mechanical), or better, the combined influence of kinetic and dynamic variables on subcritical crack growth. We have established, under conditions of static loading, the influence of microstructure on the hydrogen-induced crack growth rate as well as the dependence of this rate on stress intensity. In vacuum we have established the dynamic influence of cyclic loading on crack growth and the independence of microstructure as well as the dependence of crack growth on maximum stress intensity. We can now consider corrosion fatigue in a hydrogen environment to separate the influence of kinetic and dynamic variables, and to determine the possible existence of a synergistic effect as a result of combined chemically induced and mechanically induced crack growth.

Figure 38 is a plot of log maximum stress intensity versus log crack growth rate showing data obtained in a hydrogen environment at a cyclic frequency of 5×10^{-1} Hz for specimens having a fine acicular structure. Again, the cyclic crack growth rates have been doubled so that they can be directly compared with static crack growth rates. Also shown on this figure are the fatigue-induced crack growth rate curve in vacuum, from figure 37, and the hydrogen-induced crack growth rate curve under conditions of static loading from figure 36. Under fatigue loading, the effect of a hydrogen environment is to change the form of the crack growth rate dependence on stress intensity and increase the fatigue crack growth rate as compared to that observed in a vacuum environment. In fact, both the magnitude of the hydrogen-fatigue crack growth rate and the form of its dependence on stress intensity are nearly identical to that observed in hydrogen under conditions of static loading.

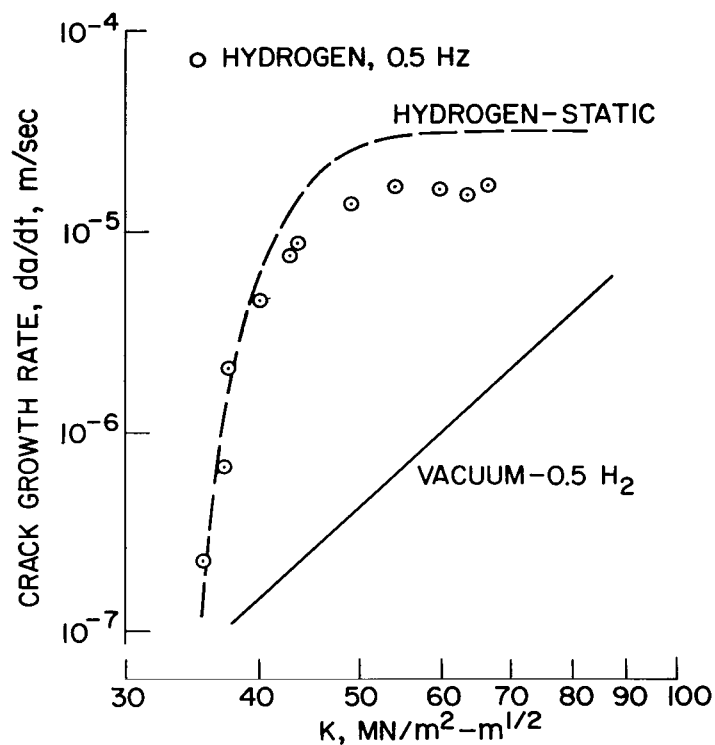


Figure 38.— The effect of maximum stress intensity on the rate of crack growth in a hydrogen environment under conditions of cyclic loading of specimens having a fine acicular microstructure.

Likewise, figure 39 is a plot of log stress intensity versus log crack growth rate showing data obtained in a hydrogen environment at cyclic frequencies of 5×10^{-1} and 5×10^{-3} Hz for specimens having a coarse acicular microstructure. Again, for comparison the fatigue-induced crack growth rate curves in vacuum and at corresponding frequencies (fig. 37) and the hydrogen-induced crack growth rate curve under conditions of static loading (fig. 36) are also shown. (The measured fatigue crack growth rates have been increased by a factor of two as explained above.) Unlike the previous structure tested (fine, acicular), at a frequency of 5×10^{-1} Hz for a coarse acicular structure, the hydrogen environment has no resolvable effect on the rate of crack growth as compared to that observed in a vacuum environment. However, at the lower frequency of 5×10^{-3} Hz, the influence of hydrogen is dramatic with a change in the form of the curve and an increase in crack growth rate as compared to that observed in a vacuum environment. Again, as in the case of the specimen having the fine acicular structure, the form and placement of the hydrogen-fatigue curve is similar to that observed in hydrogen under conditions of static loading.

It can be argued that subcritical crack growth during corrosion fatigue of the Ti-5Al-2.5Sn alloy in a hydrogen environment is not a synergistic process but can be considered, to a very good approximation, as the summation of two independent processes acting in parallel. The overall crack growth rate under cyclic loading in hydrogen is the sum of the rate of crack growth under static load in hydrogen, that is, crack growth controlled by a kinetic process (hydrogen transport in this case), and the rate of crack growth under cyclic load in an inert environment (crack growth controlled by a dynamic process). Such an interpretation is not new in corrosion fatigue; it has been postulated by Wei and Landes (ref. 172) and by Gallagher (ref. 173) for steels. All data of the present study (figs. 38 and 39) support the above interpretation. At low frequencies the contribution of the dynamic process, fatigue-induced crack growth, is negligible and the observed rate of crack growth is controlled by the kinetic process, hydrogen-induced crack growth. At high frequencies the dynamic contribution is dominant and the kinetic contribution is negligible. Within these frequencies there exists a transition where the rates of both dynamic and kinetic processes are comparable. The frequency range at which this transition is observed is dependent on the individual rates of the two processes and thus is dependent on such variables as microstructure. As a consequence, the rate of crack growth observed in

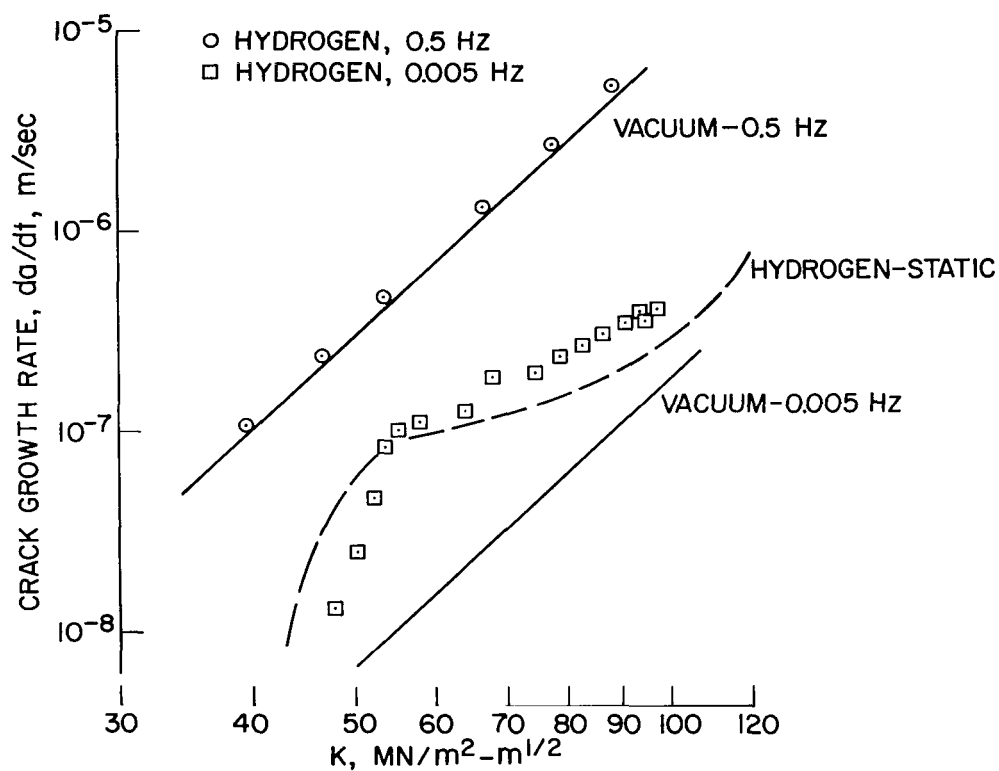
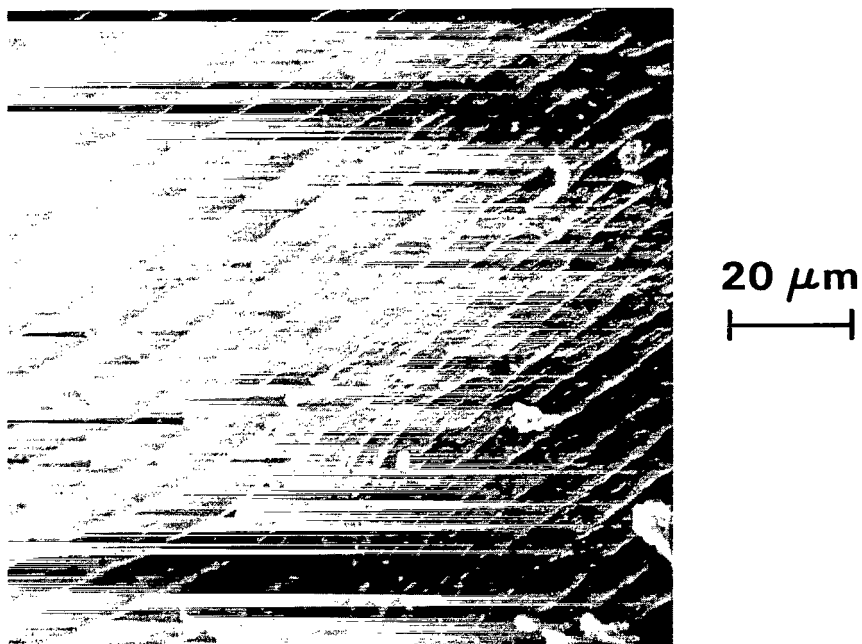


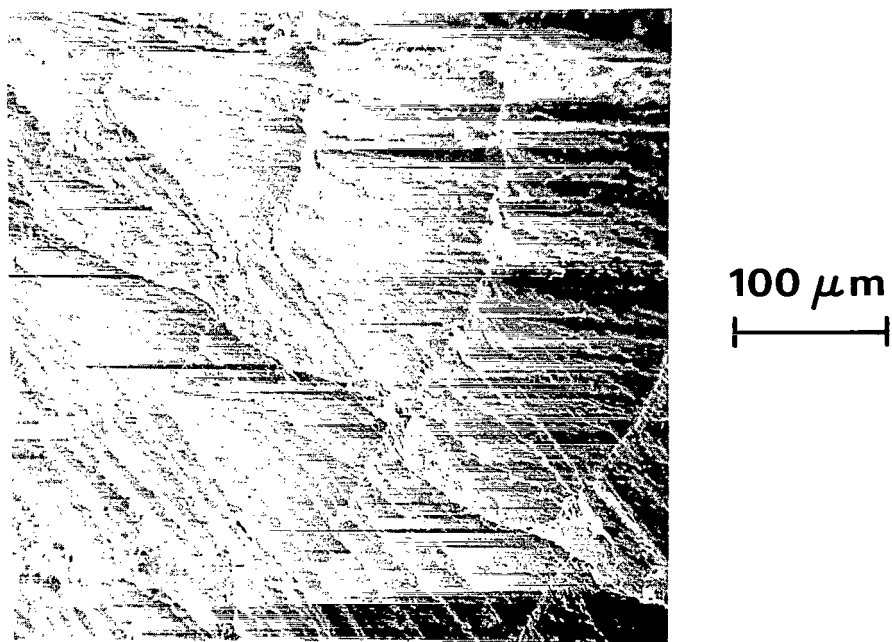
Figure 39.— The effect of maximum stress intensity on the rate of crack growth in a hydrogen environment under conditions of cyclic loading of specimens having a coarse acicular microstructure.

corrosion fatigue will never be less than that exhibited under static load in a hydrogen environment no matter what the cyclic frequency of the test.

Finally, the fracture surfaces of specimens failed under all conditions of this study were investigated with the scanning electron microscope. As would be expected, the most significant difference was observed between the fracture surfaces of specimens having a coarse acicular microstructure tested at a frequency of 5×10^{-3} Hz at a maximum stress intensity of near $55 \text{ MN/m}^2\text{-m}^{1/2}$ ($50 \text{ ksi-in.}^{1/2}$) in a vacuum and a hydrogen environment shown in figure 40. In vacuum the fatigue striations are closely spaced and definite with no evidence of intergranular fracture, whereas in hydrogen they are widely separated and less definite with evidence of intergranular separation along the prior β -phase grain boundaries as well as along the acicular α -phase boundaries.



(a)



(b)

Figure 40.— SEM fractograph of specimens having a coarse acicular microstructure fatigued at 0.005 Hz; (a) fatigued in vacuum, (b) fatigued in hydrogen.

DISCUSSION

We have presented several experimental observations concerning the influence of a gaseous hydrogen environment on both exothermic and endothermic hydrogen occluding alloys in terms of the specific influence of kinetic and mechanical variables. In this discussion we will attempt to collate these observations. First, the kinetic and mechanical influences on the type and form of hydrogen embrittlement will be considered so that the observed physical manifestations of embrittlement can be understood and cataloged. Next, these results will be interpreted in terms of embrittlement mechanisms to better understand the specific role of hydrogen in the various embrittlement processes. Finally, the physical manifestations of hydrogen embrittlement will be compared with other forms of embrittlement, particularly other forms of environmental embrittlement, to help elucidate the overall role of a chemical species in the embrittlement of metals.

KINETIC AND MECHANICAL ASPECTS OF HYDROGEN EMBRITTLEMENT

Hydrogen's deleterious effect on the behavior of a metal is primarily through its influence on the crack initiation stage or the subcritical crack growth stage of the fracture process. The susceptibility of a structure and the severity of this effect are dependent on the originating location of the hydrogen species, the relative influence of the hydrogen species on the initiation and growth stages of fracture, and the relative importance of these fracture stages in the failure of the structure.

The crack initiation stage of fracture is readily influenced in all metals of engineering significance by the presence of a supersaturation of hydrogen within the metal lattice above its solid solution concentration limit (ref. 57). A supersaturation of hydrogen can be obtained in endothermic occluding metals by cooling a saturated lattice from elevated temperatures, in exothermic occluding metals by cooling a saturated lattice below the temperature at which a hydride can precipitate, or in both by cathodically charging sufficiently large amounts of hydrogen into the metal lattice. Under conditions of a supersaturated metal lattice, crack initiation can occur in endothermic occluding metals by the precipitation of hydrogen at defects (ref. 44) and in exothermic metals by the precipitation of a brittle hydride phase (ref. 156). The propensity of a metal to "precipitate" a crack is dependent on the degree of hydrogen supersaturation, or in other words, the amount and distance that must be transported to the site of nucleation. If the

level of supersaturation is high, crack initiation is virtually spontaneous (ref. 162); if it is small, however, crack initiation is time dependent with its rate controlled by an elementary reaction of the overall transport process (fig. 1), generally lattice diffusion (ref. 174) that is a first-order kinetic process, exponentially dependent on temperature (eq. (23)). When hydrogen is present not in the metal lattice but in the environment, the influence of hydrogen on this stage of fracture becomes more random, being dependent on the fortuitous occurrence of a surface site for crack nucleation at which the environment can interact. In an endothermic steel alloy the process is truly random (fig. 26), whereas in the exothermic titanium alloy crack initiation appears dependent on a predictable process (fig. 27) of formation of a hydride layer in which crack initiation can more easily occur (fig. 29).

Most engineering structures contain preexisting cracks because of processing procedures such as welding so the crack initiation stage of fracture is of little or no importance to the failure process. This is not the case, however, for some structures and more importantly for many test specimen configurations such as the tensile bar (ref. 74) and rupture disc (ref. 161) often used to evaluate hydrogen embrittlement. In these the crack initiation stage can dominate the failure process. It is, therefore, imperative that the relative influence of the initiation and growth stages of fracture in the failure of a structure or specimen be understood, particularly when evaluating or predicting the influence of environmental hydrogen.

The subcritical crack growth stage of fracture occurs at values of stress intensity (eq. (3)) below the critical value at which unstable crack growth occurs (eq. (6)). Unlike the initiation stage, this stage of fracture is extremely sensitive to hydrogen and under conditions of noncyclic loading is the result of it. In a very simple manner, rapid unstable crack growth occurs when the applicable criteria are met, such as that proposed by Griffith for brittle materials (eq. (1)). Crack growth will occur, at stress intensity levels below this critical level, if hydrogen or any other chemical species influences the variables in the criteria (eq. (4)) in such a way as to reduce the stress intensity value determined by the criteria. If the influences of hydrogen on variables in the criteria were instantaneous and homogeneous throughout the structure, the new value of stress intensity would be the critical value, and unstable crack growth would immediately result. However, the influence

of hydrogen is localized at or near the crack tip and continued crack growth is dependent on the rate of hydrogen transport to the localized area.

The rate of hydrogen-induced crack growth in a metal will exhibit the reaction kinetics of the elementary reaction controlling the overall hydrogen transport process. The most common kinetic form is that of a thermally activated reaction expressed by an exponential dependence on temperature (eq. (19)). Under such conditions the rate of hydrogen-induced crack growth, da/dt , would be given by

$$\left(\frac{da}{dt}\right)_{K < K_c} = C a_0 \exp\left(\frac{-Q}{RT}\right) \quad (35)$$

where C is a proportionality constant dependent on factors not yet defined, a_0 and Q are the preexponential term and the activation energy of the controlling elementary reaction, respectively, T is temperature, and R is the gas constant. In general, the controlling reaction kinetics need not be this simple and can involve opposing (eq. (11)), consecutive (eq. (14)), and parallel (eq. (16)) elementary reactions. The range of control is dependent on temperature (fig. 1). For example, when hydrogen is present in a steel, subcritical crack growth of an internal crack is controlled by diffusion kinetics (ref. 76). Subcritical crack growth of a steel in water vapor is controlled by permeation kinetics (refs. 84, 86), that is, absorption and diffusion (eq. (26)). Subcritical crack growth of an α - β titanium alloy having a continuous β -matrix appears to be controlled by the hydride reaction at the α/β boundary (fig. 24). Subcritical crack growth of a steel in a molecular hydrogen environment is controlled by a surface reaction involving a physisorbed precursor (ref. 137) (eq. (28)) that can be changed to a more simple reaction process by the presence of atomic hydrogen in the environment (figs. 14 and 16).

Hydrogen-induced crack growth is also significantly influenced by the level of applied stress intensity (fig. 35). This dependence has been observed for different environments (refs. 170, 175, 176). In general, three distinct regions exist: region I where crack growth rate is strongly dependent on K and occurs at low levels of K ; region II where rate is nearly independent of K at intermediate levels of K ; and region III where rate is again strongly dependent on K at high levels of K (near K_c). These regions are interpreted in terms of a change in controlling reactions (ref. 175). Region I is controlled by the embrittlement interaction that affects the particular variable in the growth criteria.

Region II is controlled by the rate of hydrogen transport to the site of interaction, the range of applicability of equation (35). Region III is controlled by mechanical failure mechanisms as the critical stress intensity level is approached. The exact interpretation of regions I and III require further study; however, there is little doubt as to the correctness of that for region II.

The above discussion emphasizes that subcritical crack growth is a phenomenon that is complicated by processes involved in the transport of hydrogen to the site at which embrittlement can occur, and possibly further, by the embrittlement interaction and mechanical mechanisms of lattice separation. In any case, it is imperative that a total knowledge of the state and original location of hydrogen, the kinetics of the transport of this hydrogen to the site of embrittlement, and the degree of embrittlement that results from hydrogen being brought to this site be available before we can conclude unambiguously that a particular alloy will or will not exhibit hydrogen embrittlement.

Finally, subcritical crack growth can occur in a metal as a result of the influence of pure mechanical considerations under conditions of cyclic loading and in general is of simple form (fig. 36) expressed by a power dependence of applied stress intensity (eq. (34)). The combined influence of this fatigue-induced subcritical crack growth and hydrogen-induced growth appears, at least in titanium to be the sum of the two processes acting independently (figs. 37 and 38) with no synergistic effect. A similar influence has been postulated concerning the effect of water vapor on the corrosion fatigue of steels (refs. 172, 173). In terms of engineering considerations, the independent nature of these kinetically controlled and mechanically controlled processes suggests that a knowledge of each process and the influence of variables affecting each, such as alloy microstructure, temperature, purity of the environment, form and frequency of loading, can be extrapolated to predict the behavior of an engineering structure under the influence of the combined process. Like any other overall reaction made up of parallel reactions, the combined reaction will be controlled by the individual reaction occurring most rapidly (eq. (16)). For fatigue in a hydrogen environment, the rate of subcritical crack growth will never be less than that observed in hydrogen under conditions of static loading, no matter what the frequency of loading.

MECHANISM OF HYDROGEN EMBRITTLEMENT

Hydrogen embrittlement of a metal can occur when the initiation or growth stages of fracture are influenced by hydrogen. This influence can come about through the effects of hydrogen on the ability of a metal to plastically deform or on the strength of the bond between atoms in the metal lattice. In both stages of fracture, these influences are localized to a relatively small area at the site of crack nucleation or near the crack tip. A number of theories have been proposed to describe the potential influences of hydrogen on these material variables and, in general, fall into one or more of the following categories: pressure formation, surface interaction, lattice interaction, dislocation interaction, and hydride precipitation. Each category, in terms of the observed influences of hydrogen, has a strong experimental base and the occurrence of each really cannot be denied under specific sets of conditions. In this section we will first briefly discuss the theory associated with each of the above categories, and conclude with what is felt by the author to be the limit of applicability of each to the general phenomenon of hydrogen embrittlement of metals.

Pressure formation— Theories based on pressure are the oldest and, until recently, the most popular of the hydrogen embrittlement theories. The commonality of these theories is the suggestion that embrittlement results from “precipitation” of molecular hydrogen at internal voids and the expansion of these voids by the development of high pressures within them. Zapffe and Sims (ref. 165) were among the first to propose that molecular hydrogen could be precipitated and could develop significant pressures at defects within a metal lattice. De Kazinczy (ref. 177) formalized this idea by suggesting that crack propagation occurred by the diffusion of hydrogen to the nucleated voids to maintain the internal stress. Bilby and Hewitt (ref. 178) and others (ref. 179) extended the theory further to consider the contribution of plastic deformation (dislocations) to the initiation and growth of a crack by pressure. The most recent modification was accomplished by Tetelman (ref. 19) who successfully demonstrated the initiation of a crack in Fe–3%Si single crystals and the discontinuous nature of its propagation, and explained these as well as the low temperature and strain rate dependence of embrittlement in terms of pressure build-up.

Surface interaction— The surface interaction theory, first proposed by Petch and Stables (ref. 37) and later modified by Petch (ref. 34), suggests that the fracture stress is lowered by a reduction in the surface energy of a material at the surfaces of a crack by the adsorption of a chemical species. Rebinder (ref. 180) was the first to show that the

adsorption of a surface active substance (water) on the surface of a solid (glass) can greatly decrease the strength because of a decrease in surface energy. Similar effects have been observed in the embrittlement of metals by liquid metal environments (ref. 181). The surface interaction theory is most popular in the explanation of this phenomenon.

The importance of surface energy in the initiation and growth stages of fracture is virtually undisputed. Most models for crack initiation (refs. 20-23) involve a surface energy term. Petch and Stables (ref. 37) related the adsorption mechanism of hydrogen embrittlement of steel to crack initiation, and assumed that hydrogen reduces the surface energy thus favoring the formation of cracks that nucleate according to dislocation theory. Likewise, crack propagation is directly related to surface energy through the modified Griffith criteria (eq. (7)). The question still to be answered, however, is the actual influence of hydrogen on the surface energy of a metal. Numerous experiments have been conducted to explore this effect (refs. 38-40) but, unfortunately, are subject to question because of the lack of complete characterization of the system, condition of the metal surface, contaminant level in the environment, etc.

Lattice interaction— The lattice interaction theory can be considered a generality of the surface interaction theory when the latter is the limiting case of the former. In the lattice interaction theory it is suggested that hydrogen diffuses under the influence of a stress gradient to regions of high tensile stress within the metal lattice to lower the cohesive strength of the lattice. This was first proposed by Troiano and his co-workers (refs. 36, 182, 183) to explain the easier nucleation and propagation of cracks in hydrogen-charged nickel. There is little question that elastic and plastic deformation leads to the redistribution of hydrogen within a metal lattice (refs. 53, 184, 185) and that hydrogen will diffuse toward zones of maximum triaxial stress (ref. 50). These areas of maximum triaxial stress are, of course, ahead of a crack tip or near a notch. Hydrogen will be concentrated in areas that are most probable sites for the nucleation of a crack and is suggested to contribute to nucleation by the reduction of bond energy of the lattice. Crack propagation then becomes a series of nucleation events ahead of the crack tip. Like the surface interaction theory, the question of the actual influence of hydrogen on the cohesive forces of a metal lattice remains to be answered.

Dislocation interaction— The theory of dislocation interaction involves the possibility that hydrogen combines with dislocations (ref. 186) by the formation of atmospheres

reducing dislocation mobility (ref. 27) thereby reducing the plastic zone associated with the crack tip and allowing the crack to propagate at a lower stress in a more brittle manner (eq. (5)). This was first suggested by Bastien and Azou (refs. 187, 188) as applied to the embrittlement of iron alloys. These ideas have been employed extensively by the Russians (refs. 57, 189, 190) to explain hydrogen embrittlement of endothermic occluding metals but have not gained broad acceptance. Kolachev (ref. 57) expresses belief that support for the dislocation interaction theory comes from the fact that hydrogen embrittlement is influenced by but not directly dependent on crystal structure, the formation of hydrides, solubility, rate of hydrogen diffusion, etc. The dislocation nature of embrittlement, however, is common to all metals and thus embrittlement must be considered to result from the interaction of hydrogen with this common element – dislocation motion.

Hydride precipitation— A second-phase hydride precipitate appears to cause embrittlement of exothermic occluding metals. Metal hydrides are not only brittle but they are less dense than the metal matrix and thus have been proposed in a number of theories to preferentially precipitate at dislocations (ref. 191) ahead of the crack tip at regions of high triaxial stress (ref. 192) and at defects such as grain boundaries (ref. 193) influencing both the crack initiation and growth stages of fracture. There is little question that hydride embrittlement of a metal can occur; however, it is specific to a relatively small group of metals although attempts have been made to generalize its application (ref. 194).

Hydrogen embrittlement of metals— Hydrogen has been observed to influence the fracture behavior of *all* metals investigated to date. In a few metals, however, these effects are seen only when the lattice contains a supersaturated concentration of hydrogen with respect to the lattice equilibrium solubility or terminal solubility. Under this condition, exothermic occluding metals such as titanium, zirconium, and vanadium will precipitate a brittle hydride phase, and most endothermic occluding metals such as iron, copper, and aluminum will precipitate molecular hydrogen while some endothermic occluding metals such as nickel, magnesium and palladium will precipitate either molecular hydrogen or a hydride phase depending on the degree of supersaturation. The extent, location, and rate of second phase precipitation as well as the form of applied load will determine the severity of embrittlement. If precipitation is extensive, all metals can fail even without an applied load because of pressure build-up of molecular hydrogen at internal defects (ref. 76) or the stresses developed around the less dense hydride precipitate (ref. 195). If precipitation is not

this extensive but complete the metals containing hydrides can be embrittled at rapid loading rates by crack initiation and growth within the hydride phase (ref. 196) while those containing precipitated molecular hydrogen will be little affected because of the rapid reduction in hydrogen pressure because of void growth (ref. 76). At low rates of loading metals containing hydrides will be little affected because of plastic relaxation about the hydride (ref. 43) while those containing molecular hydrogen will be embrittled by the continued pressure build-up as the result of nonsteady-state hydrogen transport to the void (ref. 76). If precipitation is not complete but just beginning, no effect may be observed in metals forming hydrides of molecular hydrogen at rapid loading rates because the rate of precipitation is slow compared to the rate of loading. At slow rates of loading, embrittlement can be observed with its severity dependent on the rate process controlling precipitation.

Precipitation of a hydrogen-rich second phase in metals need not be associated only with nonequilibrium precipitation from the supersaturated bulk lattice as discussed above. It can also occur as the result of a localized supersaturation. The extreme example is the well documented hydrogen "bubble" formation observed in electrolytically charged (ref. 197) and proton charged aluminum (ref. 198). Likewise, surface hydride precipitation has been observed in columbium (ref. 159), tantalum (ref. 160), and titanium (figs. 28 and 29) exposed to a gaseous hydrogen environment at room temperature. The conditions for localized precipitation are, first, a localized hydrogen concentration greater than the equilibrium solubility or the terminal solid solubility must exist and, second, hydrogen transport within the metal lattice must be sufficiently slow to maintain the localized supersaturation during precipitation. These conditions are easily met in the exposure of exothermic-occluding hydride-forming metals to even a low-pressure gaseous-hydrogen environment. For example, in α -titanium employing the established relations for the terminal solid solubility at the $\alpha/(\alpha + \gamma)$ solvus (refs. 104, 149) the equilibrium pressure above which hydride formation will occur can be calculated as approximately 5×10^{-14} torr at room temperature; that is, at hydrogen pressures above 5×10^{-14} hydride formation should be controlled by nonequilibrium reaction kinetics and should be independent of pressure. Second-phase precipitation of molecular hydrogen will not occur in endothermic occluding metals such as steel and nickel exposed to a hydrogen environment. In these alloys the terminal solid solubility (if one exists) is greater than the lattice concentration

obtainable by normal environmental hydrogen pressures so a supersaturated lattice will not occur at a constant pressure and temperature.

Severe embrittlement of an exothermic-occluding hydride-forming metal, such as titanium, can occur in a gaseous hydrogen environment (table 3). This form of embrittlement is the result of the localized-surface, or near-surface, precipitation of the brittle hydride phase as discussed above. Severity of embrittlement is controlled either by the kinetics of the hydride reaction or hydrogen transport to the location of embrittlement. In metals that have a single phase microstructure or a mixed phase microstructure in which the hydride forming phase is continuous such as an α -phase titanium matrix containing a discontinuous β -phase, severity of embrittlement will be independent of molecular hydrogen pressure (fig. 21) with failure occurring by transgranular cleavage (fig. 10(b)) as determined by the crystallographic nature of the precipitated hydride (figs. 28 and 29) (ref. 199). If the metal is made up of a mixed microstructure in which the continuous phase is not the hydride-forming phase, such as a β -phase titanium matrix containing a discontinuous α -phase, embrittlement may be more severe (fig. 22), with the continuous phase acting as a path for rapid hydrogen transport to the hydride-forming phase. Under these conditions embrittlement might be pressure dependent (fig. 21), might be controlled by the transport reaction, and might occur by brittle intergranular separation of the α/β boundary (fig. 11(b)).

Second-phase precipitation is a sufficient but not necessary condition for the occurrence of hydrogen embrittlement. Embrittlement has been observed at hydrogen concentrations below the terminal solid solution solubility limit in the exothermic occluding vanadium alloy (ref. 200) as well as in several endothermic occluding metals subjected to deformation within a low pressure hydrogen environment (table 3). Under conditions where hydrogen is present in solid solution within the metal lattice, applied load is able to concentrate the hydrogen at areas of lattice distortion (ref. 53), for example, areas of triaxial stress ahead of a crack tip or at a grain boundary. Hydrogen in these areas, prior to the attainment of a critical concentration for precipitation, might deleteriously affect lattice cohesion to the extent that crack nucleation and propagation is possible. In a hydrogen environment the hydrogen-lattice interaction appears to occur on or just below the crack tip (at least in the 4130 steel alloy investigated in this study) and can be considered the limiting

case of lattice interaction (i.e , surface interaction). Here too, embrittlement appears to be associated with a change in lattice cohesion or a reduction in surface energy.

Embrittlement as the result of a hydrogen-lattice interaction, unlike embrittlement by second-phase precipitation, is always associated with a brittle mode of failure, either transgranular (fig. 32) or intergranular (figs. 7 and 12(b)), apparently dependent on the site of crack initiation and relative strength of the grain boundaries (ref. 166). Hydrogen-induced brittle mode of failure sometimes observed in metals embrittled by molecular hydrogen precipitation is probably associated with the hydrogen-lattice interaction at the void surface (refs. 178, 179) in much the same manner as environmental hydrogen embrittlement.

Severity of embrittlement because of a surface or lattice interaction is dependent not only on the potential reduction in cohesive strength but also on hydrogen transport processes. In environmental hydrogen, the hydrogen must be transported to the crack tip. Those metals that exhibit little or no hydrogen chemisorption, such as aluminum, copper, and magnesium, are not embrittled (table 3) while those metals in which the transport processes occur, such as nickel and steel, are severely affected by hydrogen — the rate of embrittlement determined by the particular controlling transport reaction (fig. 14). In metals where hydrogen is present in solution, it is important, first, that hydrogen be soluble in the metal lattice to the extent that sufficient hydrogen is available to interact with the lattice and, second, that lattice diffusion transport of hydrogen can occur at a significant rate.

In view of the above interpretation it is informative to qualitatively compare the relative values of hydrogen solubility and rate of transport with severity of embrittlement observed in several endothermic occluding metals. A tabulation of hydrogen solubility at 1 atm and diffusivity normalized to a common temperature of 200° C is seen in table 4. In a gaseous hydrogen environment it has been shown (table 3) that martensitic steel and nickel alloys are the most severely embrittled followed by molybdenum with copper and aluminum as well as stabilized austenitic steel not embrittled. From table 4 there appears to be a rough correlation between severity of environmental embrittlement and hydrogen solubility with the exception of austenitic steels. As mentioned previously, copper and aluminum do not chemisorb hydrogen (table 1) so they should not exhibit environmental embrittlement. It is possible that the austenitic steels do not chemisorb hydrogen near room

temperature (a point that has never been investigated), which could explain its lack of susceptibility. When hydrogen is present within the metal lattice, there is little question that martensitic steels are the most severely embrittled (refs. 87-89) followed by nickel alloys (refs. 100, 101). The alloys of molybdenum (ref. 117), copper (ref. 124), and iron having a stable austenitic structure (refs. 90, 91) can be embrittled if the lattice contains a large supersaturation of hydrogen. In these alloys, as well as the two previous, the mode of hydrogen induced failure is brittle separation along the grain boundaries. Aluminum can also be influenced by hydrogen only at very large supersaturations and, unlike the others, failure is always by ductile tearing (ref. 123). If we consider the combined values of solubility and diffusivity (the actual measure of hydrogen transport within a metal lattice), there is a rough correlation between this value and the susceptibility of these metals to this form of embrittlement. Lattice transport occurs rapidly in martensitic iron followed by nickel; is moderate to slow in molybdenum, copper, and austenitic iron; and extremely slow in aluminum. We admit that these rough correlations add little to the understanding of hydrogen embrittlement but they do not distract and in general are consistent with our interpretation.

The contribution of the hydrogen-dislocation interaction to the embrittlement of metals appears to be of secondary importance. There is little doubt that hydrogen can combine with dislocations and influence their motion in iron (refs. 201, 202), molybdenum (ref. 118), vanadium (ref. 203), columbium (ref. 204), and nickel (refs. 205, 106) as well as increase the rate of hydrogen transport within the lattice by this association with dislocation movement (ref. 207). In general, these effects require a large hydrogen concentration throughout the bulk lattice. Latanision and Staehle (ref. 208) have demonstrated an influence of a high localized concentration on deformation of nickel single crystals; however, such a localized concentration is still much higher than obtainable from a gaseous hydrogen environment at room temperature. In the present study, cleavage crack propagation across Fe-3%Si grains was observed to occur without *any* apparent evidence of deformation about the fracture surface (figs. 30 and 31). Additionally, the effects of fatigue crack growth and gaseous hydrogen-induced crack growth in titanium appear to be independent processes (figs. 38 and 39); the former, of course, associated with deformation (dislocation motion), thus eliminating any significant contribution of dislocation motion to the latter.

A COMPARISON BETWEEN HYDROGEN EMBRITTLEMENT AND OTHER FORMS OF EMBRITTLEMENT

In 1963 Nichols and Rostoker (ref. 209) made the analogy between stress corrosion cracking and liquid metal embrittlement of solid metals. Since then the analogies between these and other forms of embrittlement have become even more apparent. Based on evidence originally put forth by Williams and Nelson (ref. 138) indicating the surface or near-surface nature of gaseous hydrogen embrittlement of an endothermic occluding metal (steel) and the verification and expansion of this idea in the present investigation, it is apparent that hydrogen embrittlement may also be a specific manifestation of a more general embrittlement phenomenon involving several chemical species. The embrittlement of metals by a liquid metal environment and embrittlement by a number of stress corrosion cracking environments exhibit, at least qualitatively, similar physical characteristics as do embrittlement by a solid metal environment, a gaseous hydrogen environment, and others.

One of the more obvious similarities is the species-induced change in fracture mode of a ductile metal to brittle separation without an associated change in flow behavior in a liquid metal (ref. 210), a solid metal (ref. 211), a stress corrosion (refs. 157, 212), and a gaseous hydrogen (figs. 7 and 12(b)) environment. (As discussed in a previous section, hydrogen can influence the deformation behavior of some metals; however, this appears to be only of secondary importance.) As observed for hydrogen in this study, stress corrosion cracking is intergranular but transgranular cracking predominates in certain instances. Cracking produced by liquid metals also follows intercrystalline paths in the preponderance of instances, but transcrystalline cracking is not infrequent.

Severity of embrittlement is dependent on the strain rate of the test and is more severe the slower the strain rate or if the test is conducted under a static load. As established in this investigation, this rate effect in a gaseous hydrogen environment is related to the kinetics of hydrogen transport to the site of interaction on or very near the surface of the crack. Until only recently the observed inverse strain-rate dependence of liquid metal embrittlement was thought to result entirely from the strain-rate dependence of the stress to cause deformation at the crack tip (refs. 213, 214); however, the classic works of Mostovoy and Breyer (refs. 215, 216) on leaded steel followed by the demonstration by Fager and Spurr (refs. 211, 217) that solid cadmium can embrittle metals suggests that transport

considerations proposed for gaseous hydrogen embrittlement are important in these other forms of embrittlement as well.

Let us next consider the temperature dependence of embrittlement. In general, liquid metal embrittlement is observed to exhibit a brittle-to-ductile transition with increasing temperature (ref. 218) and numerous forms of dependency have been observed in the stress corrosion cracking behavior of metals (refs. 219, 220). Until recently the accepted explanation for these dependencies has involved the temperature dependence of plastic flow in metals; however, the works on solid metal embrittlement (refs. 211, 216, 217) together with that of this investigation suggest that the various forms of temperature dependence stems from the elementary transport reactions controlling the embrittlement process.

Finally, all forms of embrittlement are extremely sensitive to variations in the microstructure of the embrittled metal. Besides the obvious influence of microstructure on the transport reaction processes, as apparent in this investigation, species embrittlement is nothing more than a special case of the more general brittle fracture theory (eq. (1)). Thus, metallurgical parameters that tend to induce brittle fracture free of the effect of the species should be involved and include large grain size, high yield stress over modulus ratio, heterogeneous deformation, etc.

Ames Research Center

National Aeronautics and Space Administration

Moffett Field, Calif., 94035, Dec. 2, 1971

REFERENCES

1. Steigerwald, E. A.; Schaller, F. W.; and Troiano, A. R.: Discontinuous Crack Growth in Hydrogenated Steel. Met. Soc. of AIME, Trans., vol. 215, Dec. 1959, pp. 1048-1052.
2. Troiano, A. R.: Embrittlement by Hydrogen and Other Interstitials. Metal Progress, vol. 77, Feb. 1950, pp. 112-117.
3. Smialowski, M.: Hydrogen in Steel. Addison-Wesley, Reading, Mass., 1962.
4. Schuetz, A. E.; and Robertson, W. D.: Hydrogen Absorption, Embrittlement, and Fracture of Steel. Corrosion, vol. 13, July 1957, pp. 437t-458t.
5. Tetelman, A. S.; Wagner, C. N. J.; and Robertson, W. D.: An X-Ray Investigation of the Effects of Hydrogen in Iron. Acta Met., vol. 9, March 1961, pp. 205-215.
6. Geyer, N. M.; Lawless, G. W.; and Cohen, B.: A New Look at the Hydrogen Embrittlement of Cadmium Coated High Strength Steels. American Electroplaters' Society, Technical Proceedings, 1960, pp. 143-151.
7. Hofmann, W.; and Rauls, W.: Production of Fish Eyes on Steel by External Effect of Hydrogen at Room Temperature. Arch. Eisenhüttenwesen, vol. 32, March 1961, pp. 169-173.
8. Schwartz, J. H.; and Ward, J. J.: Direct Energy Conversion. NASA SP-5057, 1968, pp. 281-303.
9. Moeckel, W. E.: Propulsion Systems for Manned Exploration of the Solar System. NASA TM X-1864, 1969.
10. Griffith, A. A.: The Phenomenon of Rupture and Flow in Solids. Phil Trans., vol. A221, 1920, pp. 163-198.
11. Westergaard, H. M.: Bearing Pressures and Cracks. J. Appl. Mech., Vol. 5, 1939, pp. A-49—A-55.
12. Irwin, G. R.: Analysis of Stresses and Strains Near the End of a Crack Traversing a Plate. J. Appl. Mech., vol. 24, 1957, pp. 361-372.
13. Irwin, G. R.: Fracture. Encyclopedia of Physics. Vol. 6, Springer (Berlin), 1958, pp. 551-590.
14. Paris, P. C.; and Sih, G. C.: Stress Analysis of Cracks. Fracture Toughness Testing and Its Applications. ASTM STP 381, 1965, pp. 30-81.

15. Rice, J. R.; and Rosengren, G. F.: Plane Strain Deformation Near a Crack Tip in a Power Law Hardening Material. J. Mech. and Phys. of Solids, vol. 6, 1968, pp. 1-12.
16. Dugdale, D. S.: Yielding of Steel Sheets Containing Slits. J. Mech. and Phys. of Solids, vol. 8, 1960, pp. 100-104.
17. Drucker, D. C.; and Rice, J. R.: Plastic Deformation in Brittle and Ductile Fracture. Brown University, Div. of Engr., ARPA E57, July 1968.
18. Orowan, E.: Energy Criteria of Fracture. Weld. J. Res. Suppl., vol. 34, March 1955, pp. 1575-1588.
19. Tetelman, A. S.; and McEvelly, A. J., Jr.: Fracture of Structural Materials. John Wiley and Sons, Inc., New York, 1967.
20. Stroh, A. N.: The Existence of Microcrack After Cold-Work. Phil. Mag., vol. 2, Jan. 1957, pp. 1-4.
21. Stroh, A. N.: The Cleavage of Metal Single Crystals. Phil. Mag., vol. 3, June 1958, pp. 597-606.
22. Cottrell, A. H.: Theory of Brittle Fracture in Steel and Similar Metals. Met. Soc. of AIME, Trans., vol. 212, April 1958, pp. 192-203.
23. Gilman, J. J.: Fracture of Zin-Monocrystals and Bicrystals. Met. Soc. of AIME, Trans., vol. 212, Dec. 1958, pp. 783-793.
24. Robertson, W. D.; and Tetelman, A. S.: A Unified Structural Mechanism for Intergranular and Transgranular Corrosion Cracking. Strengthening Mechanisms in Solids, ASM, Metals Park, Ohio, 1962, pp. 217-252.
25. Head, A. K.: The Interaction of Dislocations and Boundaries. Phil. Mag., vol. 44, 1953, pp. 92-94.
26. Kramer, I. R.: Role of the Surface Layer in the Plastic Deformation of Aluminum. Environment-Sensitive Mechanical Behavior, Gordon and Breach, New York, 1966, pp. 127-146.
27. Cottrell, A. H.: Dislocations and Plastic Flow. Oxford University Press (Oxford), 1953.
28. Coulomb, P.; and Friedel, J.: On the Formation of Cavities Along Dislocations. Dislocations and Mechanical Properties of Crystals, John Wiley and Sons, Inc., New York, 1957, pp. 555-572.
29. Parkins, R. N.: Stress-Corrosion Cracking. Met. Rev., vol. 9, 1964, pp. 201-260.

30. Tromans, D.; and Nutting, J.: Electron Microscope Studies of Stress Corrosion Cracking. Fracture of Solids, John Wiley and Sons, Inc., New York 1963, pp. 637-655.
31. Boyd, J. D.; Haynie, F. H.; Moreland, P. J.; Boyd, W. K.; Wood, R. A.; Williams, D. N.; and Jafee, R. I.: The Effect of Composition on the Mechanism of Stress-Corrosion Cracking of Titanium Alloys. NASA Contract NASr-100(09), Jan. 1968.
32. Haynes, R.; and Maddocks, P. J.: Hydrogen Embrittlement of Titanium. J. Met. Sci., vol. 3, 1969, pp. 190-195.
33. Coleman, E. G.; Weinstein, D.; and Rostoker, W.: On a Surface Energy Mechanism for Stress-Corrosion Cracking. Acta Met., vol. 9, May 1961, pp. 491-496.
34. Petch, N. J.: The Lowering of Fracture-Stress Due to Surface Adsorption. Phil. Mag., vol. 1, 1956, pp. 331-337.
35. Stoloff, N. S.; and Johnston, T. L.: Crack Propagation in a Liquid Metal Environment. Acta Met., vol. 11, April 1963, pp. 251-256.
36. Troiano, A. R.: Delayed Failure of High Strength Steels. Corrosion, vol. 15, April 1959, pp. 207t-212t.
37. Petch, N. O.; and Stables, P.: Delayed Fracture of Metals Under Static Load. Nature, vol. 169, May 1952, pp. 842-843.
38. Wexler, S.: Deposition of Atomic Beams. Rev. Mod. Phys., vol. 30, April 1958, pp. 402-409.
39. Geus, J. W.: The Effect of Chemisorption on Collective Metal Properties. Surface Sci., vol. 2, 1964, pp. 48-55.
40. Swanson, L. W.; Bell, A. E.; Hinrichs, C. H.; Crouser, L. C.; and Evans, B. E.: Literature Review of Adsorption on Metal Surfaces. Vols. I and II, NASA CR 72,402, 1967.
41. Williams, D. P.; and Gasser, R. P. H.: Low Energy Electron Desorption of Mixed Adsorbates. Surface Sci., vol. 25, 1971, pp. 265-272.
42. Janssen, M. M. P.: FMR Study of Surface-Tension-Related Stress Effects in Ultraclean Ni Thin Films. J. Appl. Phys., vol. 41, Jan. 1970, pp. 384-398.
43. Coleman, C. E.; and Hardie, D.: The Hydrogen Embrittlement of α -Zirconium – A Review. J. Less-Common Met., vol. 11, 1966, pp. 168-185.

44. Tetelman, A. S.; and Robertson, W. D.: The Mechanism of Hydrogen Embrittlement Observed in Iron-Silicon Single Crystals. Met. Soc. of AIME, Trans., vol. 224, Aug. 1962, pp. 775-783.
45. Duran, Servet Ahmet: Temperature Dependence of the Creep of Metals. Ph. D. Thesis, Dept. of Engineering, Stanford Univ., Stanford, California, Feb. 1963.
46. Moore, W. J.: Physical Chemistry. Prentice-Hall, Englewood Cliffs, N. J., 1962.
47. Barrer, R. M.: Diffusion in and Through Solids. Cambridge University Press (London), 1951.
48. Ash, R.; and Barrer, R. M.: Permeation of Hydrogen Through Metals. Phil. Mag., vol. 4, 1959, pp. 1197-1206.
49. Shupe, D. S.; and Stickney, R. E.: Thermodynamics of the Solubility and Permeation of Hydrogen in Metals at High Temperature and Low Pressure. J. Chem. Phys., vol. 51, Aug. 1969, pp. 1620-1625.
50. Oriani, R. A.: Hydrogen in Metals. Fundamental Aspects of Stress Corrosion Cracking, Natl. Assoc. of Corrosion Engrs., Houston, Texas, 1969, pp. 32-49.
51. Sieverts, A.: Die Aufnahme von Gasen Durch Metalle. Z. Metallkunde, vol. 21, Feb. 1929, pp. 37-45.
52. Oriani, R. A.: On the Partial Molal Volume of Hydrogen in Alpha Iron. Met. Soc. of AIME, Trans., vol. 236, Sept. 1966, pp. 1368-1369.
53. Beck, W.; Subramanyan, P. K.; and Williams, F. S.: Interpretation of Some Hydrogen Embrittlement Phenomena. Corrosion, vol. 27, March 1971, pp. 115-118.
54. Ridley, N.; and Stuart, H.: Partial Molal Volume of Carbon in Iron. Metal. Sci. J., vol. 4, Nov. 1970, pp. 219-222.
55. Lord, A. E., Jr.: Diffusion of Hydrogen in α -Iron at About 120° K. Acta Met., vol. 15, July 1967, pp. 1241-1244.
56. Hurd, D.: Introduction to the Chemistry of Hydrides. John Wiley and Sons, Inc., New York, 1952.
57. Kolachev, B. A.: Hydrogen Embrittlement of Nonferrous Metals. Israel Program for Scientific Translations (Translated from Russian), Jerusalem, 1968.
58. Boniszewski, T.; and Smith, G. C.: A Note on Nickel Hydride. J. Phys. Chem. Solids, vol. 21, 1961, pp. 115-118.

59. Wayman, M. L.; and Smith, G. C.: The Effects of Hydrogen on the Deformation and Fracture of Nickel-Iron Alloys. Acta Met., vol. 19, March 1971, pp. 227-231.
60. Frauenfelder, R.: Permeation of Hydrogen Through Tungsten and Molybdenum. J. Chem. Phys., vol. 48, May 1968, pp. 3955-3965.
61. Gonzalez, O. D.: The Measurement of Hydrogen Permeation in Alpha Iron: An Analysis of the Experiments. Met. Soc. of AIME, Trans., vol. 245, April 1969, pp. 607-612.
62. Gulbransen, E. A.; and Andrew, K. F.: Kinetics of the Reactions of Titanium With O₂, N₂, and H₂. Metals Trans., vol. 185, Oct. 1949, pp. 741-748.
63. Zener, C.: Imperfections in Nearly Perfect Crystals. John Wiley and Sons, Inc., New York, 1952.
64. Schenck, H.; and Taxhet, H.: Diffusion und Durchgang von Wasserstoff bei Reinem Eisen und bei Stahl im Bereich Höherer Temperaturen. Arch. Eisenhüttenwesen, vol. 30, Nov. 1959, pp. 661-668.
65. Holman, W. R.; Crawford, R. W.; and Paredes, F., Jr.: Hydrogen Diffusion in Beta-Titanium Alloy. Met. Soc. of AIME, Trans., vol. 233, Oct. 1965, pp. 1836-1839.
66. Wasilewski, R. J.; and Kehl, G. L.: Diffusion of Hydrogen in Titanium. Metallurgica, vol. 50, Nov. 1954, pp. 225-230.
67. Van Ness, H. C.; and Dodge, B. F.: Effects of Hydrogen at High Pressures on the Mechanical Properties of Metals. Chem. Eng. Prog., vol. 51, 1955, pp. 266-272.
68. Cavett R. H.; and Van Ness, H. C.: Embrittlement of Steel by High-Pressure Hydrogen Gas. Weld. J. Res. Supp., vol. 42, July 1963, pp. 316s-319s.
69. Thygeson, J. R., Jr.; and Molstad, M. C.: High Pressure Hydrogen Attack on Steel. J. Chem. Eng. Data., vol. 9, April 1964, pp. 309-315.
70. Hofmann, W.; and Rauls, W.: Ductility of Steel Under the Influence of External High Pressure Hydrogen. Weld. J. Res. Supp., vol. 44, May 1965, pp. 225s-230s.
71. Hanna, G. L.; and Steigerwald, E. A.: Influence of Environment on Crack Propagation and Delayed Failures in High-Strength Steels. Tech. Doc. Report RTD-TDR-63-4225, Contract AF 33(657)-7512, Air Force Material Lab., Wright-Patterson Air Force Base, Ohio, Jan. 1964.

72. Steinman, J. B.; Van Ness, H. C.; and Ansell, G. S.: The Effect of High-Pressure Hydrogen Upon the Notch Tensile Strength and Fracture Mode of 4140 Steel. Weld. J. Res. Supp., vol. 44, May 1965, pp. 221s-224s.
73. McPherson, W. B.: Hydrogen Embrittlement-Potential Shuttle Impact. NASA TM X-64,521, 1969, pp. 59-67.
74. Walter, R. J.; and Chandler, W. T.: Effect of High-Pressure Hydrogen on Metals. ASM Report D8-14.2, ASM Report System, Metals Park, Ohio, 1968.
75. Hancock, G. G.; and Johnson, H. H.: Hydrogen, Oxygen, and Subcritical Crack Growth in a High-Strength Steel. Met. Soc. of AIME, Trans., vol. 236, April 1966, pp. 513-516.
76. Tetelman, A. S.: The Mechanism of Hydrogen Embrittlement in Steel. Fundamental Aspects of Stress Corrosion Cracking, Natl. Assoc. of Corrosion Engrs., Houston, Texas, 1969, pp. 446-460.
77. Hayward, D. O.; and Trapnell, B. M. W.: Chemisorption. Butterworths (London), 1964.
78. Pritchard, J.; and Tompkins, F. C.: Surface Potential Measurements – The Adsorption of Hydrogen by Group IB Metals. Trans. Faraday Soc., vol. 56, 1960, pp. 540-550.
79. Pritchard, J.: Surface-Potential Study of the Chemisorption of Hydrogen and Carbon Monoxide on Evaporated Copper and Gold Films. Trans. Faraday Soc., vol. 59, 1963, pp. 437-452.
80. Brown, W. F.; and Srawley, J. E.: Plane Strain Crack Toughness Testing of High Strength Metallic Materials. ASTM Publ. 410, Philadelphia, Penn., 1965.
81. Brennan, D.; and Fletcher, P. C.: The Atomization of Hydrogen on Tungsten. Proc. Roy. Soc., London, vol. A250, 1959, pp. 389-408.
82. Williams, J. C.; and Blackburn, M. J.: A Comparison of Phase Transformations in Three Commercial Titanium Alloys. Trans. ASM, vol. 60, 1967, pp. 373-383.
83. Geller, V. W.; and Sun, T. H.: Einflub von Legierungszusätzen auf die Wasserstoffdiffusion im Eisen und Beitrag zum System Eisenwasserstoff. Archiv. Eisenhüttenwesen, vol. 21, Nov.-Dec. 1950, pp. 423-430.

84. Van Der Sluys, W. A.: Mechanisms of Environment-Induced Subcritical Flow Growth in AISI 4130 Steel. Engr. Fracture Mech., vol. 1, 1969, pp. 447-462.
85. Hanna, G. L.; Troiano, A. R.; and Steigerwald, E. A.: Mechanism of the Embrittlement of High-Strength Steels by Aqueous Environments. Trans. ASM, vol. 57, 1964, pp. 658-663.
86. Johnson, H. H.; and Willner, A. M.: Moisture and Stable Crack Growth in a High Strength Steel. Appl. Mat. Res., vol. 4, Jan. 1965, pp. 34-40.
87. Toh, T.; and Baldwin, W. M., Jr.: Ductility of Steel With Varying Concentrations of Hydrogen. Stress Corrosion Cracking and Embrittlement, John Wiley and Sons, Inc., New York, 1956, pp. 176-186.
88. Barth, C. F.; Steigerwald, E. A.; and Troiano, A. R.: Hydrogen Permeability and Delayed Failure of Polarized Martensitic Steels. Corrosion, vol. 25, Sept. 1969, pp. 353-358.
89. Hill, M. L.; and Johnson, E. W.: Hydrogen in Cold Worked Iron-Carbon Alloys and the Mechanism of Hydrogen Embrittlement. Met. Soc. of AIME, Trans., vol. 215, 1959, pp. 717-724.
90. Hobson, J. D.; and Hewitt, J.: Hydrogen Embrittlement of Stainless Steel. J. Iron Steel Inst., vol. 173, 1953, pp. 131-139.
91. Benson, R. B., Jr.; Dann, R. K.; and Roberts, L. W., Jr.: Hydrogen Embrittlement of Stainless Steel. Met. Soc. of AIME, Trans., vol. 242, Oct. 1968, pp. 2199-2205.
92. Vaughan, D. A.; and Phalen, D. I.: Effect of Hydrogen on the Structural Properties of Stainless Steel. ASM Tech. Report P-12-3-64, ASM Report System, Metals Park, Ohio, 1964.
93. Holzworth, M. L.: Hydrogen Embrittlement of Type 304L Stainless Steel. Corrosion, vol. 25, March 1969, pp. 107-115.
94. Vennett, R. M.; and Ansell, G. S.: A Study of Gaseous Hydrogen Damage in Certain FCC Metals. Trans. ASM, vol. 62, 1969, pp. 1007-1013.
95. Vennett, R. M.; and Ansell, G. S.: The Effect of High-Pressure Hydrogen Upon the Tensile Properties and Fracture Behavior of 304L Stainless Steel. Trans. ASM, vol. 60, 1967, pp. 242-251.
96. Armbruster, M. H.: Hydrogen Solubility in Metals. J. Amer. Chem. Soc., vol. 65, 1943, pp. 1043-1054.

97. Chang, P. L.; and Bennett, W. D. G.: Diffusion of Hydrogen in Iron and Iron Alloys at Elevated Temperatures. J. Iron Steel Inst., March 1952, pp. 205-213.
98. Lorenz, P. M.: Effect of Pressurized Hydrogen Upon Inconel 718 and 2219 Aluminum. ASM Report W9-13.2, ASM Report System, Metals Park, Ohio, 1969.
99. Rentler, R. M.; and Welinsky, I. H.: Effect of HNO₃-HF Pickling on the Stress-Corrosion Cracking of Ni-Cr-Fe Alloy 600 in High Purity Water at 600° F. WAPD-TM-944, Bettis Atomic Power Lab., Westinghouse Electric Corp., Oct. 1970.
100. Windle, A. H.; and Smith, G. C.: The Effect of Hydrogen on the Deformation and Fracture of Polycrystalline Nickel. Metal Sci. J., vol. 4, 1970, pp. 136-144.
101. Mihelich, J. L.; and Troiano, A. R.: Delayed Failure in a Hydrogenated Face-Centered-Cubic Alloy of Nickel. Nature, vol. 197, March 1963, pp. 996-997.
102. Blanchard, P.; and Troiano, A. R.: Hydrogen Embrittlement of Metals. Mem. Sci. Rev. Metall., vol. 57, June 1960, pp. 409-422.
103. Koster, W. L.; Bangert, W. L.; and Evers, M.: Damping Phenomenon of Hydrogen Impregnated Titanium. Z. Metallkunde, vol. 47, Aug. 1956, pp. 564-570.
104. McQuillan, A. D.: An Experimental and Thermodynamic Investigation of the Hydrogen-Titanium System. Proc. Roy. Soc., London, vol. A204, Dec. 1950, pp. 309-325.
105. Wasilewski, R. J.; and Kehl, G. L.: Diffusion of Hydrogen in Titanium. Metallurgica, vol. 50, Nov. 1954, pp. 225-230.
106. Craighead, C. M.; Lenning, G. A.; and Jaffee, R. I.: Hydrogen Embrittlement of Beta-Stabilized Titanium Alloys. J. Metals, Trans. AIME, vol. 206, Aug. 1956, pp. 923-932.
107. Westlake, D. G.: Mechanical Behavior of Niobium (Columbium)-Hydrogen Alloys. Met. Soc. of AIME, Trans., vol. 245, Sept. 1969, pp. 1969-1973.
108. Clauss, A.; and Forestier, H.: Fragilité du Tantale en Présence d'Hydrogène à Température Ambiante. Comp. Rendus, vol. 246, Sept. 1958, pp. 3241-3248.

109. Sherman, D. H., Owen, C. V.; and Scott, T. E.: The Effect of Hydrogen on the Structure and Properties of Vanadium. Met. Soc. of AIME, Trans., vol. 242, Sept. 1968, pp. 1775-1784.
110. Inouye, H.; and Schaffhauser, A. C.: Low-Temperature Ductility and Hydrogen Embrittlement of Uranium – A Literature Review. Report ORNL-TM-2563, Contract W-7405-eng-26, U. S. Atomic Energy Commission, July 1969.
111. Chandler, W. T.; and Walter, R. J.: Hydrogen Effects in Refractory Metals. Proc. Symp. on Metallurgy and Technology of Refractory Metal Alloys, Washington, D. C., April 1968.
112. Powell, D. T.; and Scully, J. C.: Stress Corrosion Cracking of Alpha-Titanium Alloys at Room Temperature. Corrosion, vol. 24, June 1968, pp. 151-158.
113. Lenning, G. A., Craighead, C. M.; and Jaffee, R. I.: The Effect of Hydrogen on the Mechanical Properties of Titanium. Contract DA-33-019-ORD-938, U. S. Army, Watertown Arsenal, 1955.
114. Jaffee, R. I.; Lenning, G. A.; and Craighead, C. M.: Effect of Testing Variables on the Hydrogen Embrittlement of Titanium and a Ti-8 pct Mn Alloy. J. Metals, Trans. AIME, vol. 8, Aug. 1956, pp. 908-913.
115. Berger, L. W.; Williams, D. N.; and Jaffee, R. I.: Hydrogen in Titanium-Aluminum Alloys. Met. Soc. of AIME, Trans., vol. 212, Aug. 1958, pp. 509-513.
116. Sieverts, A.; and Gruning, K.: Das Aufnahmevermögen der Eisen-Molybden-Legierungen für Wasserstoff und Stickstoff. Arch Eisenhüttenw, vol. 7, May 1934, pp. 641-652.
117. Rengstorff, G. W. P.; and Fisher, R. B.: Cast Molybdenum of High Purity. J. Metals, Trans. AIME, vol. 4, Feb. 1952, pp. 157-160.
118. Lawley, A.; Liebmann, W.; and Maddin, R.: Effect of Hydrogen on the Yielding Behavior of Molybdenum. Acta Met., vol. 9, Sept. 1961, pp. 841-850.
119. Sharov, M. V.; and Serebryakov, V. V.: Nauchnye Doklady Vyssei Shkoly. Metallurgiya, vol. 2, 1958, pp. 307-312.
120. Day, J. H.: Embrittlement of Magnesium Alloy by Water Vapor. J. Nucl. Mater., vol. 11, 1964, pp. 249-251.
121. Bircumshaw, L. L.: Hydrogen Solubility in Aluminum. Trans. Faraday Soc., vol. 31, 1935, pp. 1439-1441.

122. Lieser, K. H.; and Witte, H.: Solubility of Hydrogen Alloys. Z. Phys. Chem., vol. 202, Jan. 1954, pp. 321-351.
123. Eichenauer, W.; Hattenbach, K.; and Pebler, A. Z.: Solubility of Hydrogen in Solid and Liquid Aluminum. Z. Metallkunde, vol. 52, Oct. 1961, pp. 682-684.
124. Opie, W.; and Grant, N.: Hydrogen Segregation in Aluminum; The Effects of Hydrogen on the Mechanical Properties of Aluminum Alloys Containing 5 pct Si. Foundry, vol. 78, 1950, pp. 104-109.
125. Moroz, L. S.; Kolgatin, N. N.; Teodorovich, V. P.; and Deryabina, V. M.: Hydrogen Embrittlement of Copper. FMM, vol. 16, 1963, pp. 737-740.
126. Broom, T.; and Nicholson, A.: Atmospheric Corrosion – Fatigue of Age-Hardened Aluminum Alloys. Inst. of Metals, J., vol. 89, Feb. 1961, pp. 183-190.
127. Bradshaw, F. J.; and Wheeler, C.: The Effect of Environment on Fatigue Crack Growth in Aluminum and Some Aluminum Alloys. Appl. Mat. Res., vol. 5, 1966, pp. 112-119.
128. Wei, R. P.: Fatigue-Crack Propagation in a High-Strength Aluminum Alloy. Intr. J. Fract. Mech., vol. 4, 1968, pp. 159-166.
129. Oriani, R. A.: The Diffusion and Trapping of Hydrogen in Steel. Acta Met., vol. 18, Jan. 1970, pp. 147-157.
130. Fletcher, E. E.; and Elsea, A. R.: Hydrogen Movement in Steel – Entry, Diffusion, and Elimination. Defense Metals Information Center, DMIC Report 219, June 1965.
131. Grimes, H. H.: The Effect of Plastic Deformation on the Diffusion of Hydrogen in Nickel. Acta Met., vol. 7, Dec. 1959, pp. 782-786.
132. Beeck, O.: Hydrogen Adsorption on Iron. Disc. Faraday Soc., vol. 8, 1950, pp. 118-120.
133. Cerny, S.; Ponec, V.; and Hlodek, L.: Hydrogen Adsorption on Molybdenum. J. Catalysis, vol. 5, 1966, pp. 27-30.
134. Brennan, D.; and Hayward, D. O.: Hydrogen Desorption. Phil. Trans., vol. A(GB)258, 1965, pp. 375-390.
135. Pritchard, J.: Surface-Potential Study of Desorption of Hydrogen From Evaporated Copper Films. Nature, vol. 194, 1962, pp. 38-51.
136. Gubanov, A. I.: Hydrogen Diffusion in Metals. Soviet Phys.-Solid State, vol. 6, Oct. 1964, pp. 790-794.

137. Nelson, H. G.; Williams, D. P.; and Tetelman, A. S.: Embrittlement of a Ferrous Alloy in a Partially Dissociated Hydrogen Environment. Met. Trans., vol. 2, April 1971, pp. 953-959.
138. Williams, D. P.; and Nelson, H. G.: Embrittlement of 4130 Steel by Low-Pressure Gaseous Hydrogen. Met. Trans., vol. 1, Jan. 1970, pp. 63-68.
139. Johnson, H. H.: On Hydrogen Brittleness in High Strength Steels. Fundamental Aspects of Stress Corrosion Cracking, Natl. Assoc. of Corrosion Engrs., Houston, Texas, 1969, pp. 439-444.
140. Dushman, S.: Scientific Foundations of Vacuum Technique. John Wiley and Sons, Inc., New York, 1962.
141. Cadenhead, D. A.; and Wagner, N. J.: Low-Temperature Hydrogen Adsorption on Copper-Nickel Alloys. J. Phys. Chem., vol. 72, Aug. 1968, pp. 2775-2781.
142. Smithells, C. J.; and Ransley, C. E.: The Diffusion of Gases Through Metals. Proc. Roy. Soc., London, vol. 150, 1935, pp. 172-196.
143. Nelson, H. G.: Environmental Hydrogen Embrittlement of Titanium – A Qualitative Comparison With Stress-Corrosion Cracking. Stress Corrosion Cracking Mechanisms in Titanium Alloys, Natl. Assoc. of Corrosion Engrs., Houston, Texas, 1971.
144. Livanov, V. A.; Bukhanova, A. A.; and Kolachev, B. A.: Hydrogen in Titanium. Israel Program for Scientific Translations, Daniel Davey and Co., New York, 1965.
145. Ripling, E. J.: Hydrogen Embrittlement of a Commercial Alpha-Beta Titanium Alloy. J. Metals, Trans. AIME, vol. 8, 1956, pp. 502-503.
146. Papazoglou, T. P.; and Hepworth, M. T.: The Diffusion of Hydrogen in Titanium. Met. Soc. of AIME, Trans., vol. 242, April 1968, pp. 682-685.
147. Blackburn, M. J.: Relationship of Microstructure to Some Mechanical Properties of Ti-8Al-1V-1Mo. Trans. ASM, vol. 59, Dec. 1966, pp. 694-708.
148. Pugh, E. N.: On the Mechanism(s) of Stress-Corrosion Cracking. Environment-Sensitive Mechanical Behavior, Gordon and Breach, New York, 1966, pp. 351-401.
149. Giorgi, T. A.; and Ricca, F.: Thermodynamic Properties of Hydrogen and Deuterium in Alpha-Titanium. Nuovo Cimento Supp., vol. 5, Feb. 1967, pp. 472-482.

150. Beevers, C. J.; Warren, M. R.; and Edmonds, D. V.: Fracture of Titanium-Hydrogen Alloys. J. Less-Common Met., vol. 14, 1968, pp. 387-396.
151. Sanderson, G.; and Scully, J. C.: Hydride Formation in Thin Foils of Dilute Ti-Al Alloys. Met. Soc. of AIME, Trans., vol. 239, Dec. 1967, pp. 1883-1886.
152. Kolachev, B. A.; Vazimov, O. P.; and Zhuravlev, L. N.: Diffusion of Hydrogen in Titanium and in the Beta-Titanium Alloy VT15. Tsvetnaya Metallurgiya, vol. 12, 1969, pp. 104-109.
153. Allen, R. P.; Taggart, R.; and Polonis, D. H.: A Resistometric Study of Hydride Precipitation in Alpha Titanium. Acta Met., vol. 14, June 1966, pp. 741-747.
154. Vitt, Ronald Sheldon: Hydride Precipitation in Titanium. Ph. D. Thesis, Dept. of Engineering, Univ. of California, Los Angeles, California, 1969.
155. Johnson, E. W.; and Hill, M. L.: The Diffusivity of Hydrogen in Alpha Iron. Met. Soc. of AIME, Trans., vol. 218, Dec. 1960, pp. 1104-1112.
156. Beton, R. H.: The Effect of Hydrogen in Quantities of up to 0.009 pct on the Room-Temperature Izod and Tensile Strength of Commercially Pure Titanium. J. Inst. Met., vol. 88, 1959-1960, pp. 93-95.
157. Boyd, W. K.: Stress Corrosion Cracking of Titanium and Its Alloys. Fundamental Aspects of Stress Corrosion Cracking, Natl. Assoc. of Corrosion Engrs., Houston, Texas, 1969, pp. 593-602.
158. Koehl, B. G.; Williams, D. N.; and Bartlett, E. S.: Investigation of the Reaction of Titanium With Hydrogen. NASA CR-92,389, 1969.
159. Walter, R. J.; and Ytterhus, J. A.: Behavior of Columbium and Tantalum in Hydrogen Environments. Research Report RR 67-7, Rocketdyne, Div. of North American Rockwell, Sept. 1967.
160. Walter, R. J.; and Chandler, W. T.: Compatibility of Tantalum and Columbium Alloys With Hydrogen. AIAA J., vol. 4, 1966, pp. 302-314.
161. Fidelle, J. P.; Roux, C.; and Rapin, M.: Essais de Fragilisation d'Aciers à Haute Résistance par l'Hydrogène et le Deutérium Sous Pression – Contribution à l'Étude du Mécanisme de la Fragilisation des Aciers par l'Hydrogène. Mem. Sci. Rev. Metallurg., vol. 66, 1969, pp. 833-844.

162. Tetelman, A. S.; and Robertson, W. D.: The Mechanism of Hydrogen Embrittlement Observed in Iron-Silicon Single Crystals. Met. Soc. of AIME, Trans., vol. 224, Aug. 1962, pp. 775-783.
163. Tetelman, A. S.; and Robertson, W. D.: Direct Observation and Analysis of Crack Propagation in Iron-3 pct Silicon Single Crystals. Acta Met., vol. 11, May 1963, pp. 415-426.
164. Gell, M.; Briant, J.-P.; and Robertson, W. D.: The Effects of Temperature and Composition on Crack Propagation in Iron-Silicon Single Crystals. Met. Soc. of AIME, Trans., vol. 239, June 1967, pp. 813-823.
165. Zapffe, C. A.; and Sims, C. E.: Hydrogen Embrittlement, Internal Stress and Defects in Steel. J. Metals, Trans. AIME, vol. 145, 1941, pp. 225-259.
166. Bernstein, I. M.: The Role of Hydrogen in the Embrittlement of Iron and Steel. Mater. Sci. Eng., vol. 6, 1970, pp. 1-19.
167. Hibbard, W. R., Jr.; and Dunn, C. G.: A Study of $\langle 112 \rangle$ Edge Dislocations in Bent Silicon-Iron Single Crystals. Acta Met., vol. 4, May 1956, pp. 306-315.
168. Tomkins, B.: Fatigue Failure in High-Strength Metals. Phil. Mag., vol. 23, March 1971, pp. 687-703.
169. Williams, D. P.; and Nelson, H. G.: Gaseous Hydrogen-Induced Cracking of Ti-5Al-2.5Sn. Met. Trans., accepted for publication, 1971.
170. Beck, T. R.; Blackburn, M. J.; and Speidel, M. O.: Stress Corrosion Cracking of Titanium Alloys: SCC of Aluminum Alloys, Polarization of Titanium Alloys in HCl and Correlation of Titanium and Aluminum SCC Behavior. NASA CR 103,236, 1969.
171. Crooker, T. W.; Judy, R. W.; and Cooley, L. A.: Subcritical Crack Growth in Several Titanium Alloys. Report 2160, Naval Research Lab., Sept. 1970.
172. Wei, R. P.; and Landes, J. D.: Correlation Between Sustained-Load and Fatigue Crack Growth in High-Strength Steels. Matr. Res. Std., vol. 9, July 1969, pp. 25-46.
173. Gallagher, J. P.: Corrosion Fatigue Crack Growth Behavior Above and Below K_{ISCC} . Report 7-64, Naval Research Lab., May 1970.
174. Barth, C. F.; and Steigerwald, E. A.: Evaluation of Hydrogen Embrittlement Mechanisms. Met. Trans., vol. 1, Dec. 1970, pp. 3451-3455.

175. Wiederhorn, S. M.: Moisture Assisted Crack Growth in Ceramics. Intern. J. Fract. Mech., vol. 4, June 1968, pp. 171-177.
176. Carter, C. S.: Observations on Stress Corrosion Crack Propagation Characteristics in High Strength Steels. Doc. D6-25274, Boeing Sci. Res. Lab., 1970.
177. De Kazinczy, F.: A Theory of Hydrogen Embrittlement. J. Iron and Steel Inst., vol. 177, 1954, pp. 85-92.
178. Bilby, B. A.; and Hewitt, J.: Hydrogen in Steel – The Stability of Microcracks. Acta Met., vol. 10, June 1962, pp. 587-600.
179. Garofalo, F.; Chou, Y. T.; and Ambegaokar, V.: Effect of Hydrogen on Stability of Microcracks in Iron and Steel. Acta Met., vol. 8, Aug. 1960, pp. 504-512.
180. Rebinder, P. A.: VI s'ezd Russkikh Fizikov. 1928, pp. 28-35.
181. Westwood, A. R. C.: Environment-Sensitive Mechanical Behavior – Status and Problems. Environment-Sensitive Mechanical Behavior, Gordon and Breach, New York, 1966, pp. 1-65.
182. Barnett, W. J.; and Troiano, A. R.: Crack Propagation in Hydrogen-Induced Fracture of Steel. J. Metals, Trans. AIME, vol. 209, April 1957, pp. 486-494.
183. Scott, T. E.; and Troiano, A. R.: Effects of Hydrogen in the Failure of Steels. Nature, vol. 185, 1960, pp. 372-376.
184. Bockris, J. O'M; Beck, W.; Genshaw, M. A.; Subramanyan, P. K.; and Williams, F. S.: The Effect of Stress on the Chemical Potential of Hydrogen in Iron and Steel. Acta Met., vol. 19, Nov. 1971, pp. 1209-1219.
185. Bockris, J. O'M; and Subramanyan, P. K.: A Thermodynamic Analysis of Hydrogen in Metals in the Presence of an Applied Stress Field. Acta Met., vol. 19, Nov. 1971, pp. 1205-1208.
186. Sturges, C. M.; and Miodownik, A. P.: The Interaction of Hydrogen and Dislocations in Iron. Acta Met., vol. 17, Sept. 1969, pp. 1197-1207.
187. Bastien, P.; and Azou, P.: Effect of Hydrogen on the Deformation and Fracture of Iron and Steel in Simple Tension. Proc. First World Met. Cong., ASM, 1951, pp. 535-552.
188. Bastien, P.; and Azou, P.: Effect of Hydrogen on Fracture of Steel. Rev. Met., vol. 49, 1952, pp. 837-848.

189. Popov, K. V.; and Nechai, E. P.: Fiziko-Khimicheskaya Mekhanika Materialov. Vol. 3, 1967, pp. 631-645.
190. Kolachev, B. A.; Livanoz, V. A.; and Bukhanova, A. A.: Nauka. 1964, pp. 88-95.
191. Wood, T. W.; and Daniels, R. D.: The Influence of Hydrogen on the Tensile Properties of Columbium. Met. Soc. of AIME, Trans., vol. 233, May 1965, pp. 898-903.
192. Westlake, D. G.: Hydrogen Embrittlement: A Resistometric Study of Niobium (Columbium)-Hydrogen Alloys. Met. Soc. of AIME, Trans., vol. 245, Feb. 1969, pp. 287-292.
193. Huber, O. J.; Gates, J. E.; Young, A. P.; Pobereskin, M.; and Frost, P. D.: Hydrogen Distribution in Heat-Treated Titanium as Established by Autoradiography. J. Metals, Trans. AIME, vol. 9, July 1957, pp. 918-923.
194. Westlake, D. G.: A Generalized Model for Hydrogen Embrittlement. Trans. ASM, vol. 62, 1969, pp. 1000-1006.
195. Robers, H. C.: Hydrogen Embrittlement of Metals. Science, vol. 159, March 1968, pp. 1057-1064.
196. Haynes, R.: Effect of Hydrogen on Room-Temperature Mechanical Properties of Titanium-5%Aluminum-2.5%Tin Alloy. J. Inst. Metals, vol. 90, 1961-1962, pp. 80-84.
197. Desorbo, W.; and Turnbull, D.: Quenching of Imperfections in Aluminum. Acta Met., vol. 7, Feb. 1959, pp. 83-85.
198. Ells, C. E.; and Evans, W.: The Agglomeration of Hydrogen in Aluminum. Met. Soc. of AIME, Trans., vol. 227, April 1963, pp. 438-446.
199. Liu, T.-S.; and Steinberg, M. A.: The Mode of Hydride Precipitation in Alpha Titanium and Alpha Titanium Alloys. Trans. ASM, vol. 50, 1958, pp. 455-477.
200. Sherman, D. H.; Owen, C. V.; and Scott, T. E.: The Effect of Hydrogen on the Structure and Properties of Vanadium. Met. Soc. of AIME, Trans., vol. 242, 1968, pp. 1775-1784.
201. Adair, A. M.; and Hook, R. E.: The Appearance and Return of a Hydrogen Yield Point in Iron. Acta Met., vol. 10, Aug. 1962, pp. 741-745.
202. Gibala, R.: Internal Friction in Hydrogen-Charged Iron. Met. Soc. of AIME, Trans., vol. 239, Oct. 1967, pp. 1574-1585.

203. Eustice, A. L.; and Carlson, O. N.: Effect of Hydrogen on the Tensile Properties of Iodide Vanadium. Met. Soc. of AIME, Trans., vol. 221, April 1961, pp. 238-241.
204. Wilcox, B. A.: Effect of Hydrogen on Dislocation Locking in Niobium. J. Less-Common Met., vol. 2 Apr.-Aug. 1960, pp. 292-303.
205. Boniszewski, T.; and Smith, G. C.: The Influence of Hydrogen on the Plastic Deformation, Ductility, and Fracture of Nickel in Tension. Acta Met., vol. 11, March 1963, pp. 165-178.
206. Wilcox, B. A.; and Smith, G. C.: The Portevin-le Chatelier Effect in Hydrogen Charged Nickel. Acta Met., vol. 12, April 1964, pp. 371-376.
207. Zapffe, C. A.: Neumann Bands and the Planar-Pressure Theory of Hydrogen Embrittlement. J. Iron and Steel Inst., vol. 254, 1946, pp. 123P-130P.
208. Latanision, R. M.; and Staehle, R. W.: The Effect of Continuous Hydrogenation on the Deformation of Nickel Single Crystals. Scripta Met., vol. 2, 1968, pp. 667-672.
209. Nichols, H.; and Rostoker, W.: Analogies Between Stress-Corrosion Cracking and Embrittlement by Liquid Metals. Trans. ASM, vol. 56, 1963, pp. 495-507.
210. Rostoker, W.; McCaughey, J. M.; and Markus, H.: Embrittlement by Liquid Metals. Reinhold, New York, 1960, p. 63.
211. Fager, D. N.; and Spurr, W. F.: Solid Cadmium Embrittlement: Steel Alloys. Corrosion, vol. 27, Feb. 1971, pp. 72-76.
212. Sprowls, D. O.; and Brown, R. H.: Stress Corrosion Mechanisms for Aluminum Alloys. Fundamental Aspects of Stress Corrosion Cracking, Natl. Assoc. of Corrosion Engrs., Houston, Texas, 1969, pp. 466-506.
213. Ichinose, H.: The Ductile-Brittle Transition of Aluminum in the Presence of Hg-3% Zn or Sn-10% Zn Liquid. Trans. JIM, vol. 9, 1968, pp. 35-41.
214. Ichinose, H.; and Couchi, C.: The Strain-Rate Dependence of the Ductile-Brittle Transition Temperature of Aluminum in Liquid Metals. Trans. JIM, vol. 9, 1968, pp. 41-47.
215. Mostovoy, S.: Embrittlement of Leaded Steel at Intermediate Temperatures. Ph. D. Thesis, Dept. of Engineering, Illinois Institute of Technology, Chicago, Illinois, 1968.

216. Mostovoy, S.; and Breyer, N. N.: The Effect of Lead on the Mechanical Properties of 4145 Steel. Trans. ASM, vol. 61, June 1968, pp. 219-232.
217. Fager, D. N.; and Spurr, W. F.: Solid Cadmium Embrittlement: Titanium Alloys. Corrosion, vol. 24, Oct. 1969, pp. 409-421.
218. Stoloff, N. S.: Liquid Metal Embrittlement. Surfaces and Interfaces II, Syracuse University Press, New York, 1968, pp. 157-182.
219. Rideout, S. P.; Ondrejcin, R. S.; Louthan, M. R., Jr.; and Rawl, D. E.: The Role of Moisture and Hydrogen in Hot-Salt Cracking of Titanium Alloys. Fundamental Aspects of Stress Corrosion Cracking, Natl. Assoc. of Corrosion Engrs., Houston, Texas, 1969, pp. 650-659.
220. Li, C.-Y.; and Johnson, H. H.: Kinetics of Sub-critical Crack Growth in High Strength Materials. Surfaces and Interfaces II, Syracuse University Press, New York, 1968, pp. 213-231.



012 001 C1 U 17 720218 S00903DS
DEPT OF THE AIR FORCE
AF WEAPONS LAB (AFSC)
TECH LIBRARY/WLOL/
ATTN: E LOU BOWMAN, CHIEF
KIRTLAND AFB NM 87117

POSTMASTER: If Undeliverable (Section 158
Postal Manual) Do Not Return

"The aeronautical and space activities of the United States shall be conducted so as to contribute . . . to the expansion of human knowledge of phenomena in the atmosphere and space. The Administration shall provide for the widest practicable and appropriate dissemination of information concerning its activities and the results thereof."

— NATIONAL AERONAUTICS AND SPACE ACT OF 1958

NASA SCIENTIFIC AND TECHNICAL PUBLICATIONS

TECHNICAL REPORTS: Scientific and technical information considered important, complete, and a lasting contribution to existing knowledge.

TECHNICAL NOTES: Information less broad in scope but nevertheless of importance as a contribution to existing knowledge.

TECHNICAL MEMORANDUMS: Information receiving limited distribution because of preliminary data, security classification, or other reasons.

CONTRACTOR REPORTS: Scientific and technical information generated under a NASA contract or grant and considered an important contribution to existing knowledge.

TECHNICAL TRANSLATIONS: Information published in a foreign language considered to merit NASA distribution in English.

SPECIAL PUBLICATIONS: Information derived from or of value to NASA activities. Publications include conference proceedings, monographs, data compilations, handbooks, sourcebooks, and special bibliographies.

TECHNOLOGY UTILIZATION PUBLICATIONS: Information on technology used by NASA that may be of particular interest in commercial and other non-aerospace applications. Publications include Tech Briefs, Technology Utilization Reports and Technology Surveys.

Details on the availability of these publications may be obtained from:

SCIENTIFIC AND TECHNICAL INFORMATION OFFICE

NATIONAL AERONAUTICS AND SPACE ADMINISTRATION

Washington, D.C. 20546